

# Solar neutrino physics

Xun-Jie Xu<sup>a,\*</sup>, Zhe Wang<sup>b,c</sup>, Shaomin Chen<sup>b,c</sup>

<sup>a</sup>*Institute of High Energy Physics, Chinese Academy of Sciences, Beijing 100049, China*

<sup>b</sup>*Center for high energy physics, Tsinghua University, Beijing 100084, China*

<sup>c</sup>*Department of Engineering Physics, Tsinghua University, Beijing 10084, China*

---

## Abstract

As a free, intensive, rarely interactive, and well directional messenger, solar neutrinos have been driving both solar physics and neutrino physics developments for more than half a century. Since more extensive and advanced neutrino experiments are under construction, being planned or proposed, we are striving toward an era of precise and comprehensive measurement of solar neutrinos in the next decades. In this article, we review recent theoretical and experimental progress achieved in solar neutrino physics. We present not only an introduction to neutrinos from the standard solar model and the standard flavor evolution, but also a compilation of a variety of new physics that could affect and hence be probed by solar neutrinos. After reviewing the latest techniques and issues involved in the measurement of solar neutrino spectra and background reduction, we provide our anticipation on the physics gains from the new generation of neutrino experiments.

*Keywords:* Solar neutrinos, Neutrino oscillations, Non-Standard Interaction, Sterile neutrinos, Neutrino detection

---

arXiv:2209.14832v2 [hep-ph] 17 Mar 2023

---

\*Corresponding author

*Email addresses:* xuxj@ihep.ac.cn (Xun-Jie Xu), wangzhe-hep@tsinghua.edu.cn (Zhe Wang), chenshaomin@tsinghua.edu.cn (Shaomin Chen)

# Contents

<b>1</b>	<b>Introduction</b>	<b>4</b>
<b>2</b>	<b>Solar neutrino physics</b>	<b>6</b>
2.1	Neutrino fluxes in the standard solar model	6
2.1.1	The pp chain and the CNO cycle	6
2.1.2	Energy spectral shapes and production rate distributions	8
2.1.3	Open issues in solar models	11
2.2	Solar neutrino propagation in matter and vacuum	11
2.2.1	The MSW-LMA solution	11
2.2.2	Measurements of solar neutrino parameters	13
2.2.3	The adiabatic approximation	16
2.2.4	The Earth matter effect	16
2.3	Search for new physics with solar neutrinos	17
2.3.1	Non-Standard Interactions (NSI)	17
2.3.2	Sterile neutrinos	21
2.3.3	Neutrino magnetic moments	22
2.3.4	Neutrino interactions with light mediators	23
2.3.5	Spin-flavor precession and solar antineutrinos	23
2.3.6	Dark matter annihilation	24
2.3.7	Neutrino decay	25
2.3.8	Others	26
<b>3</b>	<b>Detection and experimental challenges</b>	<b>28</b>
3.1	Elastic neutrino-electron scattering	28
3.2	CC scattering on nucleus	29
3.3	Coherent elastic neutrino-nucleus scattering (CE $\nu$ NS)	31
3.4	Energy and direction measurements	32
3.5	Backgrounds	34
3.5.1	Cosmogenic backgrounds	34
3.5.2	Detector-related backgrounds	37
<b>4</b>	<b>Prospects of solar neutrino experiments</b>	<b>40</b>
4.1	Water Cherenkov detectors	41
4.1.1	SK-Gd	41
4.1.2	Hyper-Kamiokande	42
4.2	Liquid scintillator detectors	43
4.2.1	JUNO	43
4.2.2	SNO+	44
4.3	Hybrid detectors	45

4.3.1	THEIA	45
4.3.2	JNE	45
4.4	DUNE	47
4.5	Other experimental approaches	48
4.5.1	Dark matter detectors	48
4.5.2	Space-based detectors	50
<b>5</b>	<b>Summary</b>	<b>51</b>

# 1. Introduction

*“How does the Sun shine? Does the neutrino have a mass? Can solar neutrinos be used to test the theory of stellar evolution? To explore the unification of strong, weak, and electromagnetic forces?”* John N. Bahcall raised these questions at the very beginning of his famous book [1]. Starting from Eddington’s speculation in 1920 [2]<sup>1</sup>, followed by the establishment of the theory of stellar nucleosynthesis (in the 1930s) and decades of experimental observations of solar neutrinos (since the 1960s) and theoretical efforts, our understanding of the Sun over a century has evolved and eventually led to a surprising and profound discovery—neutrino masses—which are of crucial importance to the most fundamental physics.

The theory of stellar nucleosynthesis anticipates that the Sun produces an enormous amount of neutrinos from nuclear fusion. They can be used as a unique probe to the solar energy production mechanism, inspiring R. Davis to carry out his pioneering experiment at Homestake in 1968 [3] via the Pontecorvo-Alvarez [4, 5] inverse  $\beta$  decay:  $\nu_e + {}^{37}\text{Cl} \rightarrow e^- + {}^{37}\text{Ar}$ . The first result [3] came out as an upper limit of 3 Solar Neutrino Units (SNU,  $1 \text{ SNU} \equiv 10^{-36} \text{ events/atom/sec}$ ) which is lower than the theoretical prediction published at the same time [6]<sup>2</sup>. From 1970 to 1994, the Homestake experiment continued data taking with improved techniques to discriminate the signal from backgrounds, and eventually obtained a precise measurement:  $2.56 \pm 0.16 \pm 0.16 \text{ SNU}$  [7], which is only one-third of the prediction [8]. Similar deficits were also confirmed by gallium experiments (GALLEX/GNO [9] and SAGE [10]) and water Cherenkov detectors (Kamiokande [11], Super-Kamiokande [12], and SNO [13]). The discrepancy between the observation of solar neutrinos and the prediction became the so-called “solar neutrino problem.”

Like Arthur B. McDonald stated in his Nobel lecture [14], *“possible reasons for the discrepancy could have been that the experiment or the theory was incorrect.”* The discrepancy motivated many theoretical efforts to address the solar neutrino problem. From the 1970s to the early 1990s, a variety of theoretical interpretations to the solar neutrino problem were proposed and investigated, including neutrino oscillation<sup>3</sup> with the Mikheyev-Smirnov-Wolfenstein (MSW) effect [19, 20, 21], oscillation in vacuum [22], spin or spin-flavor precession due to neutrino magnetic moments [23, 24, 25, 26], flavor conversion due to non-standard interactions (NSI) of massless neutrinos [19, 27, 28, 29], neutrino decays [30, 31], etc. Eventually, neutrino oscillation with the MSW effect and a large mixing angle (LMA) became the standard solution (MSW-LMA) to the solar neutrino problem.

Neutrino oscillation implies that solar neutrinos, initially being produced as  $\nu_e$ , may change their flavors to  $\nu_\mu$  or  $\nu_\tau$  along their path to the Earth. As a consequence, only a fraction of the neutrinos appear as  $\nu_e$  in the detector. The survival probability of  $\nu_e$  in the MSW-LMA solution is approximately  $\sin^2 \theta_{12} \approx 0.3$  at high energies ( $\sim 10 \text{ MeV}$ , e.g., for  ${}^8\text{B}$  neutrinos) and increases to  $\cos^4 \theta_{12} + \sin^4 \theta_{12} \approx 0.55$  at low energies ( $\lesssim 1 \text{ MeV}$ , e.g., for pp neutrinos). Both values

---

<sup>1</sup>It is worth mentioning that while the contraction hypothesis (i.e., the solar energy was from gravitational contraction) was prevailing by then, Eddington discussed abundantly contradictory consequences of the the contraction hypothesis in his paper [2] and conceived that the “sub-atomic” energy might actually power the Sun.

<sup>2</sup>In Ref. [6], the theoretical values were predicted to be 21, 11, 7.7, 4.4, and 11 SNU for five models considered by Bahcall *et al.* The differences among these models include the proton-proton reaction rate, the hydrogen/helium fraction, the metallicity, the central temperature and density, which were not well determined by then. Despite the model dependence, it was clear that the theoretical values were all higher than the experimental upper limit, 3 SNU.

<sup>3</sup>The concept of neutrino oscillation was first proposed by Pontecorvo in 1957 [15, 16], a decade earlier than Davis’s Homestake experiment. The original consideration was  $\nu \leftrightarrow \bar{\nu}$  oscillation, while oscillation due to flavor mixing was later considered by Pontecorvo, Maki, Nakagawa and Sakata in the 1960s [17, 18].

have so far been consistent with the observations. The flavor conversion to  $\nu_\mu$  and  $\nu_\tau$  has been indirectly probed by neutral current (NC) and electron scattering events in SNO [13] and Super-Kamiokande [32]. Moreover, the values of  $\theta_{12}$  and  $\Delta m_{21}^2$  in the LMA regime have been confirmed by the KamLAND experiment, which measured  $\theta_{12}$  and  $\Delta m_{21}^2$  in long-baseline reactor neutrino oscillation, independent of solar neutrino observations. Further measurements from the Borexino experiment, which is dedicated to solar neutrino observations and has identified pp,  ${}^7\text{Be}$ , pep, and CNO components [33, 34, 35, 36, 37], agree well with the MSW-LMA solution.

Next-generation large underground detectors such as Hyper-Kamiokande [38], JUNO [39], DUNE [40], JNE [41], THEIA [42], as well as dark matter (DM) detectors<sup>4</sup>, will usher in an era of precision measurement of solar neutrinos. Given the experimental prospect and the verified theory, there is a crucial question for future experiments: what can be explored in the precision measurement of solar neutrinos? The answer varies from different perspectives:

From the astrophysical viewpoint, a full spectrum of solar neutrinos of all components (e.g., pep, hep,  ${}^{13}\text{N}$ ,  ${}^{15}\text{O}$ , etc.) is valuable to the study of solar and stellar physics. Some of the spectral components are not measured precisely while some have not been detected yet. In particular, the observation of CNO neutrinos has just started—very recently the first observation is achieved by Borexino [37, 44]. The measurement of CNO neutrino fluxes will be of great importance to the poorly known metallicity of the Sun and also to the study of heavier ( $\gtrsim 1.3M_\odot$ ) stars in which the CNO cycle is believed to dominate the energy production. As the nearest star, the Sun provides the unique opportunity to measure neutrinos precisely from stellar nucleosynthesis.

From the perspective of particle physics, neutrino masses point toward new physics, while a variety of new physics might affect solar neutrino observations. The precision measurement of solar neutrino spectra allows us to search for new physics signals. Currently, the low- and high-energy regimes of the MSW-LMA solution have been measured [45, 46, 47], while the transition between the two regimes (known as the *up-turn*) is not seen yet. The *up-turn* is sensitive to new physics such as Non-Standard Interactions (NSI) or sterile neutrinos. In addition, the Sun, due to its large mass and close distance, provides an exceptional environment for the study of dark matter, which might cause observable effects on solar neutrinos. As will be comprehensively summarized in this review, all relevant new physics scenarios call for extensive investigations of solar neutrinos.

This paper aims at a timely review of theoretical and experimental progress in solar neutrino physics. We will introduce the standard solar neutrino physics, compile a variety of relevant new physics studied in the literature, review the latest techniques and issues involved in the measurement of solar neutrino spectra and background reduction, and discuss the physics gains from future experiments. Past reviews have their respective focuses on, e.g., solar models [48, 49], the detection [50], the experimental progress [51, 49, 50], or neutrino phenomenology and new physics [52]. Here, we shall highlight the feature of this review, which is to present a comprehensive summary of new physics, together with the prospects of full-spectrum precision measurements. We hope such a combination might be helpful for both theorists interested in probing their theories using solar neutrinos and experimentalists looking for new physics goals for their experiments.

---

<sup>4</sup>Solar neutrinos can be detected by DM detectors mainly via the coherent elastic neutrino-nucleus scattering (CE $\nu$ NS) process [43]. For DM detection, this is regarded as a background known as the solar neutrino floor. Currently, multi-ton scale liquid xenon detectors such as XENONnT, PandaX, and LUX are approaching the solar neutrino floor—see Sec. 4.5.1 for further details.

## 2. Solar neutrino physics

### 2.1. Neutrino fluxes in the standard solar model

The standard solar model (SSM) is constructed upon equations of hydrostatic equilibrium, energy transport, and energy production rates via nuclear reactions—see Ref. [1] for a pedagogical introduction and Ref. [53] for a recent review. With boundary conditions imposed from solar radius and luminosity, and additional inputs, including the Sun’s age, elemental abundances, and radiative opacity, these equations can be solved to predict accurate profiles of the solar density, temperature, pressure, and neutrino fluxes. Figure 2.1 depicts the distributions of these quantities obtained in recent calculations [54].

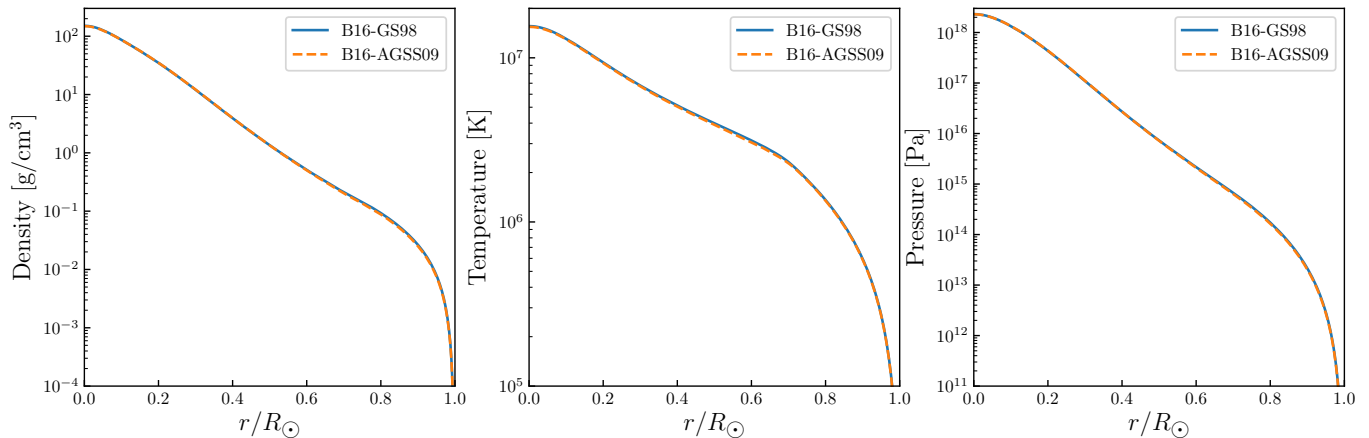


Figure 2.1: Solar density (left), temperature (middle), and pressure (right) profiles in two standard solar models B16-GS98 and B16-AGSS09 [54]. Here  $r$  denotes the distance to the solar center and  $R_{\odot}$  denotes the solar radius. The main differences between the two models are to be explained in Sec. 2.1.3.

#### 2.1.1. The pp chain and the CNO cycle

There are two sets of nuclear reactions responsible for neutrino and energy productions in the Sun, the pp chain and the CNO cycle, as illustrated in Figs. 2.2 and 2.3. The pp chain powers about 99% of the total solar energy, whereas the CNO cycle accounts for the remaining  $\sim 1\%$ . For stars with masses greater than  $1.3M_{\odot}$ , the CNO cycle dominates the energy production [57]. The total neutrino flux from the Sun should be consistent with the solar luminosity in photons, if all fusion processes are known.

As depicted in Fig. 2.2, five reactions in the pp chain produce neutrinos. They are referred to, according to the initial particles in the reactions, as pp, pep, hep,  ${}^7\text{Be}$ , and  ${}^8\text{B}$  neutrinos. The pp chain consists of four sub-chains, marked as pp-I to pp-IV in the figure. Note that all the sub-chains end up with  ${}^4\text{He}$ . Therefore, despite some heavier elements appearing at intermediate stages, the pp chain burns hydrogen only to helium. The first three sub-chains (pp-I, pp-II, and pp-III) generate most of the energy (and hence most of the neutrinos) produced in the pp-chain. The last sub-chain (pp-IV) contributes a very insignificant amount ( $10^{-5}$ ) to the energy production but produces the most energetic solar neutrinos (hep neutrinos), with energy up to 18.77 MeV [58].

In the CNO cycle<sup>5</sup>, carbon and nitrogen serve as catalysts, meaning their abundances are almost unchanged after

<sup>5</sup>Bethe first studied the CNO cycle for stellar energy production in 1939 [59]. It should be noted, however, that neutrinos were absent in

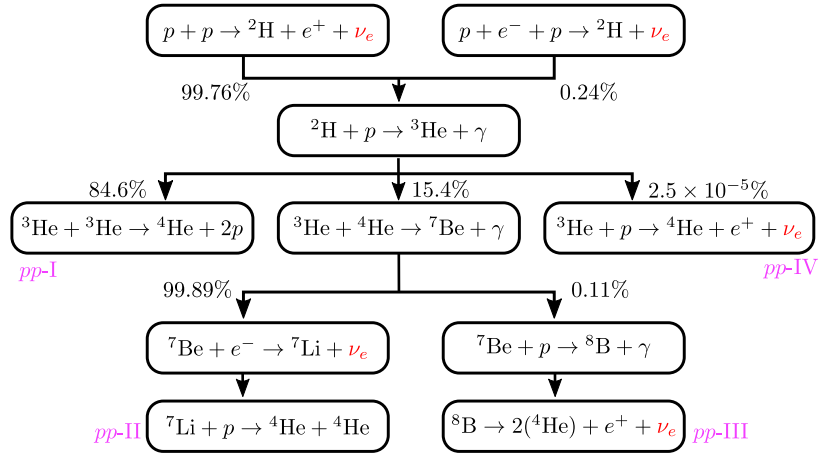


Figure 2.2: Reactions in the solar pp chain. Neutrinos ( $\nu_e$ ) produced in the five reactions in the top-down order are referred to as pp, pep, hep,  ${}^7\text{Be}$ ,  ${}^8\text{B}$  neutrinos, respectively. The theoretical branching percentages are taken from Ref. [55].

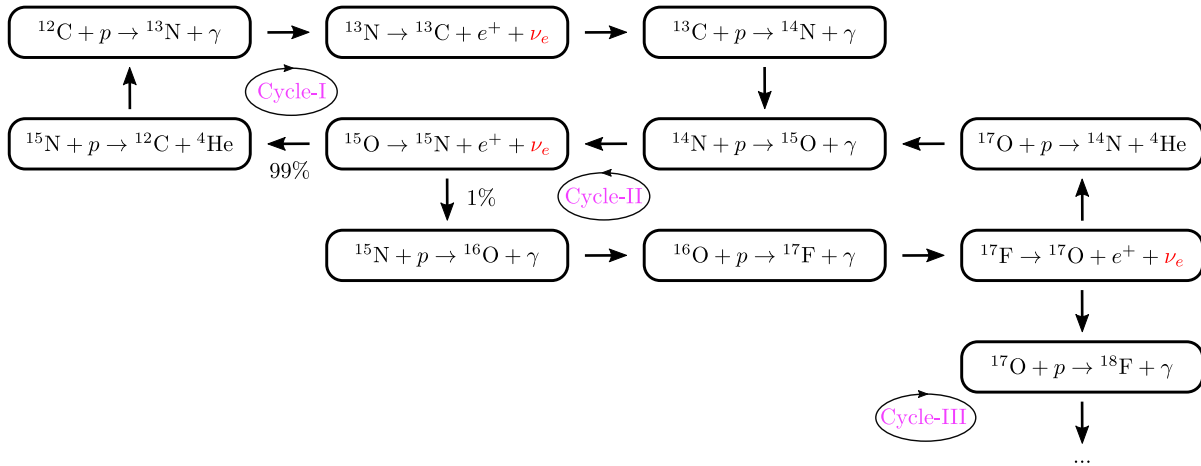


Figure 2.3: Reactions in the CNO cycle. Neutrinos ( $\nu_e$ ) are produced from decays of  ${}^{13}\text{N}$ ,  ${}^{15}\text{O}$ , and  ${}^{17}\text{F}$  in the first two cycles, Cycle-I and Cycle-II, with the latter suppressed relatively by  $\sim 1\%$ . Subsequent cycles such as Cycle-III produce heavier nuclear elements but their contributions are almost negligible for the Sun [56].

Table 2.1: Solar neutrino fluxes from two calculations, Bahcall-Serenelli-Basu (BSB) [63] and Barcelona 2016 (B16) [54], based on solar chemical composition data from GS98 [64], AGS05 [65], and AGSS09 [66].

$\nu_e$ flux [cm <sup>-2</sup> s <sup>-1</sup> ]	BSB05-GS98[63]	BSB05-AGS05[63]	B16-GS98 [54]	B16-AGSS09 [54]
$\Phi_{pp}/10^{10}$	5.99(1 ± 0.009)	6.06(1 ± 0.007)	5.98(1 ± 0.006)	6.03(1 ± 0.005)
$\Phi_{pep}/10^8$	1.42(1 ± 0.015)	1.45(1 ± 0.011)	1.44(1 ± 0.01)	1.46(1 ± 0.009)
$\Phi_{hep}/10^3$	7.93(1 ± 0.155)	8.25(1 ± 0.155)	7.98(1 ± 0.30)	8.25(1 ± 0.30)
$\Phi_{7Be}/10^9$	4.84(1 ± 0.105)	4.34(1 ± 0.093)	4.93(1 ± 0.06)	4.50(1 ± 0.06)
$\Phi_{8B}/10^6$	5.69(1 <sup>+0.173</sup> <sub>-0.147</sub> )	4.51(1 <sup>+0.127</sup> <sub>-0.113</sub> )	5.46(1 ± 0.12)	4.50(1 ± 0.12)
$\Phi_{13N}/10^8$	3.05(1 <sup>+0.366</sup> <sub>-0.268</sub> )	2.00(1 <sup>+0.145</sup> <sub>-0.127</sub> )	2.78(1 ± 0.15)	2.04(1 ± 0.14)
$\Phi_{15O}/10^8$	2.31(1 <sup>+0.374</sup> <sub>-0.272</sub> )	1.44(1 <sup>+0.165</sup> <sub>-0.142</sub> )	2.05(1 ± 0.17)	1.44(1 ± 0.16)
$\Phi_{17F}/10^6$	5.83(1 <sup>+0.724</sup> <sub>-0.420</sub> )	3.25(1 <sup>+0.166</sup> <sub>-0.142</sub> )	5.29(1 ± 0.20)	3.26(1 ± 0.18)

a complete cycle of reactions. As shown in Fig. 2.3, <sup>12</sup>C, after capturing a proton, is converted to <sup>13</sup>N, which decays and produces <sup>13</sup>C, followed by similar reactions converting <sup>13</sup>C → <sup>14</sup>N → <sup>15</sup>O → <sup>15</sup>N. Then the final element, <sup>15</sup>N, is dominantly converted back to <sup>12</sup>C. In this cycle, which we refer to as Cycle-I, neutrinos are produced via  $\beta^+$  decays of <sup>13</sup>N and <sup>15</sup>O. The net effect, hence, is that hydrogen is converted to helium with energy and neutrino emission. Besides the dominant Cycle-I, <sup>15</sup>N can be converted to <sup>16</sup>O with a small branching ratio, entering a subdominant cycle, Cycle-II, in which <sup>17</sup>F is produced and provides an additional source of neutrino emission. Due to the small branching ratio, Cycle-II is suppressed roughly by two orders of magnitude. Consequently, the <sup>17</sup>F neutrino flux is lower than <sup>13</sup>N and <sup>15</sup>O neutrino fluxes by two orders of magnitude—see Tab. 2.1.

The radioactive elements <sup>13</sup>N, <sup>15</sup>O, and <sup>17</sup>F can also produce monochromatic neutrino lines via electron capture (e.g., <sup>13</sup>N +  $e^-$  → <sup>13</sup>C +  $\nu_e$ ), which has not been extensively investigated so far [60, 61, 62]. The corresponding fluxes are suppressed by  $\sim 10^{-4}$  compared to their  $\beta^+$  decay neutrino fluxes [62]:

$$\Phi_{e^{13N}} = 7.9 \times 10^{-4} \Phi_{13N}, \quad \Phi_{e^{15O}} = 3.9 \times 10^{-4} \Phi_{15O}, \quad \Phi_{e^{17F}} = 5.8 \times 10^{-4} \Phi_{17F}. \quad (2.1)$$

Table 2.1 summarizes the neutrino fluxes calculated by Bahcall-Serenelli-Basu (BSB) [63] and the Barcelona group in 2016 (B16) [54] for different solar models. The differences of these models and related open issues will be discussed in Sec. 2.1.3.

### 2.1.2. Energy spectral shapes and production rate distributions

The shapes of solar neutrino energy distributions are not affected by model-dependent uncertainties such as those caused by the solar metallicity problem. They are determined mainly by the kinematics of the corresponding nuclear reactions, with additional corrections due to the Coulomb potentials of nuclei. Temperatures and densities hardly affect the energy distributions because the energy released by nuclear reactions is around the MeV scale and is much higher than the core temperature ( $\sim$ keV) and the chemical potential. In Fig. 2.4, we present the energy distributions using Bahcall’s results for the spectral shapes [1] and normalizing them according to B16-GS98 in Tab. 2.1, as well as the ratios in Eq. (2.1) for  $e^{13N}$ ,  $e^{15O}$ , and  $e^{17F}$  neutrinos.

---

the nuclear reactions Bethe used since the existence of neutrinos was still in question at the time.



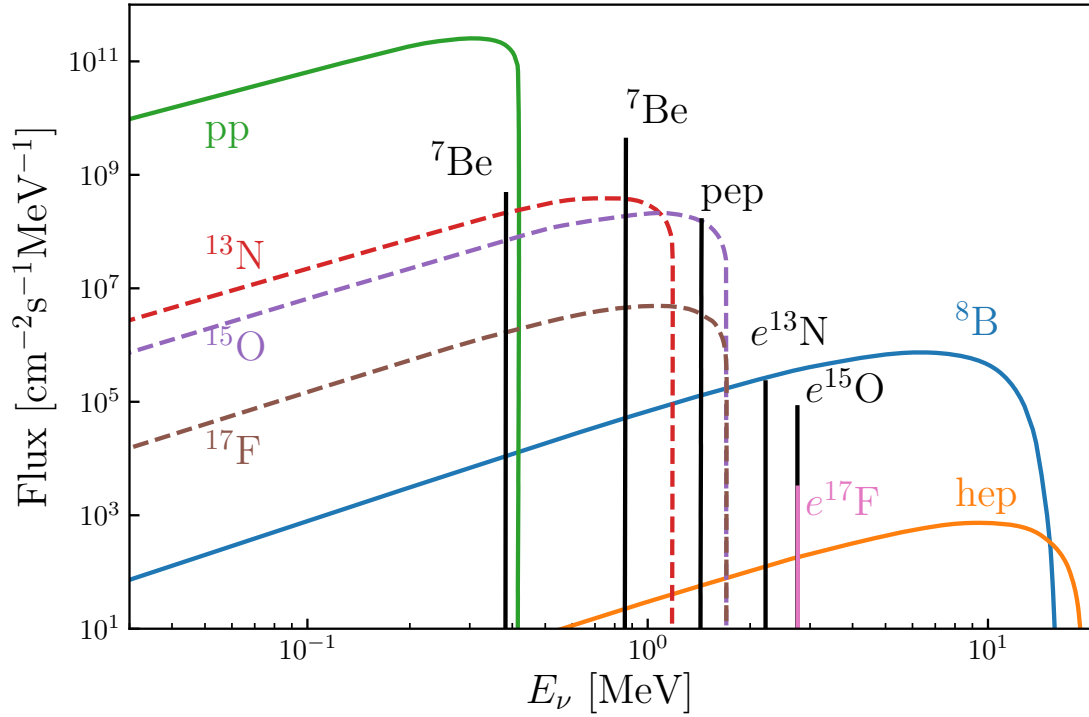


Figure 2.4: The solar neutrino spectra predicted by the SSM. Monochromatic spectra are given in units of  $\text{cm}^{-2}\text{s}^{-1}$ . Dashed lines denote neutrinos from the CNO cycle ( $^{13}\text{N}$ ,  $^{15}\text{O}$ ,  $^{17}\text{F}$ ). The figure is updated using the data from Ref. [54] (B16-GS98, see also Tab. 2.1), Bahcall's energy spectrum [1], and the electron capture rates (for  $e^{13}\text{N}$ ,  $e^{15}\text{O}$ ,  $e^{17}\text{F}$ ) in Eq. (2.1).

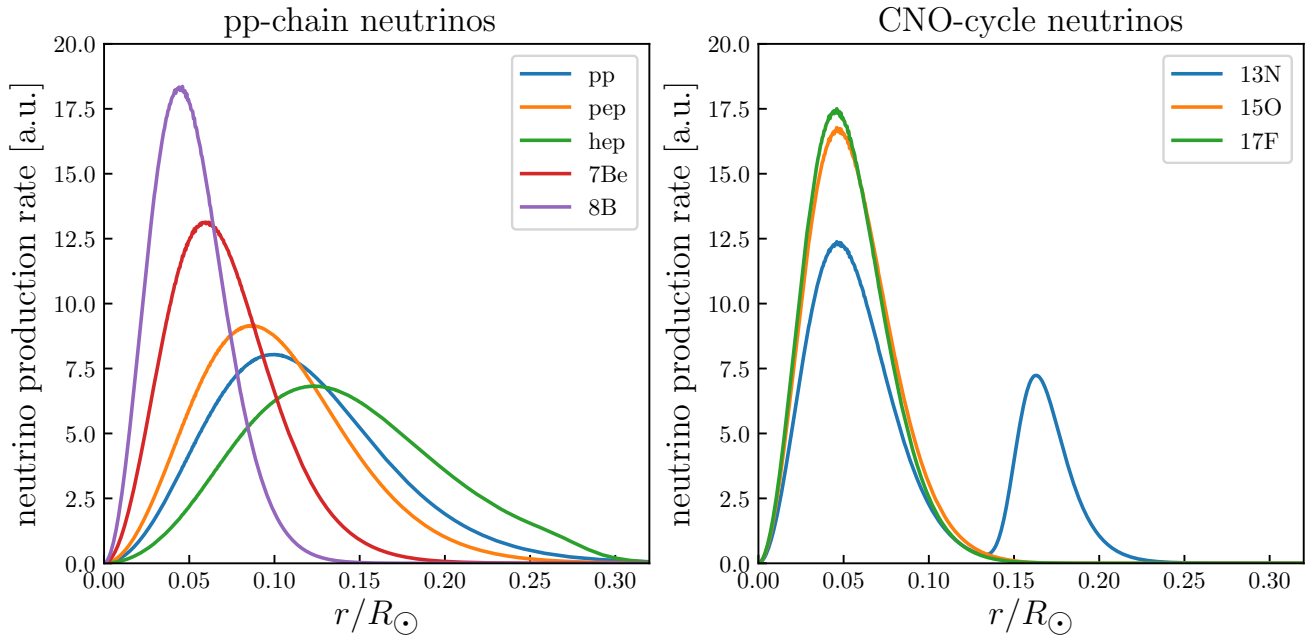


Figure 2.5: Neutrino production rates (in arbitrary unit [a.u.]) varying with the distance to the center,  $r$ . Data taken from Ref. [54] (B16-GS98).

For reactions with two particles in the final states (e.g., all the aforementioned electron-capture reactions and  $p + e^- + p \rightarrow {}^2\text{H} + \nu_e$ ), the energy spectra of  $\nu_e$  are monochromatic. The pep neutrinos have an energy of 1.442 MeV, while the  ${}^7\text{Be}$  neutrino spectrum consists of two lines: 0.861 MeV (90%) when  ${}^7\text{Li}$  is in the ground state and 0.383 MeV (10%) when  ${}^7\text{Li}$  is excited. The monochromatic energy spectra of  $e^{13}\text{N}$ ,  $e^{15}\text{O}$ , and  $e^{17}\text{F}$  have neutrino energies at 2.220, 2.754, and 2.761 MeV [61]. The widths of these monochromatic lines are around the keV scale, caused by the thermal motion of initial state particles.

For a reaction with three or more particles in the final states (e.g.,  $p + p \rightarrow {}^2\text{H} + e^+ + \nu_e$ ), the energy spectrum is continuous, with the endpoint ( $E_\nu^{\text{max}}$ ) determined by the difference between the initial and final total masses. The shape of this continuous spectrum is approximately given by [67]

$$\frac{d\Phi}{dE_\nu} \propto E_e p_e E_\nu^2 \times F_{\text{Fermi}}(Z, p_e), \quad (2.2)$$

where  $E_e$  and  $E_\nu$  are the energies of  $e^+$  and  $\nu_e$  in the final states ( $E_e = E_\nu^{\text{max}} + m_e - E_\nu$ );  $p_e = \sqrt{E_e^2 - m_e^2}$  is the momentum of  $e^+$ ;  $Z$  denotes the nucleus charge; and  $F_{\text{Fermi}}(Z, p_e)$  is the Fermi function which takes into account the influence of the Coulomb potential on the outgoing  $e^+$ . When the neutrino energy is not close to the endpoint (so that the positron keeps energetic,  $E_e \gg m_e$ ), one can ignore the Fermi function and take  $F_{\text{Fermi}}(Z, p_e) \approx 1$ . Therefore for a continuous spectrum with  $E_\nu^{\text{max}} \gg m_e$  (such as  ${}^8\text{B}$  neutrinos), the spectral shape is approximately given by  $E_e^2 E_\nu^2 \approx (E_\nu^{\text{max}} - E_\nu)^2 E_\nu^2$ . For more accurate results, we refer to Tabs. 6.2-6.4 in Ref. [1].

The spectrum with the highest endpoint is the hep neutrino spectrum, ending at 18.77 MeV. Next to it,  ${}^8\text{B}$  neutrinos have a less energetic spectrum, for which we refer to Ref. [68] for an up-to-date study of the spectrum and uncertainties. It should be noted that the usual endpoint, 15.04 MeV, is for  ${}^8\text{B}$  decaying to an excited state of  ${}^8\text{Be}$  ( $2^+$ ) which is an allowed transition. Due to the very short lifetime of this state, the forbidden decay of  ${}^8\text{B}$  to the ground state of  ${}^8\text{Be}$  can happen, though at a suppressed branching ratio [68, 69]. It would extend the  ${}^8\text{B}$  spectrum to higher energies (16.95 MeV) and might be a background for future measurements of hep neutrinos [70].

Although 18.77 MeV is the highest energy of solar neutrinos generated via nuclear fusion, the Sun can emit neutrinos of much higher energies produced via cosmic rays scattering off the solar atmosphere, known as *solar atmospheric neutrinos* [71, 72, 73, 74, 75, 76, 77]. The energy spectrum of solar atmospheric neutrinos roughly follows the power law  $d\Phi/dE_\nu \propto E_\nu^{-3}$  within  $10 < E_\nu/\text{GeV} < 10^5$  [75]. At  $E_\nu = 300$  GeV, the magnitude of the solar atmospheric neutrino flux is around  $d\Phi/dE_\nu \sim 3 \times 10^{-13} \text{cm}^{-2} \text{s}^{-1} \text{GeV}^{-1}$  [76]. Despite the low flux, solar atmospheric neutrinos would be an irreducible background for future searches for DM annihilation in the Sun.

Solar neutrinos are produced mainly within the solar core, with a radius of  $0.2 \sim 0.25 R_\odot$ . The production rates are sensitive to the temperature and density, which decrease rapidly with the distance to the center,  $r$ . In addition, the chemical composition, which also varies with  $r$ , has a significant influence. Figure 2.5 shows the distributions of the neutrino production rates, taking the B16-GS98 model from Ref. [54]. The double-peak structure of the  ${}^{13}\text{N}$  curve is because the reaction  ${}^{14}\text{N} + p \rightarrow {}^{15}\text{O} + \gamma$  is not effective in the region  $0.13 < r/R_\odot < 0.25$ . It breaks the equilibrium of the CN cycle in the region, causing an out-of-equilibrium production rate of  ${}^{13}\text{N}$  neutrinos—see, e.g. [78].

The production rate distributions in Fig. 2.5 are used in the state-of-the-art calculation of solar neutrino oscillation, in which one needs to integrate the oscillation probability weighted by the varying production rates.

### 2.1.3. Open issues in solar models

Heavy elements, or metals<sup>6</sup>, in the Sun can affect the radiative opacity and/or participate in nuclear reactions (e.g., C, N, O). Consequently, the temperature profile and neutrino fluxes are affected by them. The effects of heavy elements depend on not only the total abundance of metals (metallicity) but also the detailed chemical compositions and distributions.

Currently, there are two competing classes of solar models with prominent differences in metallicity. Models based on the chemical compositions obtained by Grevesse & Sauval in 1998 (GS98) [64] have comparatively high metallicity (often referred to as high- $Z$  models). Models based on the chemical compositions obtained by [65] (AGS05) or [66] (AGSS09) are referred to as low- $Z$  models, which incorporate new developments in simulations (e.g., changing from 1D to 3D, using non-local thermodynamic equilibrium, etc.) but are unfortunately in tension with helioseismological measurements. The sound speed at  $0.3 \lesssim r/R_{\odot} \lesssim 0.7$  computed in low- $Z$  models is significantly higher than the helioseismic constraints—see, e.g. [54]. This is known as the “solar metallicity problem.”

High- $Z$  models predict higher  ${}^8\text{B}$ ,  ${}^{13}\text{N}$ ,  ${}^{15}\text{O}$ , and  ${}^{17}\text{F}$  neutrino fluxes than low- $Z$  models, as shown in Tab. 2.1. For  ${}^{13}\text{N}$ ,  ${}^{15}\text{O}$ , and  ${}^{17}\text{F}$  neutrinos, they can be understood from that higher abundances of elements in the CNO cycles should lead to higher production rates of CNO neutrinos. Besides, higher metallicity causes higher radiative opacity, increasing the temperature gradient and the interior temperature. This effect also increases the nuclear reaction rates and the neutrino fluxes. For  ${}^8\text{B}$  neutrinos, the higher flux of high- $Z$  models is mainly affected by the higher opacity.

Precision measurements of solar neutrino fluxes will play an important role in solving the solar metallicity problem. However, the problem is much more complex than just metallicity, as it involves complicated correlations among many different ingredients in constructing solar models. Recently the authors of Ref. [79] presented a new analysis of the solar chemical composition and obtained higher metallicity, which could reduce the tension with helioseismic constraints. But this work was later questioned by Ref. [80], in which the authors showed that additional tensions would arise in such models.

## 2.2. Solar neutrino propagation in matter and vacuum

Being produced at the core of the Sun, solar neutrinos first propagate through the solar medium to the surface and then fly in vacuum to the Earth. The matter effect in the Sun is crucial to high-energy (above a few MeV) neutrinos. If arriving at night, solar neutrinos also pass through the Earth, causing a modulation signal (often known as the day-night asymmetry) due to the matter effect in the Earth.

### 2.2.1. The MSW-LMA solution

The evolution of neutrino flavors during the propagation in matter is governed by the following Schrödinger equation:

$$i \frac{d}{dL} \nu = H \nu, \quad (2.3)$$

---

<sup>6</sup>In astronomy, elements heavier than hydrogen and helium are viewed as “metals”, and metallicity refers to the abundance of these elements.

with

$$H = \frac{1}{2E_\nu} U_{\text{PMNS}} \begin{pmatrix} m_1^2 & & \\ & m_2^2 & \\ & & m_3^2 \end{pmatrix} U_{\text{PMNS}}^\dagger + \begin{pmatrix} V_e & & \\ & 0 & \\ & & 0 \end{pmatrix}, \quad (2.4)$$

$$\nu = \begin{pmatrix} \nu_e \\ \nu_\mu \\ \nu_\tau \end{pmatrix} = U_{\text{PMNS}} \begin{pmatrix} \nu_1 \\ \nu_2 \\ \nu_3 \end{pmatrix}. \quad (2.5)$$

Here  $L$  denotes the propagation distance,  $U_{\text{PMNS}}$  is the PMNS mixing matrix,  $V_e \equiv \sqrt{2}G_F n_e$  is the MSW effective potential induced by coherent forward scattering of neutrinos with electrons in matter, and  $n_e$  is the electron number density, which is  $L$  dependent. Throughout, we adopt the standard parametrization of the PMNS matrix [81],

$$U_{\text{PMNS}} = \begin{pmatrix} c_{12}c_{13} & s_{12}c_{13} & s_{13}e^{-i\delta_{\text{CP}}} \\ -s_{12}c_{23} - c_{12}s_{13}s_{23}e^{i\delta_{\text{CP}}} & c_{12}c_{23} - s_{12}s_{13}s_{23}e^{i\delta_{\text{CP}}} & c_{13}s_{23} \\ s_{12}s_{23} - c_{12}s_{13}c_{23}e^{i\delta_{\text{CP}}} & -c_{12}s_{23} - s_{12}s_{13}c_{23}e^{i\delta_{\text{CP}}} & c_{13}c_{23} \end{pmatrix}, \quad (2.6)$$

which is parametrized by three mixing angles ( $\theta_{12}$ ,  $\theta_{13}$ ,  $\theta_{23}$ ) with the abbreviation  $(c_{ij}, s_{ij}) \equiv (\cos \theta_{ij}, \sin \theta_{ij})$  and one Dirac CP phase ( $\delta_{\text{CP}}$ ). Among the four parameters,  $\delta_{\text{CP}}$  and  $\theta_{23}$  are irrelevant to the standard solar neutrino oscillation as long as  $\nu_\mu$  and  $\nu_\tau$  are indistinguishable at detection. Neutrino oscillations also involve two mass squared differences defined as  $\Delta m_{21}^2 \equiv m_2^2 - m_1^2$  and  $\Delta m_{31}^2 \equiv m_3^2 - m_1^2$ . The values of relevant oscillation parameters ( $\theta_{12}$ ,  $\theta_{13}$ ,  $\Delta m_{21}^2$ ,  $\Delta m_{31}^2$ ) and the status of their measurements will be reviewed in Sec. 2.2.2.

It is sometimes useful to define the effective mixing matrix  $U^m$  in matter by the following re-diagonalization of  $H$ :

$$H = \frac{1}{2E_\nu} U^m \text{diag}(\tilde{m}_1^2, \tilde{m}_2^2, \tilde{m}_3^2) U^{m\dagger}, \quad (2.7)$$

where  $\tilde{m}_{1,2,3}$  are effective neutrino masses in matter.

The survival probability of solar electron neutrinos can be obtained by solving the Schrödinger equation in (2.3), either numerically<sup>7</sup> or analytically. The latter employs the adiabatic approximation (to be explained in Sec. 2.2.3) and leads to the following result [52]:

$$P_{ee} = (c_{13}c_{13}^m)^2 \left( \frac{1}{2} + \frac{1}{2} \cos 2\theta_{12}^m \cos 2\theta_{12} \right) + (s_{13}s_{13}^m)^2, \quad (2.8)$$

with

$$\cos 2\theta_{12}^m \approx \frac{\cos 2\theta_{12} - \beta_{12}}{\sqrt{(\cos 2\theta_{12} - \beta_{12})^2 + \sin^2 2\theta_{12}}}, \quad (2.9)$$

$$(s_{13}^m)^2 \approx s_{13}^2 (1 + 2\beta_{13}), \quad (2.10)$$

$$\beta_{12} \equiv \frac{2c_{13}^2 V_e^0 E_\nu}{\Delta m_{21}^2}, \quad (2.11)$$

$$\beta_{13} \equiv \frac{2V_e^0 E_\nu}{\Delta m_{31}^2}. \quad (2.12)$$

---

<sup>7</sup>Numerical solutions obtained by straightforwardly solving the differential equation are highly oscillatory due to the long propagation distance ( $L\Delta m_{31}^2/E_\nu, L\Delta m_{21}^2/E_\nu \gg 1$ ). The oscillatory part can be averaged out by integrating over  $E_\nu$  within the finite energy resolution of a detector, or over  $L$  since solar neutrinos are not produced at a point-like source—see Fig. 2.5.

Here  $V_e^0$  denotes the value of  $V_e$  at the core where  $\nu_e$  is produced and the superscript “ $m$ ” denotes quantities modified by the matter effect.

The above survival probability is often referred to as the MSW-LMA (where LMA stands for Large-Mixing-Angle) solution in the literature. There are two noteworthy limits which we would like to discuss briefly.

- Low- $E_\nu$  limit (vacuum limit):

When  $E_\nu$  is sufficiently small, the matter effect is negligible ( $\beta_{12}, \beta_{13} \approx 0$ ), and Eq. (2.8) simply reduces to

$$P_{ee} \approx 1 - \frac{1}{2} \sin^2(2\theta_{12}) = c_{12}^4 + s_{12}^4, \quad (2.13)$$

where we have neglected the effect of  $\theta_{13}$ . The result is easy to understand: when  $\nu_e$  is produced, it consists of  $c_{12}\nu_1 + s_{12}\nu_2$  (assuming  $\theta_{13} = 0$ ). Each mass eigenstate propagates to the Earth independently. Due to the long distance, they lose coherence. At production, the probability of  $\nu_e$  being  $\nu_1$  ( $\nu_2$ ) is  $c_{12}^2$  ( $s_{12}^2$ ); at detection, the probability of  $\nu_1$  ( $\nu_2$ ) being detected as  $\nu_e$  is also  $c_{12}^2$  ( $s_{12}^2$ ). Hence the survival probability of  $\nu_e$  at detection is given by  $(c_{12}^2)^2 + (s_{12}^2)^2$ .

- High- $E_\nu$  limit:

When  $E_\nu$  is large so that  $\beta_{12} \gg 1$  while  $\beta_{13}$  remains small ( $\beta_{13} \ll 1$ ), Eq. (2.8) in the limit of  $\theta_{13} = 0$  reduces

$$P_{ee} \approx s_{12}^2. \quad (2.14)$$

Nonzero  $\theta_{13}$  can lead to a correction of  $\sim 5\%$  to the result. Eq. (2.14) can be seen from the adiabatic approximation. When  $\nu_e$  is produced at the center with a high electron number density, it is almost pure  $\nu_2^m$  due to the strong matter effect ( $\theta_{12}^m \approx 90^\circ$ ). As the density slowly decreases to zero, the evolution of all mass eigenstates is adiabatic, which means  $\nu_2^m$  will eventually come out of the Sun as  $\nu_2$ . Since the probability of  $\nu_2$  being detected as  $\nu_e$  is  $s_{12}^2$ , the survival probability in the high- $E_\nu$  limit is simply  $s_{12}^2$ .

Figure 2.6 shows how the survival probability varies as a function of  $E_\nu$  from the low- $E_\nu$  limit (which corresponds to  $P_{ee} \approx c_{12}^4 + s_{12}^4 \approx 0.55$ ) to the high- $E_\nu$  one ( $P_{ee} \approx s_{12}^2 \approx 0.3$ ). The probability becomes significantly energy-dependent in the range  $2 \text{ MeV} \lesssim E_\nu \lesssim 6 \text{ MeV}$ . This part, often called the *up-turn*, has not been well measured by current data but it is of crucial importance to the solar determination of  $\Delta m_{21}^2$  as well as to searches of new physics effects.

Note that the curves in Fig. 2.6 are only for illustration without including a number of subleading-order corrections, which should be taken into account in real analyses. For instance, the radical spread of neutrino production rates in Fig. 2.5 is not included (i.e. we simply assume all neutrinos are produced at  $r = 0$ ). When this is included, one should have different  $P_{ee}$  curves for different flux components (pp,  $^8\text{B}$ , CNO, etc.). When solar neutrinos propagate through the Earth, the Earth matter effect can slightly enhance  $P_{ee}$  at high  $E_\nu$ , causing a day-night difference in the observed event rates. This will be discussed in further detail in Sec. 2.2.4. The  $P_{ee}$  curves are computed assuming that the evolution is purely adiabatic while non-adiabatic corrections do exist, though they are negligibly small in the standard framework of oscillations—see Sec. 2.2.3. Finally, uncertainties of oscillation parameters also lead to variations of the  $P_{ee}$  curve. Therefore it is often shown in the literature as bands with finite widths.

### 2.2.2. Measurements of solar neutrino parameters

According to Eq. (2.8), the survival probability of  $\nu_e$  is mainly sensitive to  $\theta_{12}$  and  $\Delta m_{21}^2$ , and also weakly depends on  $\theta_{13}$  and  $\Delta m_{31}^2$ . The former can be measured not only by solar neutrino observations but also by long-baseline reactor

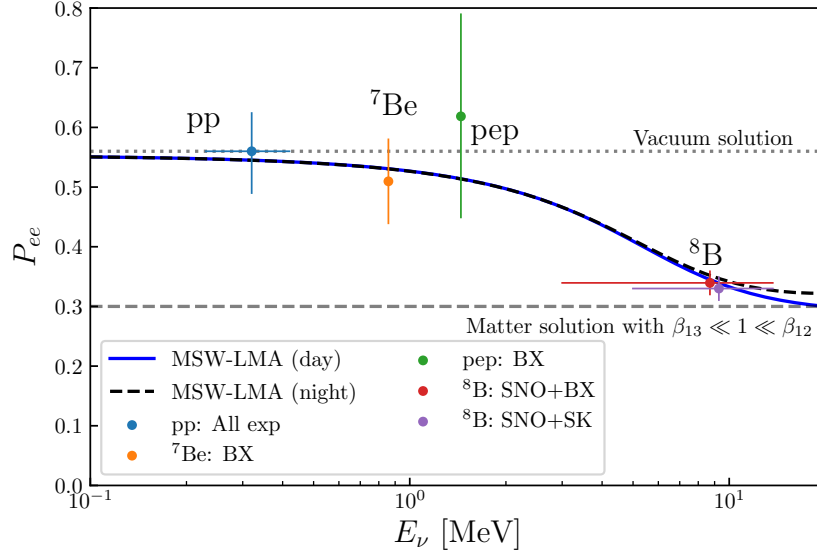


Figure 2.6: The survival probability of solar electron neutrinos  $P_{ee}$ . The MSW-LMA (day) curves is obtained using Eq. (2.8) with  $\theta_{12} = 33.4^\circ$ ,  $\theta_{13} = 8.5^\circ$ ,  $\Delta m_{12}^2 = 7.5 \times 10^{-5} \text{eV}^2$ ,  $\Delta m_{13}^2 = 2.4 \times 10^{-3} \text{eV}^2$ . The difference between the day and night curves is computed using Eq. (2.21) with the average Earth matter density,  $5.5 \text{ g/cm}^3$ . The data points are taken from Refs. [45, 47, 46]. Note that the curve and the data points are only for illustration, neglecting some subleading order effects which are discussed in the text.

neutrino experiments (KamLAND, JUNO). The latter, thanks to the high-statistics measurements of reactor neutrino experiments (Daya-Bay, RENO, Double-Chooz, etc.) in recent years, have been determined with excellent precision. The latest  $3\nu$  oscillation fit to the global data as of November 2022 (NuFit 5.2 [82, 84]) reported the following results:

$$\sin^2 \theta_{12} = 0.303_{-0.012}^{+0.012}, \quad \Delta m_{21}^2 / 10^{-5} \text{eV}^2 = 7.41_{-0.20}^{+0.21}, \quad (2.15)$$

$$\sin^2 \theta_{13} / 10^{-2} = 2.225_{-0.059}^{+0.056} (2.223_{-0.058}^{+0.058}), \quad \Delta m_{31}^2 / 10^{-3} \text{eV}^2 = +2.507_{-0.027}^{+0.026} (-2.486_{-0.028}^{+0.025}), \quad (2.16)$$

where the values in parentheses are for the inverted mass ordering if they depend on the mass ordering.

Here we would like to comment on the complementarity between solar and reactor (both long- and short-baseline) neutrino data in determining the above parameters. As a long-baseline reactor neutrino experiment, KamLAND can measure  $\Delta m_{21}^2$  with good precision because the disappearance probability ( $1 - P_{ee}$ ) is approximately proportional to  $\sin^2(\Delta m_{21}^2 L / 4E_\nu)$ . At KamLAND, the first two peaks of the probability as a function of  $L/E_\nu$  can be clearly seen [85]. By contrast, solar neutrino observations are less constraining on  $\Delta m_{21}^2$  because  $\Delta m_{21}^2$  mainly governs the *up-turn*, which as a transition from the high- to low- $E_\nu$  limits is not well measured. The well-measured values of  $P_{ee}$  in the two limits, however, are almost independent of  $\Delta m_{21}^2$  but can be used to constrain  $\theta_{12}$  very effectively. At high energies ( $10 \sim 20$  MeV), the day-night asymmetry (see Sec. 2.2.4) could be used to determine  $\Delta m_{21}^2$ , but this requires high-precision measurements of the  $^8\text{B}$  spectrum. Compared to long-baseline reactor experiments, it is more challenging to measure  $\Delta m_{21}^2$  via solar neutrinos. Consequently, the solar and KamLAND measurements are complementary to each other: one measures  $\Delta m_{21}^2$  better and the other is more constraining on  $\theta_{12}$ . The 1-3 mixing parameters,  $\theta_{13}$  and  $\Delta m_{31}^2$ , could have potentially important influence on the determination of  $\theta_{12}$  and  $\Delta m_{21}^2$ , as implied by Eq. (2.8). Since they have been measured with high precision by short-baseline reactor neutrino experiments, their uncertainties are unlikely to affect future measurements of solar neutrino parameters.

It is worth mentioning that there was a long-standing tension between solar and KamLAND measurements of  $\Delta m_{21}^2$ . More specifically, the latest result of the KamLAND experiment reported in 2013 is  $\Delta m_{21}^2 = 7.53_{-0.18}^{+0.18} \times 10^{-5} \text{ eV}^2$  [85]

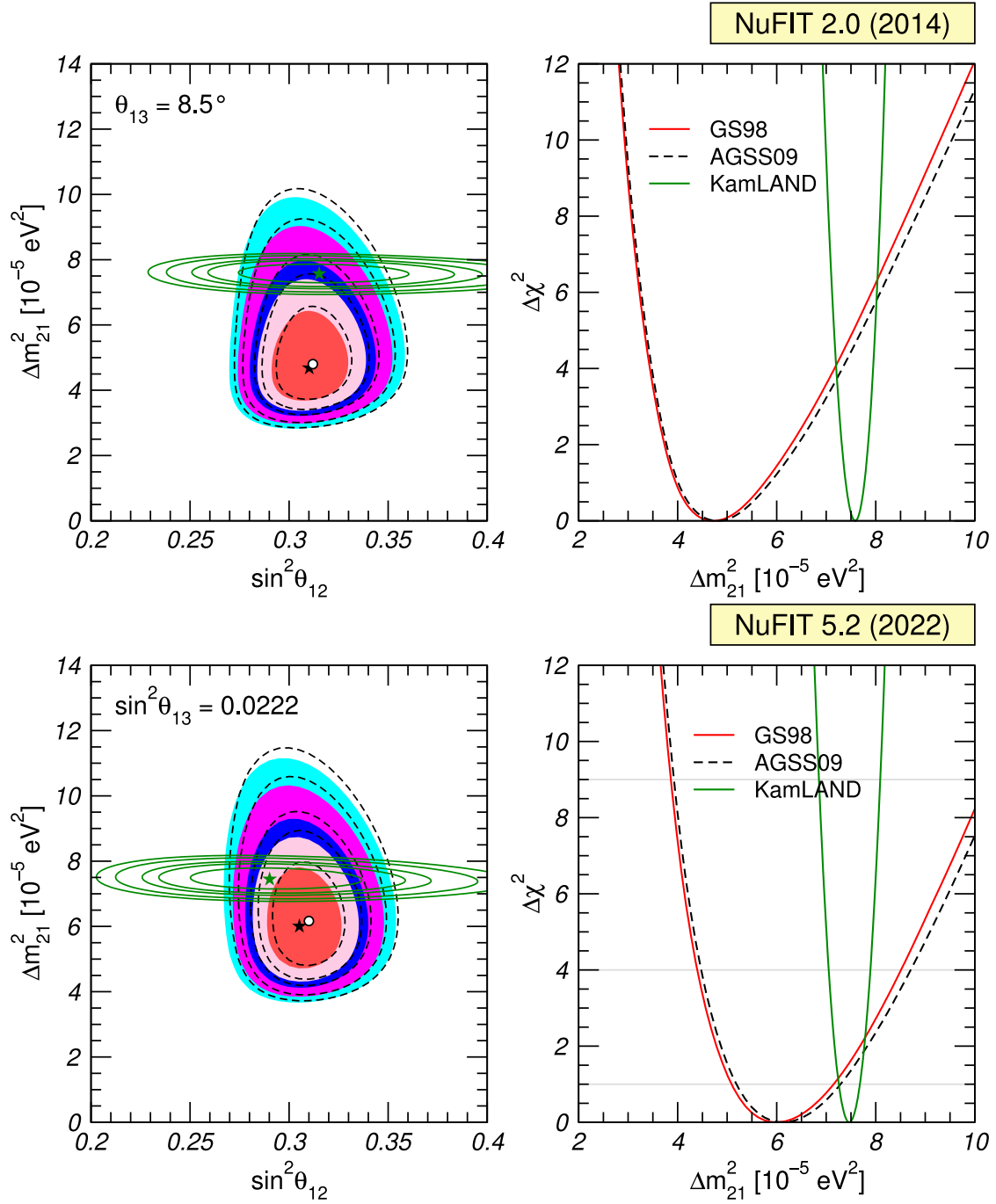


Figure 2.7: Past and present measurements of  $\Delta m_{21}^2$  and  $\theta_{12}$ . The upper panels show a  $\sim 2\sigma$  tension between the KamLAND measurement and solar neutrino data in 2014. The lower panels show that this tension has reduced to  $\sim 1\sigma$  as of 2022. Figure taken from Refs. [82, 83, 84].

while the Super-Kamiokande measurement, combining SK-I, II, III, and IV data until February 2014, gave  $\Delta m_{21}^2 = 4.8_{-0.8}^{+1.5} \times 10^{-5} \text{ eV}^2$  [86], which is  $\sim 2\sigma$  lower than the KamLAND value. Figure 2.7 shows the past and present status of this tension. From the upper right panel, one can see that the solid red curve (obtained using the GS98 solar model) crosses the green curve at  $\Delta\chi^2 \approx 4$  (corresponding to  $2\sigma$ ). Changing to a different solar model (AGSS09, dashed curves) cannot effectively alleviate the tension. However, with the very recent update of the Super-Kamiokande solar neutrino results reported in 2022 [87], the solar best-fit value of  $\Delta m_{21}^2$  shifted to  $6 \times 10^{-5} \text{ eV}^2$  and reduced the tension to  $\sim 1\sigma$ , as shown in the lower panels of Fig. 2.7. Hence the tension has eased significantly.

### 2.2.3. The adiabatic approximation

The adiabatic approximation assumes that the matter density varies sufficiently slow so that if a neutrino is in an effective mass eigenstate (say,  $\nu_i^m$ , which is  $n_e$  dependent) in the matter, then in the course of propagation it will remain  $\nu_i^m$  and will not go into another matter eigenstate. The only change is limited within the flavor composition of  $\nu_i^m$ , caused by the variation of  $n_e$ . For example, a neutrino produced in the above high- $E_\nu$  limit is almost  $\nu_2^m$ , which after propagating through the solar medium to vacuum, becomes  $\nu_2$ . Under the adiabatic approximation, the survival probability can be computed by

$$P_{ee} = \sum_i |U_{ei}^m|^2 |U_{ei}|^2, \quad (2.17)$$

where  $U^m$  is introduced in Eq. (2.7).

The validity of the adiabatic approximation and potential corrections have been addressed in Refs. [88, 89, 90, 91]. The condition of the adiabatic approximation can be formulated as [91]

$$\gamma \equiv \frac{4\Delta m_{21}^2 E_\nu^2 \sin 2\theta_{12}}{\left(\Delta m_{21}^4 \sin^2 2\theta_{12} + (\Delta m_{21}^2 \cos 2\theta_{12} - 2E_\nu V_e)^2\right)^{3/2}} \frac{dV_e}{dr} \ll 1. \quad (2.18)$$

For the standard MSW-LMA solution of solar neutrinos, Eq. (2.18) is very well satisfied. One can take the solar density profile in Fig. 2.1 and evaluate the  $\gamma$  parameter in Eq. (2.18). The result depends on both  $r$  and  $E_\nu$ . For  $E_\nu = 10 \text{ MeV}$ , we find that  $\gamma$  peaks at  $r \simeq 0.05R_\odot$  and the maximal value is  $\gamma \simeq 8 \times 10^{-4}$ . The non-adiabatic correction to  $P_{ee}$  is roughly given by

$$\delta P \sim \frac{\gamma^2}{4} \lesssim 10^{-7}. \quad (2.19)$$

Note that for large  $E_\nu$ , the solar resonance (corresponding to  $\Delta m_{21}^2 \cos 2\theta_{12} = 2E_\nu V_e$ ) can always be reached at certain  $r$ . At the solar resonance,  $\gamma$  in Eq. (2.18) can be simplified to

$$\gamma_{\text{resonance}} = \frac{4E_\nu^2}{\Delta m_{21}^4 \sin^2 2\theta_{12}} \frac{dV_e}{dr}, \quad (2.20)$$

which implies that the neutrino energy  $E_\nu$  would have to be very high to cause significant non-adiabatic effects. For the standard solar profile and oscillation parameters,  $\gamma \sim 0.1$  would require  $E_\nu \gtrsim 1 \text{ GeV}$ . Alternatively, if hypothetical neutrino states with much smaller mass squared differences or mixing angles exist (e.g. sterile neutrinos), then Eq. (2.20) could also reach  $\mathcal{O}(1)$  and therefore break the validity of the adiabatic approximation. If the adiabatic approximation fails, one can numerically solve Eq. (2.3) to obtain the solution.

### 2.2.4. The Earth matter effect

Due to the matter effect of the Earth, the survival probability of solar neutrinos arriving at nighttime is slightly different from that at daytime, causing the so-called day-night asymmetry. According to the calculations in Refs. [92, 93], the



difference of  $P_{ee}$  after averaging out oscillating parts can be approximately estimated as follows:

$$\Delta P \equiv P_{ee}^{(\text{day})} - P_{ee}^{(\text{night})} \approx \frac{1}{2} c_{13}^6 \frac{\cos 2\theta_{12}^m \sin^2 2\theta_{12} K V_{\oplus}}{K^2 - 2c_{13}^2 \cos 2\theta_{12} V_{\oplus} K + V_{\oplus}^2}, \quad (2.21)$$

where  $\cos 2\theta_{12}^m$  is given by Eq. (2.9),  $K = \Delta m_{21}^2 / (2E_{\nu})$ , and  $V_{\oplus}$  denotes the average value of  $V_e$  in the Earth. In Fig. 2.6, we plot the MSW-LMA night curve using Eq. (2.21) and Eq. (2.8). Note that in the low- $E_{\nu}$  limit,  $\Delta P$  in Eq. (2.21) is positive because  $\cos 2\theta_{12}^m \approx \cos 2\theta_{12}$  is positive and the denominator is always positive. It turns negative when  $E_{\nu}$  passes the solar resonance (around  $2 \sim 3$  MeV) above which  $\cos 2\theta_{12}^m$  becomes negative [see Eq. (2.9)]. Above the solar resonance,  $|\Delta P|$  increases as  $E_{\nu}$  increases, causing the  $P_{ee}$  curve to split into two different (day and night) curves as shown in Fig. 2.6.

In practical observation, the day-night asymmetry is usually measured by  $A_{DN} \equiv 2(R_D - R_N)/(R_D + R_N)$ , where  $R_D/R_N$  denotes the average day/night event rate. For the best-fit values in Eq. (2.15), the expected value of  $A_{DN}$  is  $-1.7\%$  at Super Kamiokande [86] (the day-night asymmetry also depends on the latitude of the observation site). In 2013, Super-Kamiokande first reported an indication of day-night asymmetry at  $2.7 \sigma$  significance. The asymmetry parameter  $A_{DN}$  is measured to be  $A_{DN} = (-3.2 \pm 1.1_{\text{stat.}} \pm 0.5_{\text{syst.}})\%$  [94]. As of 2022, the significance of day-night asymmetry at Super-Kamiokande reached  $3.1 \sigma$  with  $A_{DN} = (-2.8 \pm 0.9)\%$  [87]. So far, acquiring sufficient statistics is still the main challenge in measuring the day-night asymmetry.

If measured in the future with high statistics, the day-night asymmetry would be a direct probe of the earth matter effect. In addition, we note that there are already some discussions on the oscillation tomography of the Earth with solar neutrinos and future experiments [95, 96, 97]. Solar neutrino detectors near the equator would be more suitable in this aspect as solar neutrinos could pass the innermost part of the Earth before arriving at the detectors.

## 2.3. Search for new physics with solar neutrinos

Before the MSW-LMA became the standard solution to the solar neutrino problem, various new physics interpretations of solar neutrino data were proposed. To date, even though the standard solution has been well tested, many new physics scenarios remain indistinguishable. Since neutrinos are regarded as the portal to new physics beyond the SM, and a few experimental anomalies are still inconsistent with our current understanding of neutrinos, the search for new physics is of great importance in the era of precision measurement of solar neutrinos. Below we review a few popular new physics scenarios often considered in the literature.

### 2.3.1. Non-Standard Interactions (NSI)

A variety of neutrino mass models predict new interactions of neutrinos. As an effective field theory (EFT) approach, the so-called Non-Standard interactions (NSI), which Wolfenstein first considered in his seminal paper on the matter effect [19], have attracted increasing interest in recent years—see [98, 99, 100, 101, 102] for NSI reviews.

There are two types of NSI often considered in the literature, namely the NC-like and the CC-like NSI, formulated as

$$\mathcal{L}_{\text{NC}} = -2\sqrt{2}G_F [\bar{\nu}_{\alpha}\gamma^{\mu}P_L\nu_{\beta}] \left[ \bar{f}\gamma_{\mu} \left( \varepsilon_{\alpha,\beta}^{f,L}P_L + \varepsilon_{\alpha,\beta}^{f,R}P_R \right) f \right], \quad (2.22)$$

$$\mathcal{L}_{\text{CC}} = -2\sqrt{2}G_F [\bar{\nu}_{\alpha}\gamma^{\mu}P_L\ell_{\beta}] \left[ \bar{f}\gamma_{\mu} \left( \varepsilon_{\alpha,\beta}^{ff',L}P_L + \varepsilon_{\alpha,\beta}^{ff',R}P_R \right) f' \right], \quad (2.23)$$

where  $G_F$  is Fermi's constant,  $\alpha$  and  $\beta$  denote lepton flavors, and the  $\varepsilon$ 's quantify the strengths of neutrino interactions with matter fermions  $f$  and  $f'$ . For NC-like NSI,  $f$  can vary in  $\{e, u, d\}$  while for CC-like NSI,  $f$  and  $f'$  vary in  $\{u, d\}$

with  $f \neq f'$ . The matter effect of neutrino oscillation is only affected by the NC-like NSI. CC-like NSI could modify neutrino production and detection but they have been stringently constrained by meson decay data.

NSI can be generated in many extensions of the SM. One of the most classic example is the type-II seesaw model [103, 104, 105, 106] which introduces a Higgs triplet interacting with charged leptons and neutrinos. After integrating out the Higgs triplet and performing the Fierz transformation, it naturally gives rise to NSI in the lepton sector [107], though the strengths are found to lie below current detectability [108]. Alternatively, NSI could also be generated in  $Z'$  models [109], radiative neutrino mass models [110], or from the loop effects [111, 112].

There are two effects of NSI on solar neutrinos: they could modify (i) propagation of neutrinos in the solar medium [113, 114, 115, 116, 117, 118, 119, 120, 121, 122, 123] and (ii) neutrino scattering at detection [124, 125, 126, 127, 128, 129]. The two aspects are explained below.

### ■ Effect on propagation

In the presence of NSI, when neutrinos propagate in matter, coherent forward scattering of neutrinos with matter particles would be modified, causing an effect on the flavor evolution. As first noticed by Wolfenstein [19], neutrino oscillation could occur in matter even for massless neutrinos, provided that the neutral current had flavor off-diagonal interactions. The effect of NSI on neutrino flavor evolution can be accounted for by replacing the Hamiltonian in Eq. (2.4) with

$$H = \frac{1}{2E_\nu} U_{\text{PMNS}} \begin{pmatrix} m_1^2 & & \\ & m_2^2 & \\ & & m_3^2 \end{pmatrix} U_{\text{PMNS}}^\dagger + V_e \begin{pmatrix} 1 + \varepsilon_{ee} & \varepsilon_{e\mu} & \varepsilon_{e\tau} \\ \varepsilon_{e\mu}^* & \varepsilon_{\mu\mu} & \varepsilon_{\mu\tau} \\ \varepsilon_{e\tau}^* & \varepsilon_{\mu\tau}^* & \varepsilon_{\tau\tau} \end{pmatrix}, \quad (2.24)$$

where

$$\varepsilon_{\alpha\beta} \equiv \sum_f \frac{n_f}{n_e} \left( \varepsilon_{\alpha,\beta}^{f,L} + \varepsilon_{\alpha,\beta}^{f,R} \right) \quad (2.25)$$

includes contributions of all fermions in matter. Hence the summation is weighted by  $n_f$  which is the number density of fermion  $f$ .

Again, like the standard case, one can compute the survival probability in this case by numerically solving Eq. (2.3) with the Hamiltonian in Eq. (2.24). Analytically, one can obtain approximate solutions using the adiabatic assumption and neglecting the small correction caused by nonzero  $\theta_{13}$ . The  $\nu_e$  survival probability obtained in this way reads [113]:

$$P_{ee} \approx \frac{1}{2} + \frac{1}{2} \cos 2\theta_\epsilon \cos 2\theta_{12}, \quad (2.26)$$

where

$$\cos 2\theta_\epsilon = \frac{\cos 2\theta_{12} - x_\epsilon \cos 2\alpha}{\sqrt{1 + x_\epsilon^2 - 2x_\epsilon (\cos 2\alpha \cos 2\theta_{12} - \sin 2\alpha \sin 2\theta_{12} \cos 2\phi)}}, \quad (2.27)$$

$$\alpha = \frac{1}{2} \arctan \frac{|\epsilon_2|}{1 + \epsilon_{11}}, \quad \phi = \frac{1}{2} \arg(\epsilon_2), \quad (2.28)$$

$$x_\epsilon \equiv 2V_e^0 E_\nu \frac{\sqrt{(1 + \epsilon_1)^2 + |\epsilon_2|^2}}{\Delta m_{21}^2}. \quad (2.29)$$

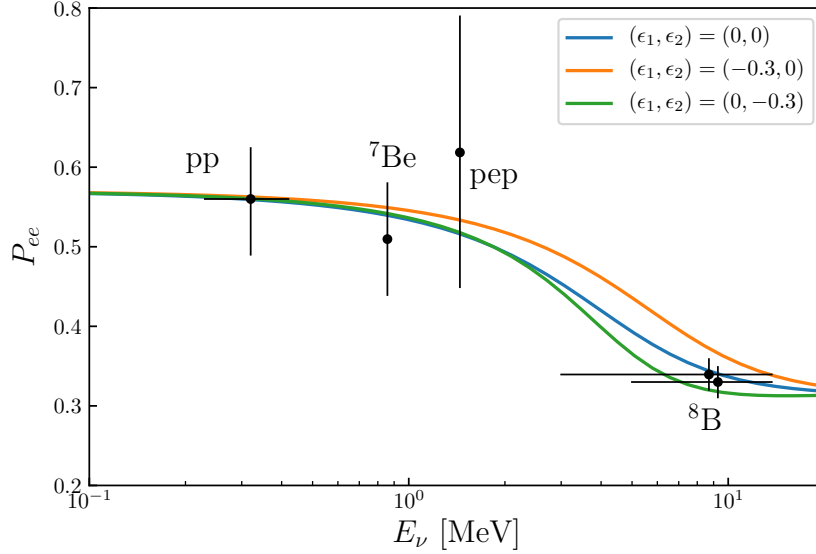


Figure 2.8: The survival probability of solar electron neutrinos  $P_{ee}$  in the presence of NSI, computed according to Eq. (2.26). The experimental measurements (black points/bars) are the same as those in Fig. 2.6. Note that the curve and the data points are only for illustration, neglecting some subleading order effects which are discussed in the text.

The effective NSI parameters  $\epsilon_1$  and  $\epsilon_2$  in the absence of  $\mu$ -flavored NSI are defined as<sup>8</sup>

$$\epsilon_1 \equiv \varepsilon_{ee} - \varepsilon_{\tau\tau} \sin^2 \theta_{23}, \quad \epsilon_2 \equiv -2\varepsilon_{e\tau} \sin \theta_{23}. \quad (2.30)$$

In the presence of NSI of all flavors and nonzero  $\theta_{13}$ ,  $\epsilon_{1,2}$  would be much more complicated combinations of  $\varepsilon_{\alpha\beta}$ . We refer to [119] for the full expressions of  $\epsilon_{1,2}$ . Note that unlike the standard solar neutrino oscillation which is independent of  $\theta_{23}$  and  $\delta_{\text{CP}}$ , the NSI  $P_{ee}$  depends on  $\theta_{23}$  which appears in Eq. (2.30), and also on  $\delta_{\text{CP}}$  which would appear in the full expressions with nonzero  $\theta_{13}$  [119].

Figure 2.8 shows how NSI might change the survival probability  $P_{ee}$ . Here all the curves are produced using Eq. (2.26) assuming the central solar density  $\rho = 10^2 \text{g/cm}^3$ ,  $\Delta m_{21}^2 = 7.5 \times 10^{-5} \text{eV}^2$ , and  $\theta_{12} = 34^\circ$ . As shown in Fig. 2.8, NSI with sizable  $\epsilon_{1,2}$  can distort the standard MSW-LMA solution significantly at intermediate energies of a few MeV (the *up-turn*). It implies that measurements at the *up-turn* would be crucial to probing new physics effects on solar neutrinos. Very recently, the Super-Kamiokande collaboration performed an analysis on the  $^8\text{B}$  solar neutrino data collected with 277 kton-yr exposure and reported that nonzero values of  $\epsilon_1$  and  $\epsilon_2$  are favored at  $1.8\sigma$  (for NSI with the  $u$  quark) or  $1.6\sigma$  (with the  $d$  quark) [123].

Another interesting consequence of introducing NSI is that they can lead to the so-called LMA-Dark (LMA-D) solution [102, 114, 130, 131, 132]. The LMA-D solution arises from a well-known degeneracy: performing the transformation  $\theta_{12} \rightarrow \pi/2 - \theta_{12}$ ,  $\Delta m_{31}^2 \rightarrow -\Delta m_{31}^2$ , and  $\delta_{\text{CP}} \rightarrow \pi/2 - \delta_{\text{CP}}$ , the Hamiltonian  $H$  in vacuum changes to  $-H^*$ , implying that the oscillation probabilities in vacuum are invariant under the above transformation. For instance, Eq. (2.13) is explicitly invariant under the transformation. In matter, the degeneracy is broken by the standard MSW effect, but it can be approximately restored by NSI parameter shifting when the energy dependence of  $P_{ee}$  is weak (e.g.  $10 \text{ MeV} \lesssim E_\nu \lesssim 20 \text{ MeV}$ ).

<sup>8</sup>The effective parameters  $\epsilon_1$  and  $\epsilon_2$  are introduced in many studies on solar neutrinos with NSI (see e.g., [113, 114, 115, 117, 119], though their specific forms may vary) due to the commonly used reduction of the  $3 \times 3$  matrix form of the Hamiltonian to a  $2 \times 2$  form, by performing a rotation between the second and third rows and columns of  $H$ .

Table 2.2: Constraints on NSI parameters from Borexino Phase-II data [35], with 90% C.L. Results taken from Ref. [128].

	$L$	$R$
$\varepsilon_{ee}^{e,L/R}$	$[-0.03, +0.06] \oplus [-1.37, -1.29]$	$[-0.23, +0.07]$
$\varepsilon_{\mu\mu}^{e,L/R}$	$[+0.58, +0.81] \oplus [-0.20, +0.13]$	$[-0.36, +0.37]$
$\varepsilon_{\tau\tau}^{e,L/R}$	$[+0.45, +0.86] \oplus [-0.26, +0.26]$	$[-0.58, +0.47]$
$\varepsilon_{e\mu}^{e,L/R}$	$[-0.17, +0.29]$	$[-0.21, +0.41]$
$\varepsilon_{e\tau}^{e,L/R}$	$[-0.26, +0.23]$	$[-0.35, +0.31]$
$\varepsilon_{\mu\tau}^{e,L/R}$	$[-0.09, +0.14] \oplus [-0.62, -0.52]$	$[-0.26, +0.23]$

Hence the observed  $^8\text{B}$  neutrino flux could be explained either by the standard MSW-LMA solution or the LMA-D solution with large NSI and the above transformation. Currently, the LMA-D solution is disfavored by elastic neutrino scattering data at  $2\sigma$  C.L. [132].

### ■ Effect on detection

Another effect of NSI on solar neutrinos is that they may modify the cross section of neutrino scattering with target particles at detection. Solar neutrinos are either detected via CC processes (e.g.  $\nu_e + {}^{37}\text{Cl} \rightarrow e^- + {}^{37}\text{Ar}$ ) or elastic scattering (e.g.  $\nu_e + e^- \rightarrow \nu_e + e^-$ ) which involves NC and/or CC interactions. Since the target particle has to be a nucleus for the former, only CC-like NSI with quarks could be relevant. However, due to existing strong constraints on CC-like NSI, most studies on the scattering effect are mainly concerned with NC-like NSI, which modifies only elastic scattering cross sections.

For elastic  $\nu_\alpha + e^-$  scattering, the cross section including NSI contributions<sup>9</sup> reads [133]:

$$\frac{d\sigma}{dT} = \frac{m_e G_F^2}{2\pi} \left[ g_1^2 + g_2^2 \left( 1 - \frac{T}{E_\nu} \right)^2 - x_{12} \frac{m_e T}{E_\nu^2} \right], \quad (2.31)$$

where  $T$  is the recoil energy of the electron, and the other parameters are defined as

$$g_1^2 \equiv (g_V + g_A + 2\varepsilon_{\alpha\alpha}^{e,L})^2 + \sum_{\beta \neq \alpha} \left( 2\varepsilon_{\alpha\beta}^{e,L} \right)^2, \quad (2.32)$$

$$g_2^2 \equiv (g_V - g_A + 2\varepsilon_{\alpha\alpha}^{e,R})^2 + \sum_{\beta \neq \alpha} \left( 2\varepsilon_{\alpha\beta}^{e,R} \right)^2, \quad (2.33)$$

$$x_{12} \equiv (g_V + g_A + 2\varepsilon_{\alpha\alpha}^{e,L}) (g_V - g_A + 2\varepsilon_{\alpha\alpha}^{e,R}) + \sum_{\beta \neq \alpha} \left( 2\varepsilon_{\alpha\beta}^{e,L} \right) \left( 2\varepsilon_{\alpha\beta}^{e,R} \right), \quad (2.34)$$

with  $g_V = 2 \sin^2 \theta_W - 1/2 + \delta_{\alpha e}$ , and  $g_A = -1/2 + \delta_{\alpha e}$ . The SM CC contribution to  $\nu_e + e^- \rightarrow \nu_e + e^-$  is included by  $\delta_{\alpha e}$  in  $g_V$  and  $g_A$ .

Note that due to the interference between flavor diagonal NSI and SM interactions, precision measurements of solar neutrinos are more sensitive to  $\varepsilon_{\alpha\alpha}$  than to  $\varepsilon_{\alpha\beta}$  with  $\beta \neq \alpha$ . As can be seen from Eqs. (2.32)-(2.34), when expanding them in terms of  $\varepsilon$ ,  $\varepsilon_{\alpha\alpha}$  and  $\varepsilon_{\alpha\beta}$  ( $\beta \neq \alpha$ ) contribute at  $\mathcal{O}(\varepsilon)$  and  $\mathcal{O}(\varepsilon^2)$  level, respectively.

Measurements of solar neutrinos via elastic  $\nu_\alpha + e^-$  scattering have produced stringent constraints on leptonic NSI [125, 128]. The latest results are summarized in Tab. 2.2, taken from Ref. [128]. NSI with quarks could be constrained by CE $\nu$ NS events, though such events have not yet been detected successfully for solar neutrinos. Future dark matter detectors

<sup>9</sup>Note that flavor-changing NSI also leads to  $\nu_\alpha + e^- \rightarrow \nu_\beta + e^-$  with  $\beta \neq \alpha$ , which is included as non-interference terms in Eqs. (2.32)-(2.34).

(e.g. multi-ton scale liquid Xenon detectors) will be capable of detecting solar neutrinos [124, 129, 134, 135, 136, 137] with significant statistics and hence constrain NSI with quarks.

### 2.3.2. Sterile neutrinos

Sterile neutrinos refer to gauge singlet (i.e. not charged under the SM gauge symmetry) fermions that have mass mixing with the SM left-handed neutrinos, such as right-handed neutrinos in the type I seesaw. As indicated by the name, sterile neutrinos do not participate in NC and CC interactions of the SM due to their singlet nature. In principle the masses of sterile neutrinos may vary rather arbitrarily from the GUT scale to values well below the sub-eV scale (i.e. the case of quasi-Dirac neutrinos [138]). However, in neutrino oscillation phenomenology, we are mainly concerned about light ( $\lesssim \mathcal{O}(1)$  eV) sterile neutrinos, initially motivated by several experimental anomalies, including the LSND and MiniBooNE excesses (see [139] for a review) that cannot be accommodated in the standard three-neutrino paradigm. While the sterile neutrino explanation for these anomalies often leads to some inconsistency when confronted with searches in neutrino experiments [140, 141, 142] and cosmological observations [143, 144], the possible existence of new oscillation modes caused by sterile neutrinos remains far from being excluded.

In the presence of a sterile neutrino  $\nu_s$ , one needs to generalize the  $3 \times 3$  PMNS mixing to

$$(\nu_s, \nu_e, \nu_\mu, \nu_\tau)^T = U (\nu'_s, \nu_1, \nu_2, \nu_3)^T, \quad U = U' U_{\text{PMNS}}^{(4)}, \quad (2.35)$$

where  $\nu'_s$  denotes the mass eigenstate approximately identical to  $\nu_s$ ,  $U_{\text{PMNS}}^{(4)} = \text{diag}(1, U_{\text{PMNS}})$ , and  $U'$  is a unitary matrix that accounts for the small active-sterile mixing. Since  $\nu_s$  does not have NC or CC interactions, the Hamiltonian reads [142]

$$H = \frac{1}{2E_\nu} U \begin{pmatrix} m_s^2 & & & \\ & m_1^2 & & \\ & & m_2^2 & \\ & & & m_3^2 \end{pmatrix} U^\dagger + V_e \begin{pmatrix} \frac{n_n}{2n_e} & & & \\ & 1 & & \\ & & 0 & \\ & & & 0 \end{pmatrix}, \quad (2.36)$$

where  $n_n$  is the neutron number density<sup>10</sup>. While Eq. (2.36) allows one to numerically solve the Schrödinger equation to obtain the oscillation probability, the adiabatic approximation is still valid if the mass splitting  $\Delta m_s^2 \equiv m_s^2 - m_1^2$  is not too small. More specifically, one needs to evaluate the  $\gamma$  parameter in Eq. (2.18) with  $\Delta m_{12}^2 \rightarrow \Delta m_s^2$  to determine whether adiabaticity is violated or not. For  $E_\nu = 10$  MeV,  $\gamma \ll 1$  corresponds to  $\Delta m_s^2 \gg 6 \times 10^{-8} \text{eV}^2$ . For  $\Delta m_s^2$  well above this value, the adiabatic approximation can be used.

The impact of sterile neutrinos on solar neutrino physics has been explored extensively in the literature [138, 145, 146, 147, 148, 149, 150, 151, 152, 153, 154, 155, 156, 157, 158]. It has been shown that sterile neutrinos with a mass squared difference of  $(0.7 - 2) \times 10^{-5} \text{eV}^2$  and a small mixing ( $|U'_{12}|^2 \sim 10^{-4} - 10^{-3}$ ) would modify the up-turn of the MSW-LMA solution and might cause a dip of the survival probability at a few MeV [148, 151]. In Fig. 2.9, we use Eqs. (2.36) and (2.17) to reproduce such an effect of sterile neutrinos, assuming  $U'_{12} = -U'_{21} = 0.05$  and  $\Delta m_s^2 = \pm 2 \times 10^{-5} \text{eV}^2$ . Ref. [138] studied the scenario of sterile neutrinos with Majorana masses well below the sub-eV scale, rendering neutrino quasi-Dirac. Solar neutrino data can impose strong constraints on such a scenario, and it was found that the Majorana

<sup>10</sup>Its presence is due to the fact that the NC contribution to the MSW potential was subtracted for active neutrinos of all flavors in Eq. (2.4). The subtraction should be added back for  $\nu_s$ , which makes no such contribution. Usually only neutrons are considered here because protons have a much smaller effective vector coupling to  $Z$  (suppressed by  $1 - 4 \sin^2 \theta_W$ ).

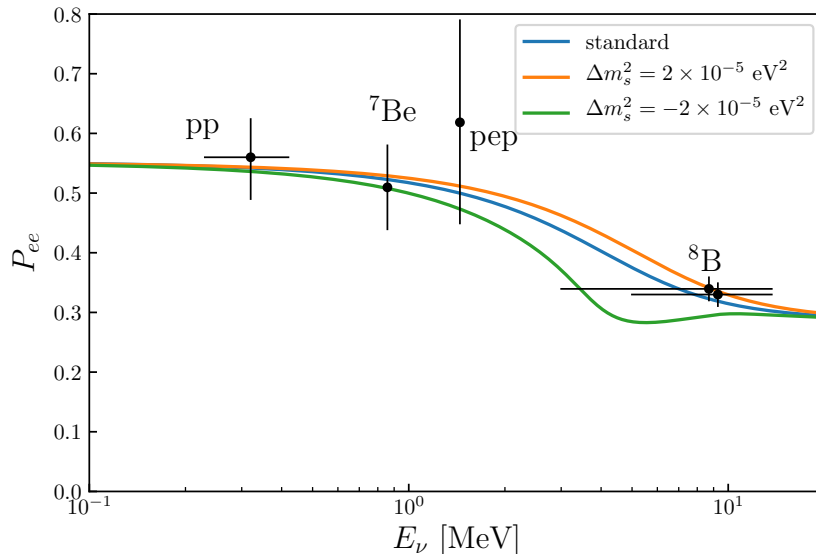


Figure 2.9: The survival probability of solar electron neutrinos  $P_{ee}$  in the presence of sterile neutrinos, computed according to Eqs. (2.36) and (2.17). The orange and green curves assume  $U'_{12} = -U'_{21} = 0.05$  for the sterile-active neutrino mixing. The experimental measurements (black points/bars) are the same as those in Fig. 2.6. Note that the curve and the data points are only for illustration, neglecting some subleading order effects which are discussed in the text.

masses in this regime need to be below  $10^{-9}$  eV. Apart from the aforementioned cases of small mass splittings, one can also consider sterile neutrinos at the eV scale (as possible explanations for various short-baseline anomalies) and test them in solar neutrino measurements [155, 158]. A recent study in Ref. [158] shows that the current solar neutrino data have excluded significant regions of the parameter space responsible for some recent anomalies.

### 2.3.3. Neutrino magnetic moments

Despite being electrically neutral, neutrinos can interact with the photon via loop processes. In the SM, such loop diagrams are mediated by the  $W^\pm$  or  $Z$  boson with the photon leg attached either to the  $W^\pm$  boson, or to the charge fermion running in the loop. It is well-known that these diagrams give rise to neutrino magnetic moments [159, 160, 161, 162, 163, 164], provided that neutrinos have small masses. However, neutrino magnetic moments generated in this way are extremely small, typically around  $10^{-20} \mu_B$  ( $\mu_B = 0.296 \text{ MeV}^{-1}$  is the Bohr magneton) for Dirac neutrinos. For Majorana neutrinos, the theoretical values are further suppressed. In new physics models, loop interactions of neutrinos with the photon might potentially lead to much larger magnetic moments [165, 166, 167, 168, 169, 170, 171]. In addition to the magnetic moment, neutrinos could also possess other electromagnetic form factors such as electric dipole moments, charge radii, and anapoles—see [172] for a comprehensive review.

Neutrino electromagnetic interactions would affect both solar neutrino propagation and detection. Here we concentrate on the latter and leave the former to Sec. 2.3.5. In fact, constraints on neutrino magnetic moments derived from the latter are generally much more stringent and more robust than those from the former.

In the presence of significant neutrino magnetic moments or other electromagnetic form factors, the photon can mediate elastic neutrino scattering. Due to its massless feature, it could drastically enhance the cross section in the soft-scattering limit. The cross section of elastic  $\nu + e$  scattering including the contribution of a neutrino magnetic moment

reads [172, 173]:

$$\frac{d\sigma}{dT} = \frac{d\sigma_{\text{SM}}}{dT} + \frac{\pi\alpha^2}{m_e^2} \left( \frac{1}{T} - \frac{1}{E_\nu} \right) \left( \frac{\mu_\nu}{\mu_B} \right)^2, \quad (2.37)$$

where  $\frac{d\sigma_{\text{SM}}}{dT}$  denotes the SM cross section [see Eq. (2.31) with NSI parameters set to zero],  $\alpha = 1/137$ , and  $\mu_\nu$  is the neutrino magnetic moment. As is implied by Eq. (2.37), to gain the sensitivity to  $\mu_\nu$ , one needs to focus on low  $T$  or low  $E_\nu$ , which is the advantage of solar neutrino data. Therefore, testing neutrino electromagnetic interactions via elastic scattering of solar neutrinos has been investigated in many studies [128, 129, 174, 175, 176, 177, 178, 179, 180, 181, 182], with some being motivated by the recent XENON1T excess, which could be explained by  $\mu_\nu \in [1.4, 2.9] \times 10^{-11} \mu_B$  (90% C.L.) [183]. This value was close to the best limit by then from Borexino [176]:  $\mu_\nu < 2.8 \times 10^{-11} \mu_B$  at 90% C.L. Unfortunately, the XENON1T excess disappeared with the latest updates from LUX-ZEPLIN [184, 185] and XENONnT [186]. Nevertheless, the investigation of possible signals of neutrino magnetic moments in solar neutrinos have led to so far the most stringent constraints:  $\mu_\nu < 6.2 \times 10^{-12} \mu_B$  from LUX-ZEPLIN [185] and  $\mu_\nu < 6.3 \times 10^{-12} \mu_B$  from XENONnT [186], both at 90% C.L.

In addition to elastic  $\nu + e^-$  scattering, CE $\nu$ NS of solar neutrinos at dark matter detectors could be used to test neutrino electromagnetic interactions. Due to the comparatively high momentum transfer required in order to produce observable nuclear recoils, it is unlikely that CE $\nu$ NS in future experiments will lead to stronger constraints than  $\nu + e^-$  scattering [187, 188, 189]<sup>11</sup>.

### 2.3.4. Neutrino interactions with light mediators

Neutrino interactions with light mediators such as dark gauge bosons could be tested by elastic scattering of solar neutrinos off electrons as well [128, 129, 190, 191, 192, 193, 194]. The most extensively studied case is a neutral gauge boson similar to the  $Z$  boson in the SM, often denoted by  $Z'$ . For a generic vector mediator  $Z'$ , one can take the cross section in Eq. (2.31) with  $g_1$  and  $g_2$  modified as follows [133, 195]:

$$g_1 = g_1^{\text{SM}} + \frac{g_{eL}g_\nu}{\sqrt{2}G_F(2m_eT + m_{Z'}^2)}, \quad g_1^{\text{SM}} = 2s_W^2 - 1 + 2\delta_{\alpha e}, \quad (2.38)$$

$$g_2 = g_2^{\text{SM}} + \frac{g_{eR}g_\nu}{\sqrt{2}G_F(2m_eT + m_{Z'}^2)}, \quad g_2^{\text{SM}} = 2s_W^2, \quad (2.39)$$

where  $m_{Z'}$  is the mass of  $Z'$ ,  $(g_{eL}, g_{eR}, g_\nu)$  are  $Z'$  couplings defined in the Lagrangian terms  $\mathcal{L} \supset Z'_\mu \bar{e} \gamma^\mu (g_{eL} P_L + g_{eR} P_R) e + Z'_\mu \bar{\nu} \gamma^\mu g_\nu P_L \nu$ . When  $Z'$  is light, the cross section could be significantly enhanced at low energies by  $2m_eT + m_{Z'}^2$  in the denominators in Eqs. (2.38) and (2.39). In fact, since among all  $\nu_\mu$  and  $\nu_\tau$  sources for practical detection solar neutrinos have the lowest energy, they have been used to constrain the  $L_\mu - L_\tau$  model which, after imposing all experimental constraints, can still successfully accommodate the muon  $g - 2$  anomaly [193] for  $10^{-2}$  GeV  $\lesssim m_{Z'} \lesssim 10^{-1}$  GeV [196]. The lower bound of  $m_{Z'}$  for the muon  $g - 2$  is mainly determined by the Borexino data —see [193] for a recent update.

### 2.3.5. Spin-flavor precession and solar antineutrinos

In addition to the effect on elastic neutrino-electron scattering as elucidated in Sec. 2.3.3, neutrino magnetic moments may cause another particularly interesting effect, the spin-flavor precession [25, 26, 182, 197]. When a neutrino propagates in the solar magnetic field with a nonzero magnetic moment, the magnetic field could flip the spin of a neutrino and convert

<sup>11</sup>See Fig. 4 in Ref. [187] and Fig. 11 in Ref. [188], which implies that the CE $\nu$ NS bounds would only be competitive if the solar neutrino floor could be measured at extremely low nuclear recoils ( $10^{-3} \sim 10^{-2}$  keV).

Table 2.3: Summary of experimental searches for the measurement of solar  $\nu_e \rightarrow \bar{\nu}_e$ .

Expt.	Target	$E_{\bar{\nu}_e}$ (MeV)	$P_{\nu_e \rightarrow \bar{\nu}_e}$ (90% C.L.)
KamLAND [200]	Liquid Scintillator	8.3-31.8	$5.3 \times 10^{-5}$
Borexino [201]	Liquid Scintillator	1.8-16.8	$7.2 \times 10^{-5}$
SNO [202]	Heavy Water	4.0-14.8	$8.1 \times 10^{-3}$
SK-IV [203]	Pure Water	9.3-17.3	$4.7 \times 10^{-4}$

it to an antineutrino. The spin flipping effect combined with flavor oscillations results in the conversion of  $\nu_e \rightarrow \bar{\nu}_e$ , with the probability given by [182, 197]:

$$P_{\nu_e \rightarrow \bar{\nu}_e} \simeq 1.1 \times 10^{-10} \times \left[ \frac{\mu_\nu}{10^{-12} \mu_B} \frac{B_\perp(r_0)}{10 \text{kG}} \right]^2, \quad (2.40)$$

where  $\mu_\nu$  is the neutrino magnetic moment and  $B_\perp(r_0)$  represents the strength of the solar magnetic field at  $r_0 \approx 0.05 R_\odot$ . Note that Eq. (2.40) is not universally valid for all neutrino energies. For low and high energy parts of the solar neutrino spectra one should use numerical calculations—see Ref. [182] for such a discussion.

Historically the idea that the solar magnetic field could lead to the neutrino-antineutrino conversion was proposed as a solution to the solar neutrino problem [23, 24, 25, 26]. However, this explanation has faded due to experimental confirmation of the MSW-LMA solution. Nevertheless, the neutrino-antineutrino conversion has motivated experimental searches for solar antineutrinos. It should be noted that the standard solar model can produce a highly suppressed amount of antineutrinos due to the existence of  $\beta^-$  decay elements such as  $^{40}\text{K}$ ,  $^{238}\text{U}$ , and  $^{232}\text{Th}$ . The expected antineutrino flux from the standard solar model is around  $200 \text{ cm}^{-2}\text{s}^{-1}$  on the Earth’s surface, with energies up to 3 MeV. They are buried under the much higher flux of geo-neutrinos ( $\sim 10^8 \text{ cm}^{-2}\text{s}^{-1}$ ) [198] and the global reactor antineutrino flux (At CJPL [199], e.g., this is around  $10^5 \text{ cm}^{-2}\text{s}^{-1}$ ). Photofission reactions occurring in the solar interior, on the other hand, can produce a more energetic flux  $\sim 10^{-3} \text{ cm}^{-2}\text{s}^{-1}$  at 3-9 MeV, which is far below existing antineutrino fluxes on the Earth. Therefore, observations of solar  $\bar{\nu}_e$  above the known background would be a powerful probe of new physics.

Table 2.3 summarizes the results of experimental searches for  $\nu_e \rightarrow \bar{\nu}_e$ . The KamLAND and Super-K experiments focus on neutrino energies above  $8 \sim 9$  MeV to reduce the reactor antineutrino background. Borexino and SNO, with their much lower reactor antineutrino backgrounds, can perform such searches at lower energies, with the lower energy bounds being only limited by their detection thresholds.

The experimental searches rely crucially on the experimental ability to detect and identify  $\bar{\nu}_e$  events. In the aforementioned experiments,  $\bar{\nu}_e$  is detected either by the inverse beta decay (KamLAND, Borexino, and Super-K) or the charged-current reaction on deuterium,  $\bar{\nu}_e + d \rightarrow e^+ + n + n$  in heavy water (SNO). Neutron tagging at Super-K is important for the background reduction, which can be significantly improved by adding Gd to the detector.

### 2.3.6. Dark matter annihilation

The local density of the galactic dark matter (DM) halo is known to be around  $0.4 \text{ GeV}/\text{cm}^3$  in the solar system. As the Sun moves in the halo, it can capture DM particles that fall into its gravitational potential well and scatter with normal matter particles or, in the presence of DM self-interactions, with DM particles. The theory of DM being captured by the Sun or other large celestial bodies has been developed since the 1980s [204, 205, 206].



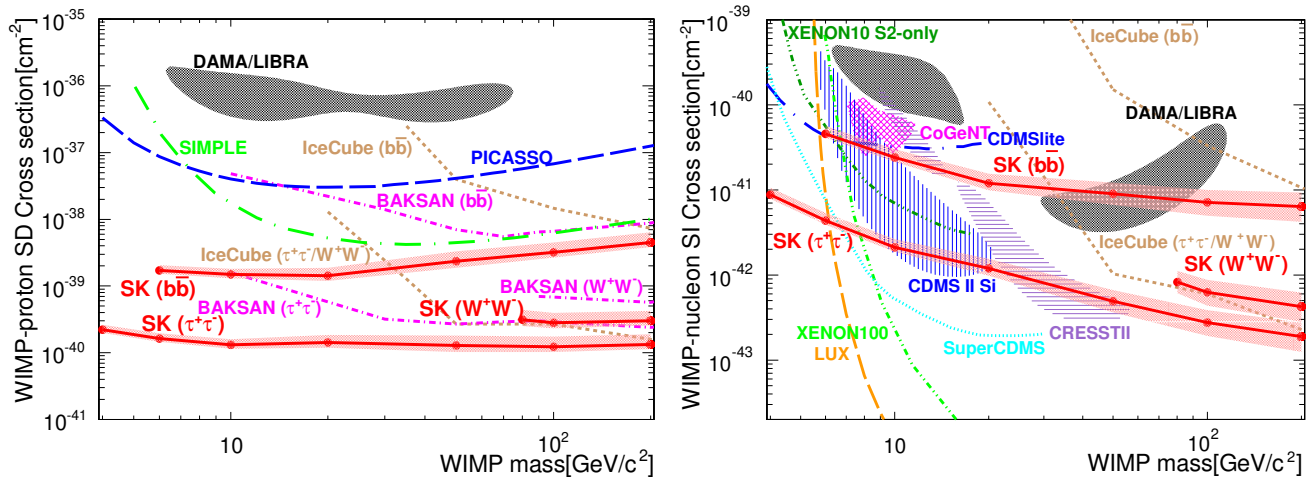


Figure 2.10: Super-Kamiokande (SK) limits of DM annihilation in the Sun on SD (left) and SI (right) WIMP-proton cross sections, taken from Ref. [219].

The accumulation of DM in the Sun can be used to constrain DM annihilation, which may produce various SM particles, including quarks, leptons, etc. While most of them cannot escape the Sun except for neutrinos, they may decay to neutrinos and other final states. Hence neutrinos from DM annihilation in the Sun could be used to constrain or probe DM properties—see, e.g., Refs. [207, 208, 209, 210, 211, 212, 213, 214, 215, 216, 217, 218]. Most of these studies focused on Weakly Interacting Massive Particles (WIMP), which is so far the most extensively studied DM candidate. The mass of WIMP typically varies from a few GeV to hundreds of GeV, implying that neutrinos from WIMP annihilation should have similar energies (i.e., around the same orders of magnitude). It requires that neutrino detectors have the capability to detect high-energy neutrinos within the above energy window<sup>12</sup>. An interesting exception is Quark Nugget Dark Matter [215, 216], which leads to neutrino signals in the 20–50 MeV range.

Several experiments have conducted searches for neutrinos from DM annihilation in the Sun, including Super-Kamiokande [219], IceCube [220, 221], and ANTARES [222]. All experiments found no significant excess, putting stringent constraints on WIMP-proton cross sections. In particular, the most stringent limits on spin-dependent (SD) WIMP-proton cross section are obtained from these experiments. Figure 2.10 shows the 90% C.L. upper limits on SD and spin-independent (SI) WIMP-proton cross sections reported by Super-Kamiokande [219]. Depending on the mass and the annihilation channel of WIMP, the limits vary from  $10^{-38} \sim 10^{-40} \text{ cm}^{-2}$  and  $10^{-40} \sim 10^{-43} \text{ cm}^{-2}$  for the SD and SI cross sections, respectively. The SI bounds are generally weaker than those from direct detection due to the coherent enhancement of large nuclei in the SI case.

### 2.3.7. Neutrino decay

Massive neutrinos are not absolutely stable. Even with pure SM interactions, due to loop-level processes, massive neutrinos can decay as  $\nu_i \rightarrow \nu_j \gamma$  or  $\nu_i \rightarrow \nu_j \nu_k \nu_l$ ,<sup>13</sup> though the lifetime is much longer than the universe’s age [223, 224]. Nevertheless,

<sup>12</sup>Within this energy window, the dominant background is atmospheric neutrinos, which could be reduced by improving the directional resolution. However, as previously discussed, solar atmospheric neutrinos remain as an irreducible background even if the direction can be well measured.

<sup>13</sup>This case is similar to lepton flavor violating decays of charged leptons such as  $\mu \rightarrow e + \gamma$  and  $\mu \rightarrow 3e$ , which are present (though highly suppressed) when neutrino masses and the PMNS mixing are introduced to the SM.

like the situation of neutrino magnetic moments, new physics of neutrinos might potentially enhance the decay rates to an experimentally accessible level.

Since, so far, all neutrinos being successfully detected are relativistic, the lifetime of a neutrino during flight,  $\tau_{\text{flight}}$ , is dilated by the Lorentz factor, which is equal to  $E_\nu/m_\nu$ , i.e.  $\tau_{\text{flight}} = \tau_{\text{rest}} E_\nu/m_\nu$  where  $\tau_{\text{rest}}$  is the lifetime in the rest frame. As neutrinos decay during propagation, the flux is depleted by the factor  $\exp(-L/\tau_{\text{flight}})$  where  $L$  is the distance of propagation. Increasing  $L$  can drastically enhance experimental sensitivity to neutrino decay. Hence the strongest constraints on neutrino decay are derived from observations of supernova neutrinos (SN1987A) and solar neutrinos.

Using solar neutrinos to constrain neutrino lifetimes was first studied in Refs. [225, 226], followed by several studies further exploring various aspects [157, 177, 227, 228, 229, 230, 231]. The lower bound on  $\tau_{\text{rest}}/m_\nu$  varies within  $10^{-4} \sim 10^{-3} \text{ sec/eV}$  [226, 229], depending on how the standard MSW-LMA solution and its uncertainties are taken into account and also on which mass eigenstate decays. The bound is about ten orders of magnitude weaker than that from supernova neutrinos of SN1987A. However, the solar neutrino bounds have the merit that they can be applied to a specific mass eigenstate, while the constraint from SN1987A would be invalid if any of the three mass eigenstates is stable.

### 2.3.8. Others

In addition to those mentioned above, there have been a variety of other new physics scenarios that solar neutrinos could probe. Below we briefly mention some interesting examples.

1. New long-range forces could be present with very weak couplings. Such forces could induce additional flavor-dependent effective potentials and hence be probed by neutrino oscillation, as has been studied in Refs. [232, 233, 234, 235, 236, 237, 238, 239, 240, 241, 242, 243, 244, 245, 246]. Solar neutrinos have the advantage that the new potential caused by the Sun is much larger than that caused by the Earth for the same strength of a long-range force. For a generic vector mediator with a mass  $m_A$  and a universal coupling  $g$ , solar neutrinos can probe  $g \sim 10^{-25}$  when  $m_A$  is around the inverse of the solar radius [245]. This exceeds other known experimental bounds significantly.
2. Dark matter-neutrino interactions could affect neutrino oscillation when neutrinos propagate on a DM background [247, 248, 249, 250, 251, 252, 253]. For instance, Ref. [247] showed that for the fuzzy DM scenario, current solar neutrino data are more sensitive to the neutrino-DM coupling than CMB limits by more than two orders of magnitude. Ref. [249] proposed a framework which connects DM and sterile neutrinos via a dark gauged  $U(1)$  and studied the solar MSW effect caused by DM, dubbed Solar Dark MSW. The authors showed that Solar Dark MSW is characterized by comparatively large modifications of  $^8\text{B}$ ,  $^{15}\text{O}$ , and  $^{13}\text{N}$  neutrinos, with the other fluxes less affected.
3. In addition to interactions with dark matter, neutrinos could also interact with dark energy, as exemplified by the idea of Mass-Varying Neutrinos (MaVaN) [254] which has drawn considerable interest in cosmology. If neutrinos are coupled to a dark scalar field whose background value accounts for the dark energy, then neutrino masses are connected to dark energy. It explains the intriguing coincidence of today's dark energy density  $\rho_\Lambda \sim (2 \times 10^{-3} \text{ eV})^4$  with the neutrino mass scale,  $\rho_\Lambda^{1/4} \sim m_\nu$ . The neutrino oscillation probe of MaVaN was proposed and investigated in Ref. [255, 256, 257].
4. DM accumulated in the Sun could affect the energy transport in the Sun and modify the solar core temperature [258, 259, 260, 261, 262, 263, 264, 265, 266]. For non-annihilating DM accumulated in the Sun, the central temperature could be reduced by a few percent. Consequently, neutrino production rates in the very central region are reduced

and enhanced in the outer part. This feature allows one to use precision measurements of the solar neutrino spectrum to constrain GeV DM effectively—see, e.g., Ref. [260, 263] for further details.

### 3. Detection and experimental challenges

Neutrinos are detected when they scatter on particles such as electrons or nuclei in a detector and generate observable signals. Neutrino scattering processes are mediated by charged-current (CC) or neutral-current (NC) interactions. NC interactions are flavor universal, whereas CC interactions are, for solar neutrinos, only relevant to the detection of  $\nu_e$  since  $\nu_\mu$  and  $\nu_\tau$  do not have sufficient energy to produce their corresponding heavy charged lepton partners  $\mu$  and  $\tau$ .

For solar neutrino scattering on electrons, it has to be elastic ( $\nu + e^- \rightarrow \nu + e^-$ ) and only the final-state electron is observable. The elastic  $\nu + e^-$  scattering process is particularly important for measuring low-energy solar neutrino fluxes due to its zero threshold. Its disadvantage is that the neutrino energy usually cannot be constructed on an event-by-event basis, unless both the electron energy and direction are well measured.

For scattering on nuclei, there are several possibilities including elastic scattering ( $\nu + N \rightarrow \nu + N$ ), CC scattering ( $\nu_e + N \rightarrow N' + e^-$ ), and NC inelastic scattering (e.g.,  $\nu + {}^2\text{H} \rightarrow \text{p} + \text{n} + \nu$ ), etc. The last two types of reactions have been successfully applied to solar neutrino observations (Homestake, GALLEX/GNO, SNO). In contrast, elastic scattering on nuclei has not yet been observed for solar neutrinos. In the foreseeable future, with the improvement of ultra-low nuclear recoil detection in, e.g., DM detectors, elastic scattering on nuclei, which is a coherent process due to the low energy of solar neutrinos, will soon become an effective way to detect solar neutrinos.

Below we focus our discussions on two predominant processes in solar neutrino detection, elastic scattering on electrons and CC scattering on nucleus.

#### 3.1. Elastic neutrino-electron scattering

Elastic neutrino-electron scattering applies to all three neutrino flavors:

$$\nu_\alpha + e^- \rightarrow \nu_\alpha + e^-, (\alpha = e, \mu, \tau). \quad (3.1)$$

Note that the total cross section of  $\nu_e + e^-$  scattering is about 6 times greater than that of  $\nu_{\mu,\tau} + e^-$  when the recoil electron is relativistic. This difference is because the former receives contributions from both CC and NC interactions, while the latter is mediated only by NC interactions. More specifically, for  $E_\nu \gg m_e$ , we have  $\sigma(\nu_e + e^-)/10^{-46}\text{cm}^2 \approx 93s/\text{MeV}^2$  and  $\sigma(\nu_{\mu,\tau} + e^-)/10^{-46}\text{cm}^2 \approx 15s/\text{MeV}^2$  with  $s = 2E_\nu m_e$  [267, 268]. Towards low energy, e.g. from 10 MeV to 1 MeV,  $\sigma(\nu_{\mu,\tau} + e^-)/\sigma(\nu_e + e^-)$  increases, and this needs to be considered for the relevant experimental study for the solar neutrino up-turn effect.

In elastic neutrino-electron scattering, the electron recoil kinetic energy  $T_e$  is related to the initial neutrino energy  $E_\nu$  by

$$T_e = \frac{2m_e E_\nu^2 \cos^2 \theta}{(m_e + E_\nu)^2 - E_\nu^2 \cos^2 \theta}, \quad (3.2)$$

where  $\theta$  denotes the angle between the outgoing electron and the incoming neutrino (solar) directions, varying from  $0^\circ$  to  $90^\circ$ . Given a fixed  $E_\nu$ ,  $T_e$  reaches its maximum,  $T_{\text{max}}$ , at  $\theta = 0^\circ$  and vanishes when  $\theta = 90^\circ$ . The maximum is given by

$$T_{\text{max}} = \frac{2E_\nu^2}{2E_\nu + m_e}. \quad (3.3)$$

Theoretically, with the measured electron scattering angle  $\theta$  and its recoil  $T_e$ , we can obtain  $E_\nu$  from

$$E_\nu = \frac{m_e}{\sqrt{1 + 2m_e/T_e \cos \theta} - 1}. \quad (3.4)$$

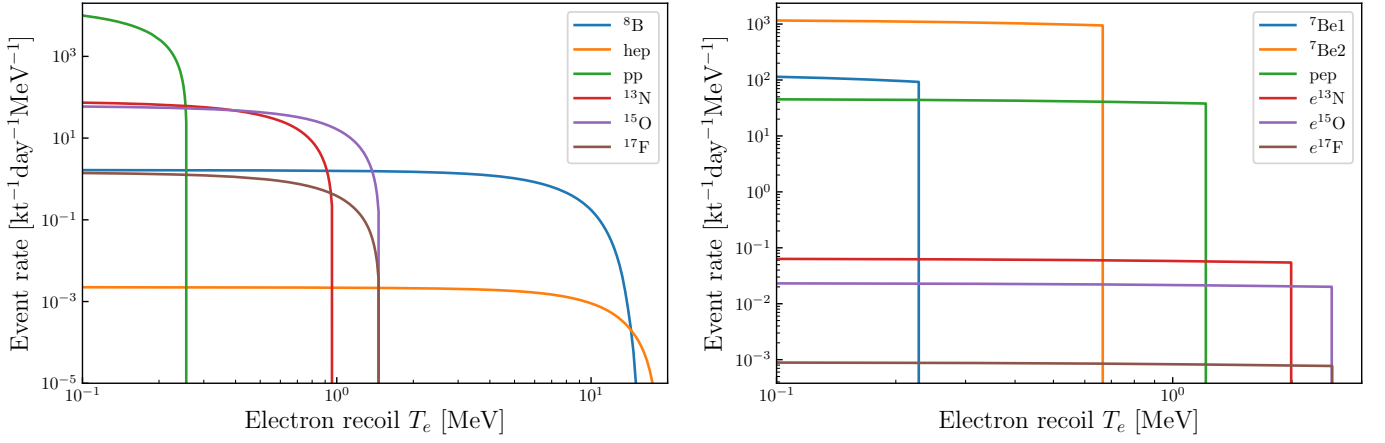


Figure 3.1: Electron recoil distributions of elastic  $\nu_e + e^-$  scattering for continuous (left) and monochromatic (right) solar neutrino spectra.

In practice, the angle  $\theta$  cannot be measured accurately at low energies. For instance, water Cherenkov detectors have angular resolution  $\sim 40^\circ$  ( $20^\circ$ ) for  $T_e = 5$  (15) MeV (see Sec. 3.4), while conventional liquid scintillator detectors are hardly able to measure the direction. For this reason, the recoil energy spectrum with respect to  $T_e$  is primarily used in the data analyses. The  $T_e$  spectrum is related to the neutrino energy spectrum by

$$\frac{dN}{dT_e} = N_e t_{\text{exposure}} \int_0^{E_\nu^{\text{max}}} \phi(E_\nu) \frac{d\sigma}{dT_e} \Theta(T_{\text{max}} - T_e) dE_\nu, \quad (3.5)$$

where  $\frac{dN}{dT_e}$  denotes the event rate;  $N_e$  is the total number of electrons in the detector ( $N_e = 3.3 \times 10^{32}$  for 1kt water);  $t_{\text{exposure}}$  is the exposure time;  $\phi(E_\nu)$  is the neutrino flux;  $\frac{d\sigma}{dT_e}$  is the differential cross section for which we refer to Eq. (2.31); and  $\Theta(T_{\text{max}} - T_e)$  is the Heaviside step function.

Figure 3.1 shows the electron recoil spectra of solar neutrinos obtained using the fluxes presented in Fig. 2.4 and Eq. (3.5), assuming no flavor conversion. One can see that although the continuous and monochromatic neutrino spectra in Fig. 2.4 are rather distinct from each other, their electron recoil spectra are quite similar, all being flat at low  $T_e$  and quickly falling to zero when  $T_e$  increases to  $T_{\text{max}}$ . The main difference is at the turning point where the monochromatic case has a sharp cut-off, but resolving this difference would require very high precision measurements of the spectrum. In general, it is difficult to use electron recoils to distinguish between continuous and monochromatic neutrino spectra, and unfolding the solar neutrino spectra based on elastic scattering data is challenging.

### 3.2. CC scattering on nucleus

At solar neutrino energies, CC scattering of neutrinos with a nucleus usually cannot break the nucleus, simply converting one of the neutrons in the nucleus to a proton,  $\nu_e + n \rightarrow p + e^-$ , which we refer to as neutrino-capture beta decay ( $\nu$ BD). It differs from inverse beta decay (IBD),  $\bar{\nu}_e + p \rightarrow n + e^+$ , which has been extensively used to detect antineutrinos. Because free neutrons are unstable, in a practical  $\nu$ BD process, the neutron has to be bound in a nucleus  ${}^A_Z N$  which after absorbing  $\nu_e$  becomes  ${}^A_{Z+1} N'$ :

$$\nu_e + {}^A_Z N \rightarrow {}^A_{Z+1} N' + e^-. \quad (3.6)$$

Table 3.1: Thresholds of  $\nu_e$ -capture reactions. Most reactions are ground-to-ground transitions except for  $\nu_e + {}^{40}\text{Ar} \rightarrow {}^{40}\text{K}^* + e^-$  in which the final nucleus is an excited nuclear state (further details explained in the text). Data obtained from Ref. [269].

Reaction	$E_\nu$ threshold	Experiments
$\nu_e + {}^{163}\text{Dy} \rightarrow {}^{163}\text{Ho} + e^-$	2.8 keV	-
$\nu_e + {}^{205}\text{Tl} \rightarrow {}^{205}\text{Pb} + e^-$	50.6 keV	LOREX [270, 271]
$\nu_e + {}^{123}\text{Sb} \rightarrow {}^{123}\text{Te} + e^-$	51.9 keV	-
$\nu_e + {}^{193}\text{Ir} \rightarrow {}^{193}\text{Pt} + e^-$	80.2 keV	-
...		
$\nu_e + {}^{55}\text{Mn} \rightarrow {}^{55}\text{Fe} + e^-$	0.231 MeV	-
$\nu_e + {}^{71}\text{Ga} \rightarrow {}^{71}\text{Ge} + e^-$	0.232 MeV	GALLEX [9], SAGE [10]
$\nu_e + {}^{73}\text{Ge} \rightarrow {}^{73}\text{As} + e^-$	0.345 MeV	-
...		
$\nu_e + {}^{37}\text{Cl} \rightarrow {}^{37}\text{Ar} + e^-$	0.814 MeV	Homestake [3]
$\nu_e + {}^{57}\text{Fe} \rightarrow {}^{57}\text{Co} + e^-$	0.836 MeV	-
$\nu_e + {}^7\text{Li} \rightarrow {}^7\text{Be} + e^-$	0.862 MeV	Refs. [272, 273, 274, 275]
$\nu_e + {}^{75}\text{As} \rightarrow {}^{75}\text{Se} + e^-$	0.865 MeV	-
...		
$\nu_e + {}^{40}\text{Ar} \rightarrow {}^{40}\text{K}^* + e^-$	5.888 MeV (Fermi)	
	3.8 ~ 4.6 MeV (GT)	DUNE [40]

Such a process has been applied to solar neutrino detection since the very early stage of experimental studies<sup>14</sup>. For example, the Homestake experiment employed  $\nu_e + {}^{37}\text{Cl} \rightarrow {}^{37}\text{Ar} + e^-$ , which is a typical  $\nu\text{BD}$  reaction.

The CC cross section calculation can be found in Ref. [1, 280, 281, 282]. Unlike elastic  $\nu + e^-$  scattering, the neutrino energy  $E_\nu$  in  $\nu\text{BD}$  can be well determined from the electron kinetic energy  $T_e$  and the masses of initial and final particles<sup>15</sup>:

$$E_\nu = T_e + m_{N'} - m_N + m_e, \quad (3.7)$$

where  $m_N$  and  $m_{N'}$  are the masses of the initial and final nuclei, respectively. The kinetic energy of the final nucleus is negligible since it is of the order  $\sim E_\nu^2/m_{N'}$ , much smaller than  $E_\nu$ . Note that when the final nucleus is in an excited state, then  $m_{N'}$  denotes the mass of the excited nucleus mass, which can be obtained by adding the excitation energy to the ground-state nucleus mass. In the presence of multiple allowed transitions to different excited states, one needs to take into account their branching ratios, which depend on the corresponding nuclear matrix elements. The experimental determination of the nuclear matrix elements is usually done with (p, n) or ( ${}^3\text{He}$ , t) reactions. More details can be found in, e.g. Ref. [283, 284].

The usage of  $\nu\text{BD}$  in solar neutrino detection concerns two limitations. First,  $\nu\text{BD}$  is only applicable to the detection of  $\nu_e$ , irrelevant to neutrinos of other flavors. Second, it has a threshold given by

$$E_\nu^{\text{thre}} = m_{N'} - m_N + m_e = m_{N'}^{(\text{atom})} - m_N^{(\text{atom})},$$

<sup>14</sup>In the 1930s, Crane and Halpern used such reactions to look for neutrinos by measuring the energy of the emitted  $\beta$ -ray and the recoil atom [276, 277, 278, 279].

<sup>15</sup>This feature is rather important for the Earth matter effect measurement.

where  $m_N^{(\text{atom})}$  and  $m_{N'}^{(\text{atom})}$  denote the masses of  $N$  and  $N'$  atoms. For some final state isotopes, the nuclear excitation energy levels can be rather complicated and some low-energy excitation states may have very low transition rates. In such cases, the complicated energy levels might smear the threshold.

In Tab. 3.1, we present a list of low-threshold  $\nu$ BD processes obtained by looking for electron capture (i.e., the inverse of  $\nu$ BD) interactions with low  $Q$  values. Due to technical difficulties, many low-threshold  $\nu$ BD processes have not been used in solar neutrino detection. The successful examples  $^{71}\text{Ga}$  and  $^{37}\text{Cl}$  have a common feature: they can be used in liquid form, and the final-state nuclei can be extracted and counted using radiochemical methods. In the Homestake experiment,  $^{37}\text{Cl}$  was used in the form of tetrachloroethylene ( $\text{C}_2\text{Cl}_4$ ), which is liquid at room temperature. Metal  $^{71}\text{Ga}$  melts at  $29.8^\circ\text{C}$  and was used in the SAGE experiment. In the GALLEX experiment,  $^{71}\text{Ga}$  is contained in the detector as an aqueous solution of gallium chloride.

In addition, we also include in Tab. 3.1 the process  $\nu_e + {}^{40}\text{Ar} \rightarrow {}^{40}\text{K}^* + e^-$  which is important to DUNE. Its threshold depends on the excited states of  ${}^{40}\text{K}^*$  [285, 286]. The Fermi transition of  ${}^{40}\text{Ar}(0^+)$  to the second  $0^+$  excited state of  ${}^{40}\text{K}$  has the largest nuclear matrix element (hence the largest cross section for sufficiently high  $E_\nu$ ). The threshold is given by  $E_\nu^{\text{thre}} = E_{\nu 0}^{\text{thre}} + E_i$  where  $E_{\nu 0}^{\text{thre}} = 1.504$  MeV is the would-be threshold if the ground-state transition were allowed and  $E_i = 4.384$  MeV is the excitation energy. Apart from the Fermi transition, several Gamow-Teller (GT) transitions to  ${}^{40}\text{K}(1^+)$  with the excitation energy  $E_i = 2.290, 2.730, \text{ and } 3.110$  MeV have lower thresholds but smaller nuclear matrix elements.

J. Bahcall proposed that lithium could be used to detect solar neutrinos in 1964 [287]. This possibility has recently been investigated in Refs. [272, 273, 274, 275]. The ground-state-to-ground-state transition  $\nu_e + {}^7\text{Li} \rightarrow {}^7\text{Be} + e^-$  has a threshold of  $E_\nu^{\text{thre}} = 0.862$  MeV. In addition, the final-state nucleus can be in its first excited state:  $\nu_e + {}^7\text{Li} \rightarrow {}^7\text{Be}^* + e^-$ , which has a threshold of  $E_\nu^{\text{thre}} = 1.291$  MeV. Both GT and Fermi transitions contribute to the ground-state reaction, while for the excited case, only the GT transition is possible [274]. The cross section of this reaction is about 60 times the cross section of elastic  $\nu_e + e^-$  scattering when applied to  ${}^8\text{B}$  neutrino detection [275]. A lithium detector might be possible by exploiting the high solubility of LiCl, 74.5g per 100g of water at  $10^\circ\text{C}$ . An initial test reported in Ref. [275] indicates that a saturated LiCl solution shows excellent optical transparency. The attenuation length of the solution under 430nm LED light is measured to be  $11 \pm 1$  m. Hence the use of LiCl solution in a 10-m diameter detector seems promising.

Some other isotopes such as  ${}^{11}\text{B}$  [288] and  ${}^{115}\text{In}$  [289] have been well discussed and explored by experimentalists. The naturally high radioactivity limits the usage of  ${}^{115}\text{In}$ . Xenon as a dark matter detection medium has been considered as a neutrino target [290]. People have also thought about finding delayed coincidence to reduce the experimental difficulty for  ${}^{115}\text{In}$  [291],  ${}^{100}\text{Mo}$  [292],  ${}^{176}\text{Yb}$  [293],  ${}^{116}\text{Cd}$  [294], and  ${}^{71}\text{Ga}$  [295].

### 3.3. Coherent elastic neutrino-nucleus scattering (CE $\nu$ NS)

At  $E_\nu \lesssim 50$  MeV, elastic scattering of a neutrino with a nucleus via NC interactions is generally considered to be coherent, which implies that the cross section can be substantially enhanced by the large number of nucleons in the nucleus. This process is known as coherent elastic neutrino-nucleus scattering (CE $\nu$ NS), with the following differential cross section [43, 296]:

$$\frac{d\sigma}{dT} = \frac{G_F^2 [N - (1 - 4s_W^2)Z]^2 F^2(T)M}{4\pi} \left(1 - \frac{T}{T_{\text{max}}}\right), \quad (3.8)$$

where  $N$  and  $Z$  are the neutron and proton numbers of the nucleus;  $T$  and  $M$  denote the recoil energy and the mass of the nucleus;  $T_{\max}$  is the maximal value of  $T$  determined by

$$T_{\max} = \frac{2E_\nu^2}{M + 2E_\nu}. \quad (3.9)$$

The form factor  $F$ , which quantifies the coherency of the scattering, can be computed using Helm's approximate formula [297]:

$$F = 3 \frac{j_1(qr_n)}{qr_n} e^{-(qs)^2/2}, \quad (3.10)$$

where  $q \approx \sqrt{2TM}$ ,  $s \approx 0.9$  fm,  $r_n \approx 1.14A^{1/3}$  fm with  $A = N + Z$ , and  $j_1$  is the spherical Bessel function of the first kind. At  $q = 0$ , the form factor should be  $F = 1$ . For solar neutrino scattering on Xe nuclei, the deviation  $1 - F$  typically varies around 5%.

CE $\nu$ NS has received increasing interest since the first successful observation by the COHERENT experiment in 2017 [298]. Despite the large cross section of CE $\nu$ NS, the main challenge of detecting neutrinos via this process is the low nucleus recoil energy ( $\sim$ keV for 10 MeV neutrinos) which is basically invisible in liquid scintillator or water Cherenkov detectors. Dark matter detectors are generally sensitive to such low nucleus recoils. With the rapid development of dark matter detectors (larger scales and lower backgrounds), CE $\nu$ NS becomes a promising process to detect solar neutrinos in the near future—see Sec. 4.5.1 for further discussions on the experimental progress.

### 3.4. Energy and direction measurements

As elucidated above, after neutrino scattering with particles in a detector, the neutrino energy is partially (for elastic scattering) or fully (for CC scattering on nucleus) transferred to charged particles such as electrons and nuclei. The kinetic energy of a final-state nucleus is negligible since it is typically below keV. Here we concentrate on the energy and directional measurements of electrons.

Electrons produced from solar neutrino scattering can only travel a very short distance in the detector medium before it stops. For MeV electrons in water, the propagation distance is around  $0.5 \text{ cm} \times (T_e/\text{MeV})$  [299]. Within this short distance, electrons lose energy due to ionization, bremsstrahlung, and Cherenkov radiation.

The effects of ionization and Cherenkov radiation are employed in modern neutrino detectors filled with water (Super-K, SNO) or liquid scintillator (Borexino) and equipped with PMTs. Water-based Cherenkov detectors can provide important directional information using Cherenkov light, whereas liquid scintillator detectors excel at energy resolution using uniform scintillation light caused by ionization.

#### ■ Water Cherenkov detectors

In water Cherenkov detectors, the Cherenkov light emitted by relativistic charged particles such as electrons propagates as a cone in the water and reaches the surrounding PMTs as a ring—see Fig. 3.2. The Cherenkov cone has an opening angle given by

$$\theta_c = \arccos \frac{1}{\beta n} \approx 41^\circ, \quad (3.11)$$

where  $n \approx 1.33$  is the refractive index for water, and  $\beta \approx 1$  is the speed of the particle. Theoretically, the emission of Cherenkov light from a moving electron only requires  $\beta > 1/n$ , corresponding to  $E_e > m_e/\sqrt{1 - 1/n^2}$  or  $T_e > 0.26$  MeV. In practice, the threshold of detecting electrons via Cherenkov light is higher (e.g., 3.49 MeV at Super-K [86]) due to a sharp increase in event rate caused by radioactive backgrounds and PMT dark noises, as described in Sec. 3.5.1.



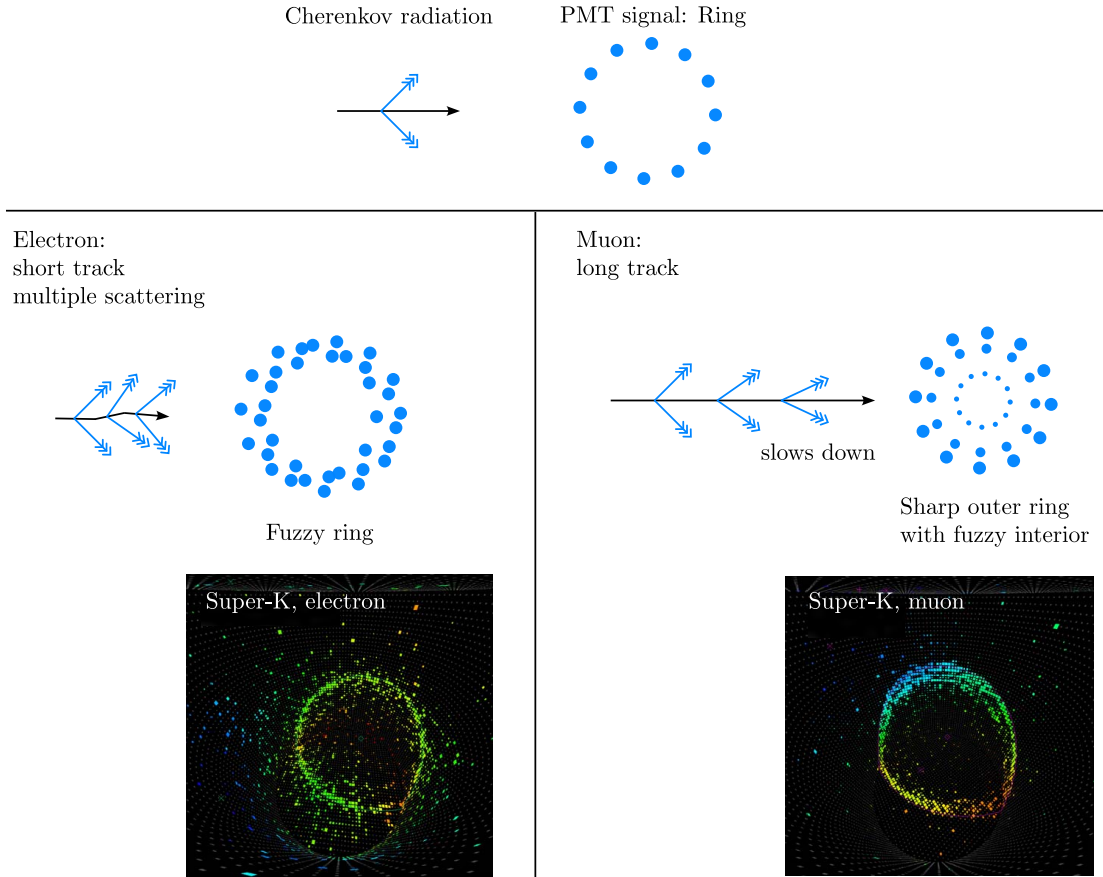


Figure 3.2: Cherenkov rings caused by relativistic electrons and muons. A relativistic electron leaves a short track deflected by multiple soft scattering, leading to a fuzzy ring. By comparison, a muon track is straight and much longer, with a sharp outer ring and a fuzzy interior due to the slow-down of the muon.

The light emission follows from the Frank–Tamm formula:

$$\frac{d^2E}{dLd\omega} = \alpha\omega \sin^2 \theta_c, \quad (3.12)$$

where  $\alpha \approx 1/137$  is the fine-structure constant,  $\omega$  is the frequency of the Cherenkov light, and  $L$  is the propagation distance. For electrons, the total energy of Cherenkov radiation takes only a very minor fraction of the kinetic energy since the major energy loss is ionization. The electron energy can be inferred from the number of Cherenkov photons. The electron energy determined from Cherenkov light is less accurate than that from the measurement of ionization energy, which so far is only possible in liquid scintillator.

The directional measurement plays an essential role in event reconstruction and background reduction. Due to its small mass, the electron undergoes multiple soft (i.e. the momentum transfer is much smaller than the electron energy) scattering processes during Cherenkov radiation. As illustrated in Fig. 3.2, each of the multiple scattering processes deflects the direction of the electron and hence the direction of the Cherenkov cone. Consequently, the signal arriving at surrounding PMTs is a fuzzy ring. This is to be compared with a muon track which can hardly be deflected due to  $m_\mu \gg m_e$  and features a sharp outer ring with fuzzy interior rings caused by the slow-down of the muon.

In the Super-K detector, the energy resolution varies from 10% (for  $E_e \approx 40$  MeV) to 20% (for  $E_e \approx 4$  MeV) and the angular resolution varies from  $20^\circ$  (for  $E_e \approx 18$  MeV) to  $40^\circ$  (for  $E_e \approx 4$  MeV) [300]. The energy resolution improves when  $E_e$  increases because of the statistics of photoelectrons detected by PMTs increases for larger  $E_e$ . The angular

resolution improves when  $E_e$  increases because of the aforementioned multiple scattering, which occurs more often for low-energy electrons and reduces the capability of Cherenkov detectors to measure the electron direction.

### ■ Liquid scintillator detectors

Because most of the electron kinetic energy deposited in the detector is transferred to ionization instead of Cherenkov radiation, the electron kinetic energy can be more straightforwardly (and hence more precisely) measured from the ionization energy. Liquid scintillator (LS) offers an effective way to measure the energy deposited in ionization by converting it to optical photons.

The working mechanism of LS is the subject of fluorescence. The most widely used LS is organic solvent doped with fluorophores (often briefly referred to as fluor). Both the solvent and fluorophore molecules possess aromatic rings. The ionization leads to excitation of the aromatic solvent molecules, which then transfer their excited energy to fluorophore molecules. Due to an effect known as the Stokes shift, the fluorophore, when undergoing deexcitation, emits photons with considerably larger wavelengths than the photon spectrum of the solvent.

The primary advantage of LS is its high light yield,  $\sim 10^4$  photons/MeV for deposit energy, which is about 50 times higher than that in water Cherenkov detectors [301]. Only a small fraction of these photons are detected due to the attenuation length of LS and the coverage and detection efficiency of PMTs. For example, the Borexino detector receives  $\sim 500$  photoelectrons per MeV.

The energy resolution of a LS detector mainly relies on the number of photoelectrons,  $N_{pe}$ , of which the statistical fluctuation is  $\sqrt{N_{pe}}$ . For Borexino,  $N_{pe} \sim 500E_e/\text{MeV}$  implies that the energy resolution is approximately  $1/\sqrt{N_{pe}} \sim 5\% \sqrt{E_e/\text{MeV}}$  [302].

Measuring directions in LS is challenging since the scintillation light emission from ionization is isotropic. An electron path length is about  $0.5 \text{ cm} \times (T_e/\text{MeV})$  [299], which is sufficiently short to be treated as nearly point-like in comparison to the resolution of position reconstruction ( $\sim 10 \text{ cm}$  in Borexino [301]). The Cherenkov light emission is directional but usually overwhelmed by the scintillation light. Observation of Cherenkov light in LS might be possible if the detector is capable of making use of the time separation between them (the Cherenkov light is emitted almost instantaneously while the scintillation light is emitted at the nanosecond level) or if the scintillation light is reduced (e.g., in water-based LS). The former has recently been demonstrated feasible by Borexino [303].

## 3.5. Backgrounds

The solar neutrino spectrum spans from  $\mathcal{O}(0.1)$  MeV (pp neutrinos) to 18.77 MeV (the endpoint of hep neutrinos). Within this range, there are two categories of backgrounds: cosmogenic and detector-related. The latter comes from external (e.g., surrounding rock) and internal (contamination in the fiducial volume) radioactivity.

### 3.5.1. Cosmogenic backgrounds

Cosmic-ray muons on the ground can trigger the data acquisition system of a neutrino detector, causing a sharp increase in event rate and a production of radioactive background, which are not desirable for a rare-event experiment. Therefore, neutrino experiments usually go underground to utilize the thick rock overburden to shield these muons as much as possible. The flux of cosmic-ray muons can be parametrized by Gaisser's formula [304] and further modifications [305, 306]. Figure 3.3 shows how the muon flux decreases with the depth in units of *meter of water equivalent* (m.w.e).

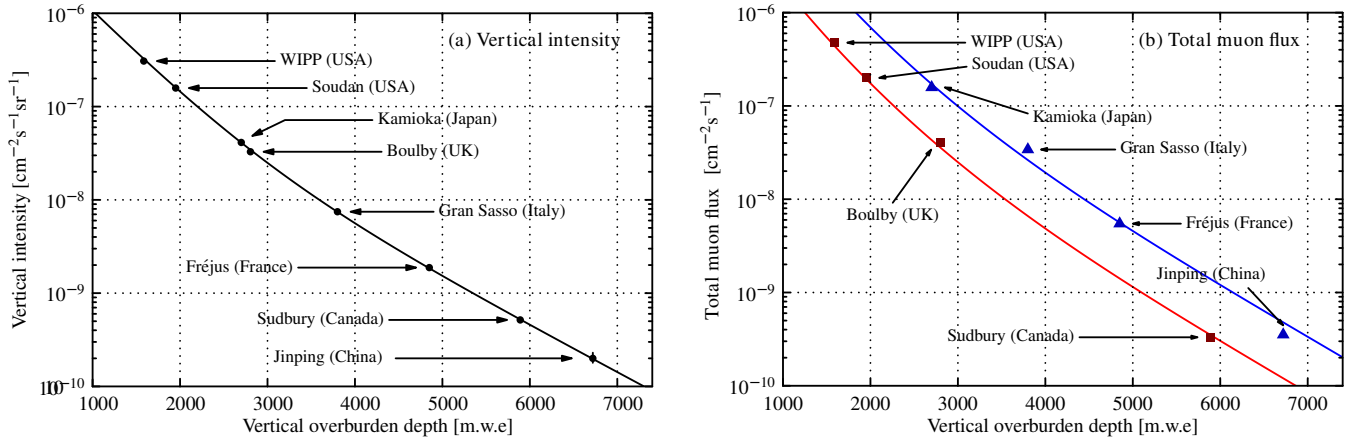


Figure 3.3: Measured muon fluxes in underground laboratories compared with theoretical calculations. The left/right panel is for vertical/total muon fluxes. The black, red, and blue lines represents fits using the empirical formula. The difference between red and blue lines in the right panel is caused by the shape of the overburden. A flat overburden (e.g., Sudbury) with the same depth can shield better from large-zenith-angle cosmic muons. Figure taken and modified from Ref. [306].

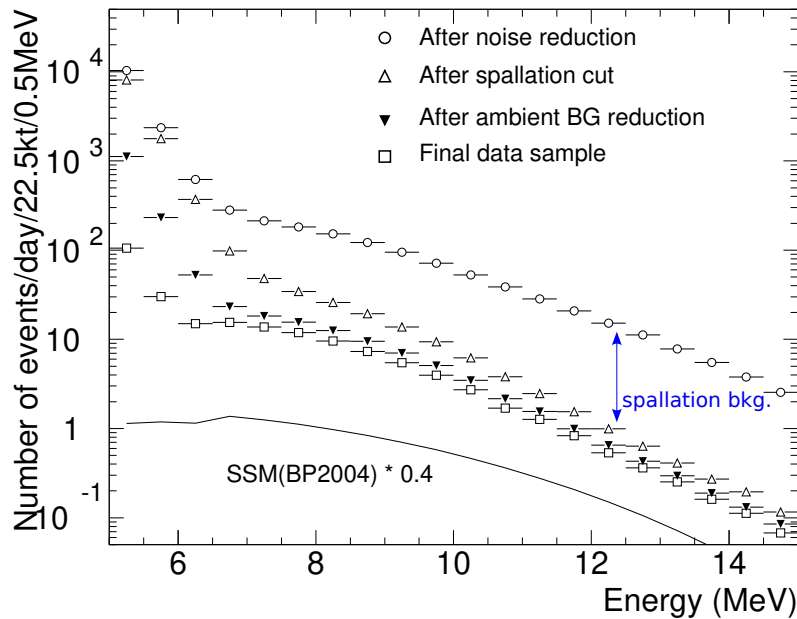


Figure 3.4: Background reduction at multiple steps in Super-Kamiokande [307]. Above  $\sim 6$  MeV, the spallation background which comes from decays of radioactive isotopes ( $^{12}\text{B}$ ,  $^{12}\text{N}$ ,  $^9\text{Li}$ ,  $^8\text{Li}$ , etc.) generated by cosmic muons scattering off  $^{16}\text{O}$  becomes dominant.

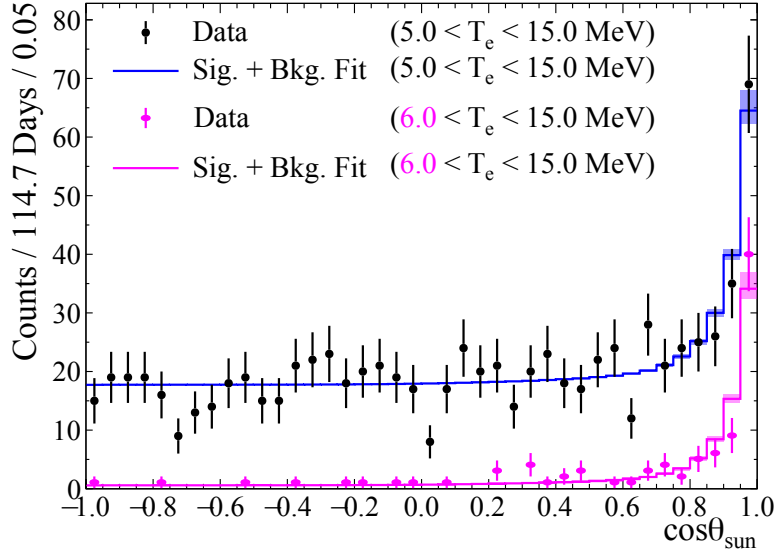


Figure 3.5: Angular distributions of solar neutrino-electron scattering events in SNO+. The original figures are taken from Ref. [308], we combine both figures to give a better illustration. The elastic scattering rate peaks at  $\cos\theta_{\text{sun}} = 1$ , and the non-vanishing flat part with  $\cos\theta_{\text{sun}} < 0$  can be viewed as either the spallation background or the detector-related background since, theoretically, the solar neutrino signal always has  $\cos\theta_{\text{sun}} > 0$ . See more discussion in the text.

When an energetic cosmic muon impinges on a nucleus, it may break up the nucleus and cause a spallation process, thereby generating many short-lived radioactive isotopes. These isotopes then undergo  $\alpha$ -,  $\beta$ - or  $\gamma$ - decays to produce radiations, mimicking solar neutrino signals [309, 310, 311].

In water-based detector, since the heaviest element abundantly contained in the fiducial volume is  $^{16}\text{O}$ , radioactive isotopes generated via spallation are lighter than  $^{16}\text{O}$ . For example,  $\mu^\pm + ^{16}\text{O} \rightarrow \mu^\pm + ^{12}\text{B} + 3\text{p} + \text{n}$  gives rise to  $^{12}\text{B}$  which decays in the  $\beta^-$  mode within  $\sim 10^{-2}$  sec. In Super-K, the significant background from cosmic muon spallation arises from  $^{12}\text{B}$ ,  $^{12}\text{N}$ ,  $^9\text{Li}$ ,  $^8\text{Li}$ ,  $^{15}\text{C}$ , etc. These isotopes decay and emit  $\beta^\pm$  rays of  $\mathcal{O}(10)$  MeV [307]. In addition, the muon capture process  $\mu^- + ^{16}\text{O} \rightarrow \nu_\mu + ^{16}\text{N}$  generates  $^{16}\text{N}$  which has a relatively long lifetime, 7.13 sec. In Super-K, this background is reduced by imposing a cut based on spatial and time correlations of the stopping muon with  $^{16}\text{N}$  decays [307]. Figure 3.4 shows the event rates at multiple steps of background reduction [307]. As shown in the figure, the background above 6 MeV majorly comes from spallation.

The spallation background has no angular preference because the generated non-relativistic radioactive isotopes decay isotropically. Hence the spallation background and solar neutrino signals can be differentiated in angular distributions of event rates. Figure 3.5 shows angular distributions of solar neutrino-electron scattering events in SNO+ [308]. Here  $\theta_{\text{sun}}$  is defined as the angle between the reconstructed recoil electron direction and the expected neutrino direction, which is known from the Sun's position at the event time. The elastic scattering rate peaks at  $\cos\theta_{\text{sun}} = 1$  and becomes flat at smaller  $\cos\theta_{\text{sun}}$  (corresponding to large  $\theta_{\text{sun}}$ ). Theoretically, elastic neutrino-electron scattering does not allow a negative  $\cos\theta_{\text{sun}}$ . Therefore, the non-vanishing flat rate with  $\cos\theta_{\text{sun}} < 0$  indicates the background level. For SNO+, thanks to its substantial overburden (2000m below a flat ground), the cosmic spallation background is reduced to a signal-to-noise level of four for the energy region above 6 MeV.

For liquid scintillator experiments, the dominant cosmogenic background comes from carbon spallation:  $\mu + ^{12}\text{C} \rightarrow \mu + ^{11}\text{C} + \text{n}$ . The neutron in the above spallation process is captured by hydrogen in liquid scintillator, releasing a 2.225

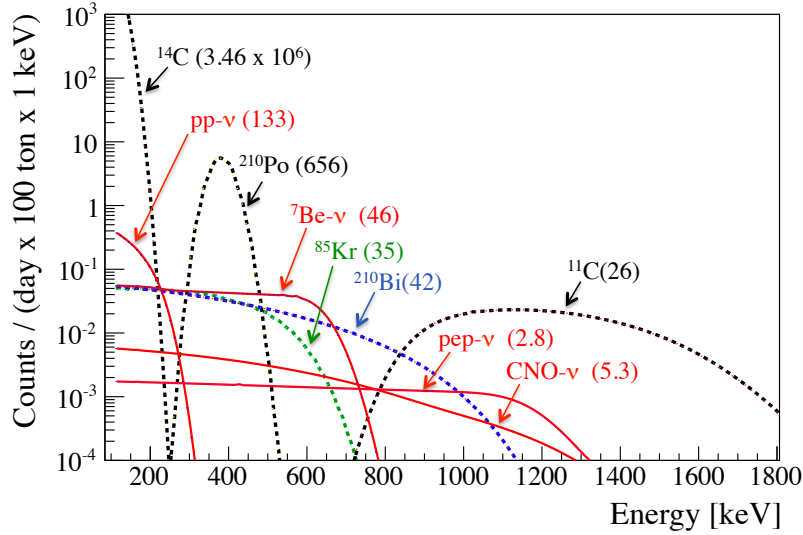


Figure 3.6: Borexino backgrounds (dashed lines) compared with solar neutrino signals (solid lines) in the low energy regime [301].

Table 3.2: Summary of natural radioactive background levels for water and liquid scintillator detectors. Note that radioactive background levels are based on studies for SNO and Borexino. Hence they should not be considered a priori as generic expectations for future detectors.

	Water (g/gH <sub>2</sub> O)	Liquid Scintillator (g/gLS)
<sup>238</sup> U Chain	$6.6 \times 10^{-15}$ [312]	$1.6 \times 10^{-17}$ [313, 314]
<sup>232</sup> Th Chain	$8.8 \times 10^{-16}$ [312]	$6.8 \times 10^{-18}$ [313, 314]
<sup>40</sup> K	$6.1 \times 10^{-16}$ [315]	$1.3 \times 10^{-18}$ [313, 316]

MeV  $\gamma$ -ray. The unstable isotope <sup>11</sup>C decays with a half-life time of 20.34 minutes. Its dominant<sup>16</sup> decay channel is positron emission:  $^{11}\text{C} \rightarrow ^{11}\text{B} + e^+ + \nu_e$  with a  $Q$  value of 0.96 MeV. As  $e^+$  will eventually annihilate with  $e^-$  in the detector, the total energy released from <sup>11</sup>C decay in the detector ranges from  $2m_e = 1.02$  MeV to  $2m_e + Q = 1.98$  MeV. As shown in Fig. 3.6, the <sup>11</sup>C background in Borexino dominates the event rates in this range (the energy resolution effect is taken into account), posing a substantial challenge to the measurement of pep and CNO neutrinos [301].

Due to its relatively long lifetime, <sup>11</sup>C is difficult to tag. Borexino has developed a Three-Fold Coincidence (TFC) method for <sup>11</sup>C tagging through the spatial and time coincidence among (i) the positron from <sup>11</sup>C decay, (ii) the parent muon, and (iii) the neutron capture. Using this method has successfully reduced the <sup>11</sup>C background by  $\sim 10\%$  (see Fig. 40 in Ref. [301]).

Deeper underground laboratories such as SNO or CJPL can almost eliminate the cosmogenic backgrounds. A precise <sup>8</sup>B measurement and search for hep neutrinos can go down to the level at which the low-energy atmospheric neutrino background starts to be significant.

### 3.5.2. Detector-related backgrounds

Detector-related backgrounds can be categorized as internal or external.

External backgrounds come from the radioactivity of surrounding materials, mainly from the glass of PMTs, the vessel,

<sup>16</sup>The electron capture process is also possible (0.19 – 0.23%):  $^{11}\text{C} + e^- \rightarrow ^{11}\text{B} + \nu_e$  with a  $Q$  value of 1.98 MeV.

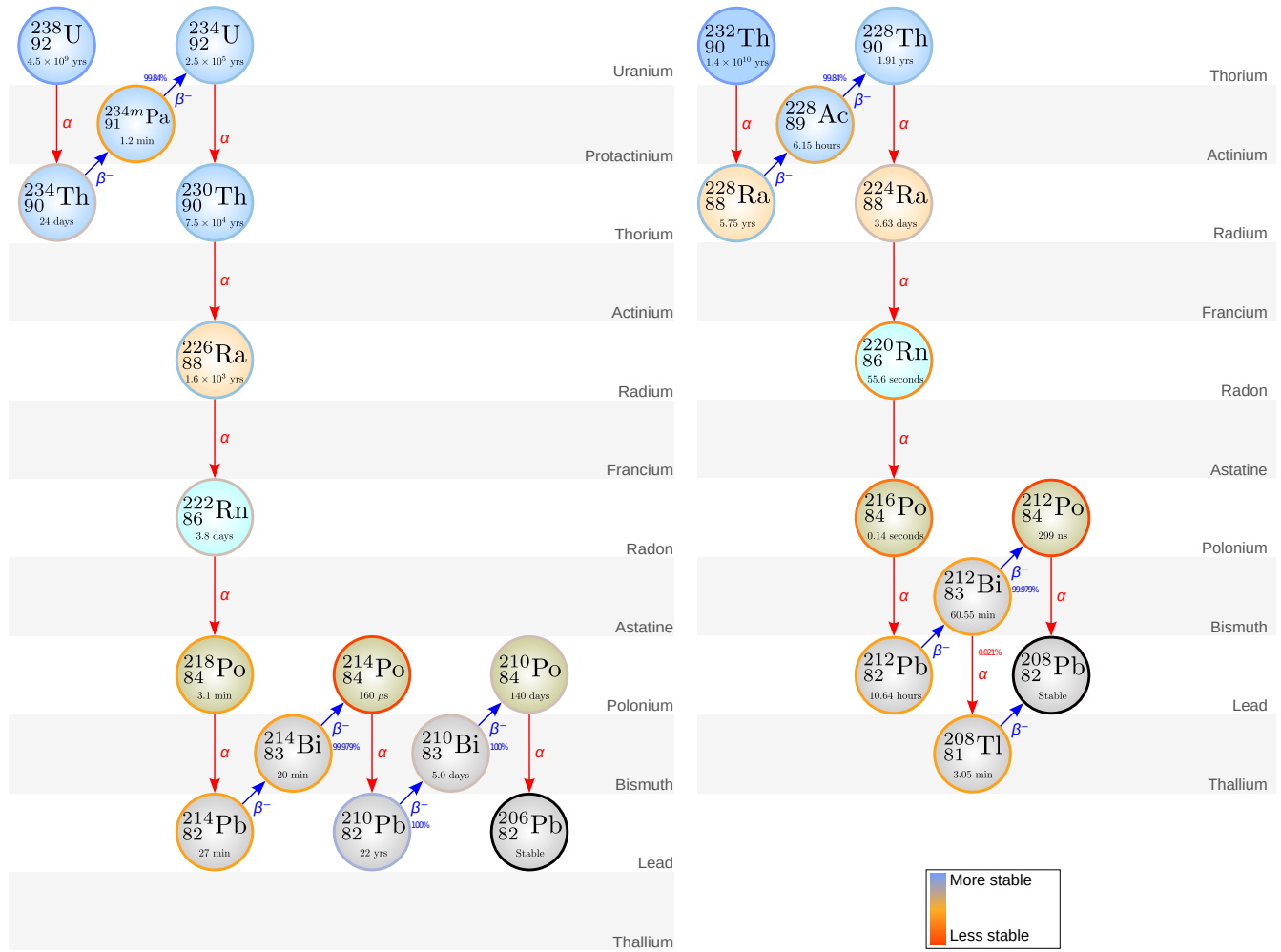


Figure 3.7: Decay chains of  $^{238}\text{U}$  and  $^{234}\text{Th}$ , with the half-life time indicated below each element.

the support structure, rock, and cement. Typical radioactive backgrounds include  $\alpha$ ,  $\beta$ ,  $\gamma$  rays and neutrons. Among them,  $\gamma$  rays and neutrons need a careful detector design. A buffer layer (e.g., water, mineral oil, or LS with quenched material) can significantly reduce the external background.

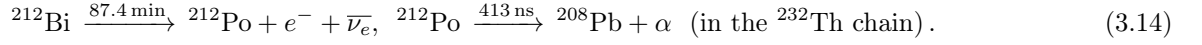
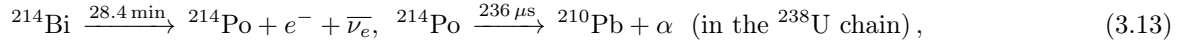
Internal backgrounds come from radioactive isotopes in the fiducial volume. Radioactive ions (e.g.,  $^{40}\text{K}$ ), noble gas ( $^{85}\text{Kr}$ ,  $^{39}\text{Ar}$ ), and products of  $^{238}\text{U}$  and  $^{234}\text{Th}$  decay chains (see Fig. 3.7) can be dissolved in water or liquid scintillator.

Table 3.2 summarizes natural radioactive background levels for water and liquid scintillator detectors, according to studies for SNO and Borexino [312, 313, 314, 315, 316]. Backgrounds from  $^{238}\text{U}$  and  $^{232}\text{Th}$  chains and  $^{40}\text{K}$  in water are significantly higher (roughly by two orders of magnitude) than those in liquid scintillator. This is because the binding ability of water molecules with inorganic ions is stronger than that of organic liquid scintillator. Hence the solubility of inorganic ions in water is higher than that in liquid scintillator.

It is important to note that both the  $^{238}\text{U}$  and  $^{232}\text{Th}$  chains contain the inert gas element radon ( $^{222}\text{Rn}$ ,  $^{220}\text{Rn}$ ), which is difficult to be removed chemically. The radon isotopes can continuously enter the fiducial volume emanation from external materials.

Tagging some of decays in the  $^{238}\text{U}$  and  $^{232}\text{Th}$  chains is possible by exploiting a fast decay sequence existing in each

of the chains:



Here  ${}^{214}\text{Bi}$  and  ${}^{212}\text{Bi}$  are  $\beta$  emitters, and their decays are followed by  $\alpha$  decays with a mean life of 236  $\mu\text{s}$  or 413 ns. This feature allows one to evaluate the amount of radon in the detector and to infer the contamination by isotopes in the  ${}^{238}\text{U}$  and  ${}^{232}\text{Th}$  chains. However, successful tagging  ${}^{214}\text{Bi}$ - ${}^{214}\text{Po}$  and  ${}^{212}\text{Bi}$ - ${}^{212}\text{Po}$  does not imply that the background caused by other isotopes in the  ${}^{238}\text{U}$  and  ${}^{232}\text{Th}$  chains can be effectively suppressed. For example, the  ${}^{210}\text{Bi}$ - ${}^{210}\text{Po}$  decay sequence has mean-life times of 7.23 and 200 days. Hence the background of  ${}^{210}\text{Bi}$  and  ${}^{210}\text{Po}$  (shown in Fig. 3.6) can not be reduced by time coincidence.

## 4. Prospects of solar neutrino experiments

Future neutrino experiments will feature higher statistics, lower backgrounds, better energy and angular resolution, and new detection channels. Table 4.1 summarizes past, present and future (including under-construction and proposed) neutrino detectors for solar neutrino measurements.

Table 4.1: Summary of past, present, and future solar neutrino detectors.

Detectors	Depth [m]	Cosmic $\mu^\pm$ flux [ $\text{cm}^{-2}\text{s}^{-1}$ ]	Type	Fiducial mass [ton]	Live period	Location
Homestake [7]	1478	$4.4 \times 10^{-9}$ [42]	$\text{C}_2\text{Cl}_4$	615	1968-1994	South Dakota, USA
GALLEX/GNO [317]	1400	$3.3 \times 10^{-8}$ [302]	$\text{GaCl}_3$	$30.3_{(\text{Ga})}$	1991-2003	Gran Sasso, Italy
SAGE [318]	2100	$3 \times 10^{-9}$ [318]	Ga metal	50	1989-2007	Baksan, Russia
SNO [319]	2092	$3.3 \times 10^{-10}$ [320]	$\text{D}_2\text{O}$	1k	1999-2006	Sudbury, Canada
SK I-IV [86]	1000	$\sim 10^{-7}$ [321]	Water	22.5k	1996-2018	Kamioka, Japan
KamLAND [322, 323]	1000	$\sim 10^{-7}$ [321]	LS	1k	2002-2011	Kamioka, Japan
Borexino [301]	1400	$3.3 \times 10^{-8}$ [302]	LS	278	2007-2021	Gran Sasso, Italy
SNO+ [324]	2092	$3.3 \times 10^{-10}$ [320]	LS	800	2018-	Sudbury, Canada
SK-GD [325, 326]	1000	$\sim 10^{-7}$ [321]	Water	22.5k	2020-	Kamioka, Japan
JUNO [327]	700	$4 \times 10^{-7}$ [327]	LS	20k	Future	Jianmeng, China
Hyper-K [38, 321]	650	$\sim 10^{-6}$ [321]	Water	187k	Future	Kamioka, Japan
DUNE [40, 328]	1500	$4.4 \times 10^{-9}$ [42]	LAr	40k	Future	South Dakota, USA
THEIA [42]	1500	$4.4 \times 10^{-9}$ [42]	WbLS	25k/100k	Future	South Dakota, USA
JNE [41]	2400	$2.6 \times 10^{-10}$ [306]	SLS	2k	Future	Jinping, China

As can be seen from the table, water Cherenkov and liquid scintillator (LS) detectors are still taking their roles in current and future solar neutrino observations. The low-background LS experiment Borexino has succeeded dramatically as a solar neutrino observatory. The measurement of  ${}^7\text{Be}$  neutrinos, which was its primary scientific goal, has achieved excellent precision ( $\sim 5\%$ ) [329]. Moreover, it measured the pp neutrino flux with a precision of  $\sim 10\%$  [34]. It has been able to resolve (at  $7\sigma$  C.L.) the component of CNO neutrinos from complex backgrounds and other solar signals [44].

It is worth mentioning that these remarkable achievements were accomplished by Borexino with only 278 ton LS in the fiducial volume, while its successors, including SNO+ and JNE, will have significantly larger fiducial masses (800 tons and 2 kilotons, respectively) and lower backgrounds (by two orders of magnitude in terms of cosmic muon flux)—see Tab. 4.1 and Fig. 3.3. KamLAND, as a long-baseline reactor neutrino experiment, has played an important role in both the measurements of solar neutrino mixing parameters ( $\theta_{12}$  and  $\Delta m_{12}$ ) and solar neutrino fluxes [322, 323], and JUNO can be viewed as its successor, with the fiducial mass 20 times as large as that of KamLAND.

On the other hand, the capability of water-based detectors to detect solar neutrinos will be substantially improved with the Super-Kamiokande detector running in the Gd-doped phase (since 2020), and the future upgrade—Hyper-Kamiokande. THEIA, a Water-based Liquid Scintillator (WbSL) experiment, has been proposed, with a 25 kt fiducial mass at the initial phase and a possible upgrade to 100 kt [42]. WbSL features the directionality of water Cherenkov detectors, LS-like energy measurement (low energy thresholds, high energy resolution), and high chemical solubility for



loading isotopes like  ${}^7\text{Li}$  to measure low-energy neutrino spectroscopy.

In addition, the technology of liquid noble gas (liquid Ar, liquid Xe) detectors advances rapidly, and the scale of such detectors will expand considerably in the upcoming years. It might provide new insight into solar neutrino physics. For example, the low-threshold elastic scattering in such detectors can be sensitive to new physics related to neutrino magnetic moments and light mediators, as reviewed in Sec. 2.3.

Below, we elucidate the improvement and novelty of the next-generation neutrino detectors and discuss the expected gains in physics from these experiments.

## 4.1. Water Cherenkov detectors

Historically, Kamiokande [330, 331, 332, 333] and Irvine-Michigan-Brookhaven (IMB) [334, 335] experiments based on the water Cherenkov technique have made groundbreaking contributions to solar and atmospheric neutrino observations and the discovery of supernova 1987A neutrinos. Today water-based Cherenkov detectors, due to their low costs, mature technologies, and the feature of being easy to expand, are still a good option for future neutrino experiments.

### 4.1.1. SK-Gd

As the successor of Kamiokande, Super-Kamiokande (SK) is a gigantic water Cherenkov detector located 1 km underground in the Kamioka mine in Hida City, Gifu Prefecture, Japan. It consists of a cylindrical tank measuring 39.3 m in diameter and 41.4 m in height, filled with 50 kilo-ton water, and equipped with 11129 inner<sup>17</sup> and 1885 veto PMTs [86]. Since 1996, it has undergone four data-taking phases, SK-I to SK-IV, and accomplished a series of profound measurements of solar, atmospheric, and accelerator neutrino oscillations, which are crucial to the now-established framework of three neutrino mixing.

Since 2020, SK has entered the SK-Gd phase in which Gadolinium (Gd) in the form of  $\text{Gd}_2(\text{SO}_4)_3 \cdot 8\text{H}_2\text{O}$  has been added to the pure water for high efficiency of neutron tagging, as initially proposed by Beacom and Vagins [336]. The neutron capture by Gd has a much larger cross section than that by Hydrogen (which would be the case if it is pure water) and also produces a clear signal presenting as an 8 MeV gamma cascade. With only a 0.02% concentration of Gd sulfate octahydrate in water, the neutron-Gd capture rate can reach approximately the same as the neutron-Hydrogen capture rate [325]. For a 0.2% concentration, 90% of neutrino captures will be on Gd. The high efficiency of neutron tagging will drastically enhance SK's capability to detect the diffuse supernova background (DSNB) [337]<sup>18</sup>.

For solar neutrinos, this operation also makes an impact. With the loading of Gd, SK will be able to separate well solar  ${}^8\text{B}$  neutrino events from cosmogenic background events, which are usually accompanied by the production of neutrons in  ${}^{16}\text{O}$  spallation—see Sec. 3.5.1. Hence the measurement of solar  ${}^8\text{B}$  neutrinos will be improved, due to the reduced background. Consequently, the measurements of the upturn due to the MSW effect in the Sun and the day-night asymmetry due to the Earth's matter effect are also expected to be improved. The SK-Gd detector, with its reduced background, might be able to see a hint of hep neutrinos since the expected event rate of hep neutrinos in the 15.5-19.5 MeV range is about 0.064 event/year/kt [86], high enough for the 22.5 kt detector to detect a few events within several

---

<sup>17</sup>Initially, the number of inner PMTs was 11146, reduced to 5182 after an accident of chain-reaction PMT implosions in 2001, and finally replenished to 11129 in 2006.

<sup>18</sup>Also referred to as Supernova Relic Neutrinos (SRN) in the literature—see, e.g., SK measurements [338, 339] and early theoretical calculations [340, 341, 342]. The name of DSNB occurred later [343, 344, 345] but has become more frequently used in recent years.

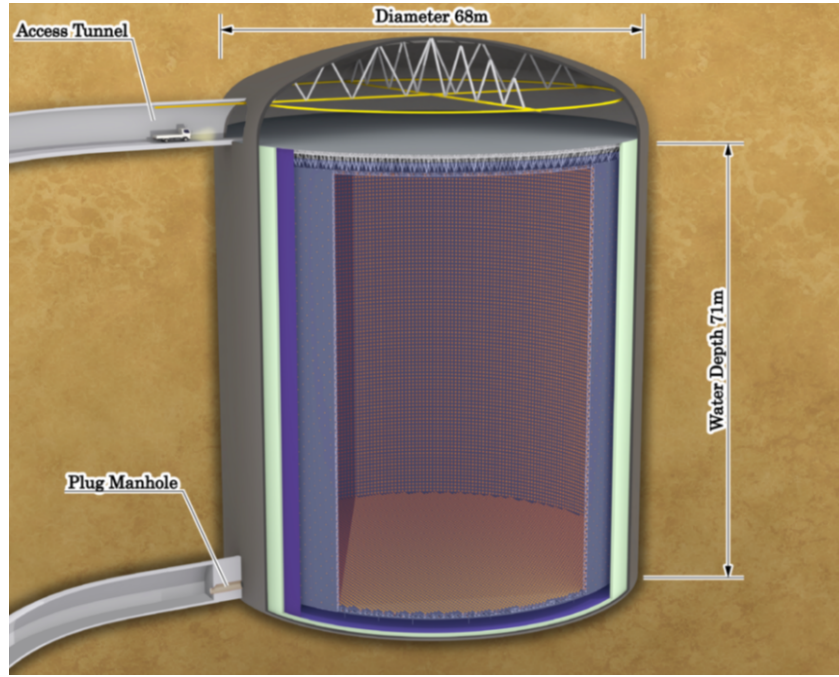


Figure 4.1: The schematic view of the Hyper-Kamiokande water Cherenkov detector [38].

years (In this case, the background reduction is crucial). In addition, searches for solar antineutrinos (see Sec. 2.3) will benefit substantially from the high efficiency of neutrino tagging in an IBD event.

#### 4.1.2. Hyper-Kamiokande

The Hyper-Kamiokande (HK), located 8 km south of the SK site, is a next-generation water Cherenkov detector. It will expand the scale enormously to promote its goals for various physics topics [38]. The primary goal is to study CP violation in neutrino oscillation. Meanwhile it also serves as one of the most important experiments for high-statistics solar neutrino observations and proton decay searches. Figure 4.1 shows a schematic view of the HK detector. The cylindrical tank of HK has a double-cylinder structure, with the outer (inner) cylinder measuring 74 m (70.8 m) in diameter and 60 m (54.8 m) in height. It will be filled with 258 kt water (fiducial mass 187 kt) and equipped with 40,000 inner and 6,700 outer PMTs [38]. The construction has been undertaken since 2020 and is expected to collect data starting from 2027 [346].

HK uses PMTs with higher single-photon detection efficiency, 24% (to be compared with 12% in SK), and better single-photon timing resolution, 1 ns (to be compared with 2-3 ns in SK)—see Table VII in Ref. [38]. Therefore, the energy threshold of detecting low-energy electrons might be further improved, possibly below 3.5 MeV<sup>19</sup>. With this threshold, the up-turn predicted by the MSW effect could be probed at  $3\sigma$  ( $5\sigma$ ) C.L. within 2 (11) years of exposure to solar  $^8\text{B}$  neutrinos [38]. However, due to the thinner rock overburden, the cosmic-ray spallation background will be higher, affecting the solar neutrino study. A specific analysis of this background is necessary and has already been performed at SK. The sensitivity of the day-night asymmetry measurement is within the range of  $4-8\sigma$  depending on the systematics for 10 years of exposure. With a 10-year exposure, HK would be able to measure hep solar neutrinos at  $3.2\sigma$  C.L. if the spallation background could be neglected.

<sup>19</sup>At pointed out in Ref. [38], page 185, the background caused by  $^{214}\text{Bi}$  beta decay which has an endpoint energy of 3.27 MeV may severely limit the energy threshold.

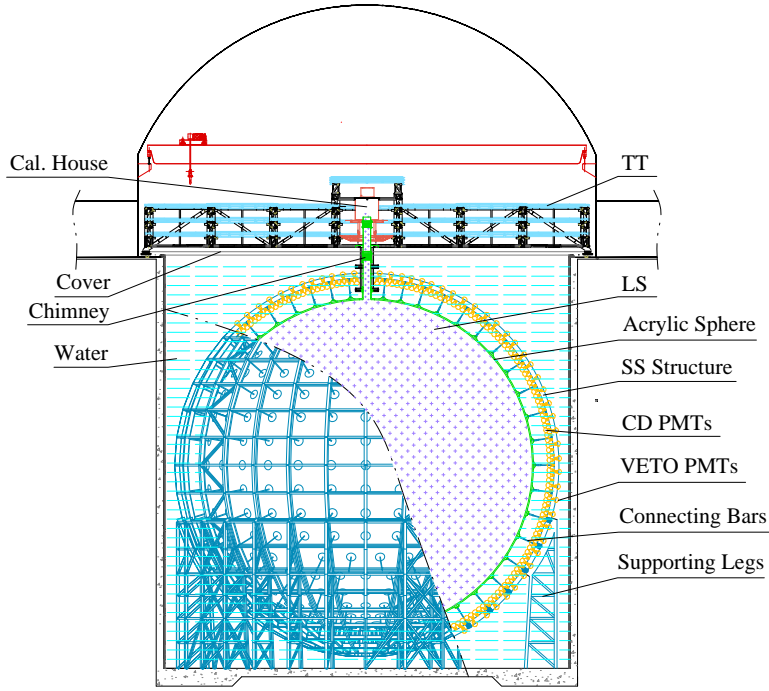


Figure 4.2: A schematic view of the JUNO detector [327].

## 4.2. Liquid scintillator detectors

Liquid scintillator, due to its high light yield, is commonly used for MeV neutrino detection. In Borexino, the LS used for detection is a solution of 2,5-diphenyloxazole (PPO) in pseudocumene (PC, 1,2,4-trimethylbenzene) [301]. Now linear-alkyl-benzene (LAB) is more commonly adopted as the solvent (e.g. the JUNO LS is a solution of 2.5 g/L PPO in LAB, with additional bis-MSB as a wavelength shifter) due to a number of optical advantages as well as the comparability with acrylic vessels [324, 327].

### 4.2.1. JUNO

The Jiangmen Underground Neutrino Observatory (JUNO) is currently the largest LS detector ever built, containing 20 kt LS in a spherical acrylic vessel with an inner diameter of 35.4 m. The acrylic vessel is submerged in a water pool and roofed by Top Tracker (TT) for muon veto—see Fig. 4.2 for a schematic view of the detector [327].

The detector is equipped with 15,000 Microchannel-Plate (MCP) PMTs and 5,000 dynode-type PMTs. The PMTs have high photon detection efficiencies: 28.9% for MCP PMTs and 28.1% for dynode PMTs. Due to the high performance of the PMTs deployed, together with 80% PMT coverage, JUNO features an unprecedented energy resolution. The expected yield of photoelectrons can reach 1345 per MeV, which is significantly higher than Borexino ( $\sim 500$  photoelectrons/MeV). Consequently, the relative energy resolution, mainly determined by the statistics of photoelectrons, will reach an unprecedented level,  $3\%/\sqrt{E/\text{MeV}}$  [327].

Like KamLAND, JUNO is primarily a long-baseline reactor neutrino experiment that is sensitive to the long oscillation mode (subject to  $\theta_{12}$  and  $\Delta m_{21}^2$ ) of reactor neutrinos. The oscillation parameters,  $\sin^2 \theta_{12}$  and  $\Delta m_{21}^2$ , which are relevant to the flavor conversion of solar neutrinos, will be measured to 0.5  $\sim$  0.7% relative precision [39]. The high precision

measurements of  $\theta_{12}$  and  $\Delta m_{21}^2$  at JUNO are very important to future solar neutrino physics because they can be used to calibrate solar neutrino oscillations.

JUNO has the advantage of conducting a high-statistics measurement of solar neutrino fluxes. However, the cosmogenic background is high due to the relatively shallow overburden (700 m). This shortcoming, which was also a concern in KamLAND’s measurement of solar neutrinos, can be partially compensated by stringent muon spallation cuts, enormously high statistics, and significantly improved energy resolution in JUNO.

The primary channel for solar neutrino detection in JUNO is elastic  $\nu + e^-$  scattering. According to the study in Ref. [347], a 10-year data taking will generate 60,000 recoil electrons and 30,000 background events. Therefore, in addition to the aforementioned precision measurements of  $\theta_{12}$  and  $\Delta m_{21}^2$  using reactor neutrinos, JUNO is also capable to measure them using solar neutrinos. The precision is expected to be around 7% and 16%  $\sim$  21% for  $\sin^2 \theta_{12}$  and  $\Delta m_{21}^2$  respectively [347].

In addition to elastic scattering, a considerable amount of  $^{13}\text{C}$  nuclei in LS ( $9 \times 10^{30}$  per 20kt) can also allow JUNO to detect solar neutrinos via the CC and NC reactions [348, 349]:

$$\text{CC} : \nu_e + {}^{13}\text{C} \rightarrow e^- + {}^{13}\text{N}, \quad E_\nu^{\text{thre}} = 2.2\text{MeV}, \quad (4.1)$$

$$\text{NC} : \nu + {}^{13}\text{C} \rightarrow \nu + {}^{13}\text{C}^*(3^-/2), \quad E_\nu^{\text{thre}} = 3.7\text{MeV}. \quad (4.2)$$

A preliminary estimation assuming 100% detection efficiency and a 200 kt-year exposure indicates that the CC (NC) channel would observe 3768 (3165) and 14 (13.5) events for  $^8\text{B}$  and hep neutrinos, respectively [327]. However, background-driven cuts imposed on them may substantially reduce the actual numbers of signal events, which requires a more dedicated study.

#### 4.2.2. SNO+

Upgraded from SNO, the SNO+ experiment replaces the heavy water in SNO with LAB-PPO LS (PPO concentration 2g/L). It recycles SNO’s acrylic vessel, PMTs, support structure, light water system, and electronics and trigger system [324, 350]. Although the primary scientific goal is to search for neutrino-less double beta decay, SNO+ can still continue its solar neutrino study. One of the most significant advantages that SNO+ inherits from SNO is the ultra-low cosmogenic background, which is almost negligible above 6 MeV for solar neutrino events—see previous discussions in Sec. 3.5.1 and Fig. 3.5.

Serving as a low-background solar neutrino detector, SNO+ can provide precision measurements of solar neutrinos. According to the sensitivity study in Ref. [350], with one year of data in the LS phase, the  $^7\text{Be}$  and  $^8\text{B}$  fluxes can be measured to 4% and 8%, respectively. Due to its low cosmogenic background and large target volume compared to Borexino, SNO+ may significantly contribute to observing CNO neutrinos. But it will rely on how well the radioactive background can be obtained and if the direction information can be extracted as what Borexino has achieved. Assuming a conservative uncertainty for separating the  $^{210}\text{Bi}$  background and CNO, the predicted uncertainty of the CNO flux measurement is 15% [350]. It should be emphasized that even in the phase of neutrino-less double beta decay searches with Te loaded, SNO+ can still detect  $^8\text{B}$  neutrinos down to the endpoint of Te double beta decay, 2.53 MeV. Precision measurements of  $^8\text{B}$  neutrinos above this endpoint allows SNO+ to probe the up-turn predicted by the MSW mechanism.

### 4.3. Hybrid detectors

Can the virtues of water Cherenkov detectors (good directionality) and pure LS detectors (good energy resolution, low-energy thresholds) be combined in MeV-scale neutrino detectors? Recent efforts in developing water-based LS (WbLS) and slow LS will make the combination possible in future hybrid detectors.

#### 4.3.1. THEIA

THEIA (after the Titan Goddess of light) [42] is a proposed large-scale (25-100 kt) multi-purpose detector with a broad range of physics goals, including measurements of long-baseline neutrino oscillations (e.g., serving as one of DUNE’s far detectors), solar neutrinos, supernova neutrinos, neutrinoless double beta decay, etc. The experiment intends to adopt WbLS, which has been actively investigated as a future alternative to LS [351]. The basic idea of WbLS is to mix LS with water so that ionization (the dominant energy deposited by a recoil electron) can be effectively converted to optical signals. Meanwhile, the observability of Cherenkov light is retained with new PMTs or ultrafast LAPPDs (Large Area Picosecond Photo-Detectors). The amount of LS added to water typically varies from 1% to 10%, depending on the designed light yield, the PMTs’ capability of Cherenkov/scintillation separation, as well as the cost and environmental concerns. After considering these issues, Ref. [42] suggested that the light yield can be as high as 10% of LS. Hence WbLS can partially inherit the excellent energy resolution from LS.

With the capability to perform both direction and energy measurements, THEIA would be a powerful solar neutrino observatory featuring high-statistics, low-threshold (MeV-scale) observations. For instance, it could improve the CNO neutrino measurement to the precision of 4%  $\sim$  10%, assuming 100 kt WbLS with 5% LS is used—see Fig. 9 and Tab. 4 in Ref. [42]. Such a high precision measurement would allow THEIA to resolve the solar metallicity problem conclusively. The collaboration is also studying the physics potential of adding  $^7\text{Li}$  to the detector, and the impact of isotope loading.

#### 4.3.2. JNE

The Jinping Neutrino Experiment (JNE) [41, 306, 352] is a neutrino observatory for low-energy neutrino physics, astrophysics, and geophysics, to be built in the China JinPing underground Laboratory (CJPL) [353], located around 2400 m below Jinping Mountain, Sichuan Province, China. CJPL was constructed in two phases (CJPL-I and CJPL-II) and completed all the tunnel excavation in 2016, as shown in Fig. 4.3. Among all underground laboratories, CJPL has the lowest vertical cosmic muon flux and also the lowest reactor neutrino background. The total cosmic-ray muon flux at CJPL-I is measured to be  $(3.53 \pm 0.22_{\text{stat.}} \pm 0.07_{\text{sys.}}) \times 10^{-10} \text{cm}^{-2} \text{s}^{-1}$  [306]. The expected flux for the four major lab halls at CJPL-II varies with the individual hall location. Using the CJPL-I measurement extrapolated to CJPL-II gives about  $2.6 \times 10^{-10} \text{cm}^{-2} \text{s}^{-1}$ . Figure 4.4 compares its cosmic-ray muon flux and reactor neutrino flux with other underground laboratories, using data from Refs. [41, 306, 354]. The low background makes CJPL an ideal site for low-energy neutrino observations.

JNE plans to employ a new type of LS, known as slow LS, which features both high light yield and the capability of Cherenkov/scintillation separation [355, 356]. By reducing the concentration of the primary fluor, the pulse shape of the scintillation light is stretched to several tens of nanoseconds, allowing the prompt Cherenkov light component to be distinguishable. This new technique will enable JNE to measure both the electron direction and its energy, which are crucial in solar neutrino experiments.

Suppose JNE can fulfill its proposal of multi-kilo-ton fiducial target mass. In that case, it will provide high-precision

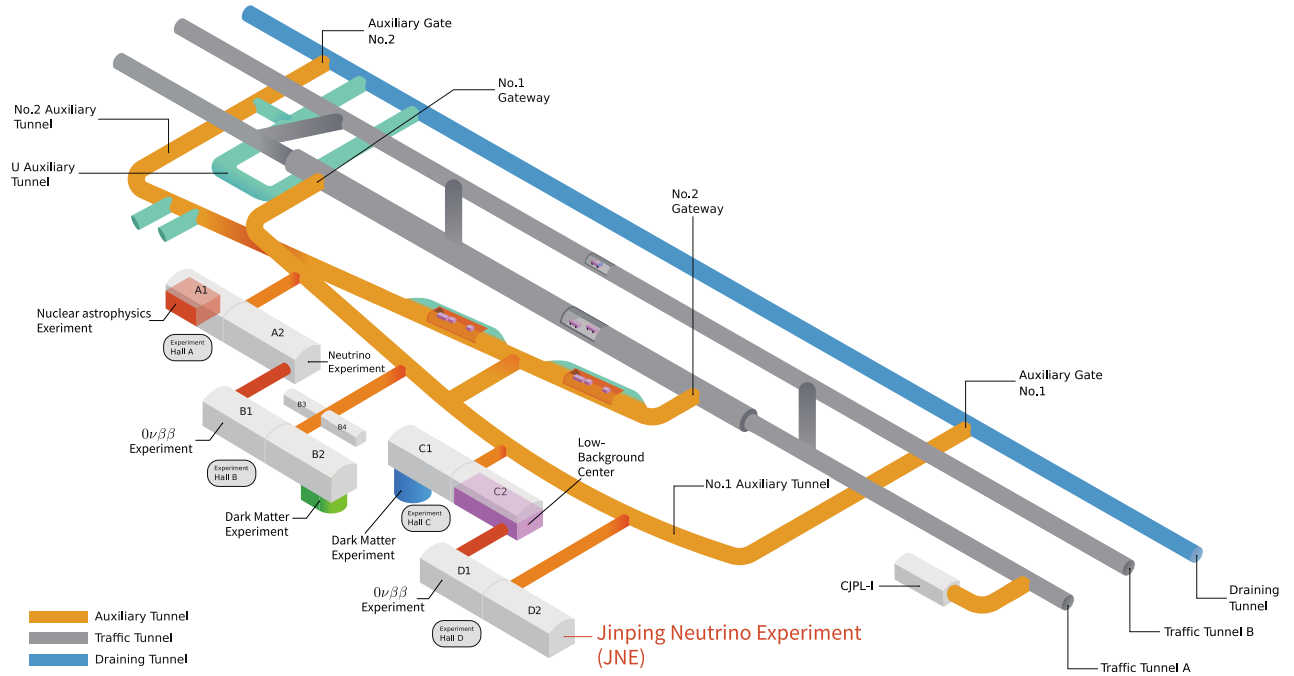


Figure 4.3: The layout of CJPL, including CJPL-I and CJPL-II. It may be subject to changes with new hall excavations. Figure provided by CJPL.

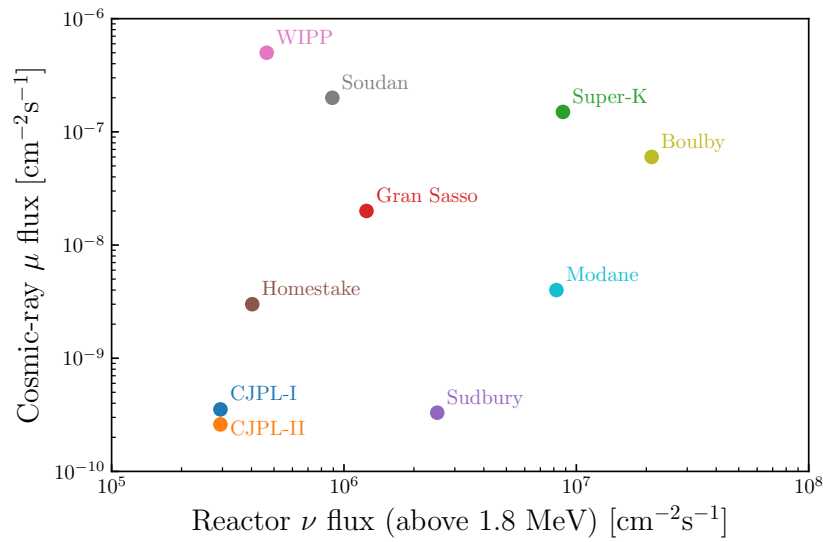


Figure 4.4: A comparison of cosmic-ray muon fluxes and reactor neutrino fluxes among underground laboratories. The muon flux data is taken from Ref. [41] and updated according to Ref. [306]. The reactor neutrino data is taken from Ref. [354].



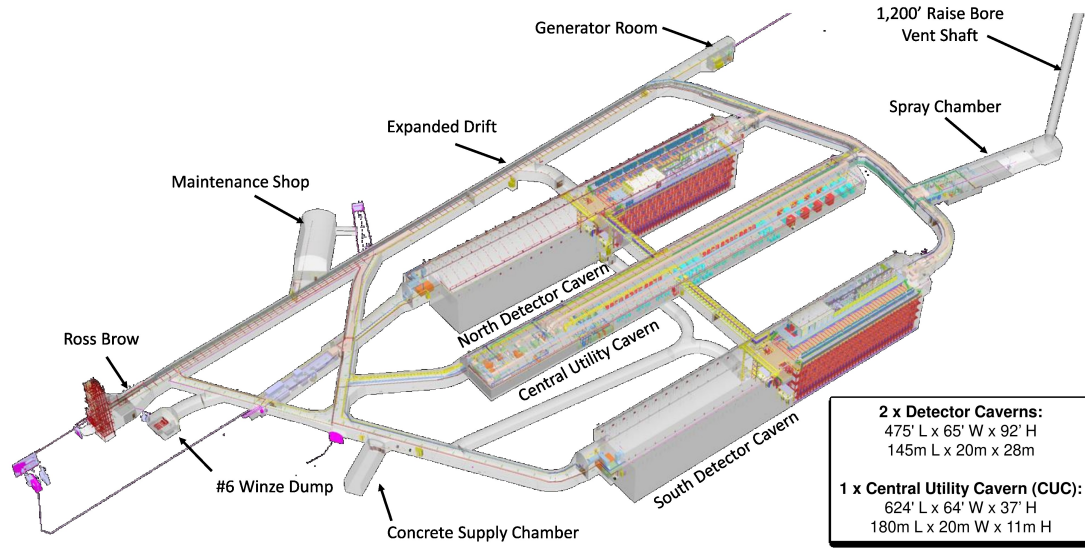


Figure 4.5: Far-site underground caverns for DUNE at SURF, with an overburden of 1478 m ( 4300 m.w.e). The vertical shaft is on the right. Phase I will have two detector modules. Figure taken from Ref. [328]

measurements of solar neutrino fluxes, particularly the low-energy components like pp and  ${}^7\text{Be}$  neutrinos. Assuming 500 photoelectrons per MeV can be attained (depending on the light yield and the PMT efficiency), these two neutrino fluxes can be measured within 0.5% and 0.4% statistical uncertainties, respectively—see Tab. 3.5 in Ref. [41]. In addition, JNE will also be able to observe CNO neutrinos with more than  $5\sigma$  statistical significance. Assuming the oscillation parameters are well determined with high precision, the high and low metallicity hypotheses can be resolved at more than  $5\sigma$  C.L. [41]. These achievements require demonstrating the Cherenkov scintillator technique in a large-volume neutrino detector. It needs the PMT waveform output and analysis in both online and offline stages. Despite the lowest cosmogenic background, low energy radioactive background control will be another challenging issue. The group is also investigating the possibility of loading lithium [275] or gallium [295] to enrich its solar neutrino research program.

#### 4.4. DUNE

The Deep Underground Neutrino Experiment (DUNE) [40, 328] is an accelerator-based long-baseline experiment at Sanford Underground Research Facility (SURF) in South Dakota, with the primary goal of discovering matter-antimatter asymmetries in neutrino flavor mixing. It consists of near and far detectors and is currently under the construction phase. According to the design, DUNE will eventually be equipped with four Liquid Argon (LAr) TPC<sup>20</sup> far detectors. In practical considerations, DUNE will be built in two phases. In Phase I, the far site will accommodate two 17-kt detector modules, as shown in Fig. 4.5. Each will have at least a 10-kt fiducial liquid argon target mass. The first physics results will appear around 2030. Phase II will fulfill the whole DUNE design goal within the next decade after the completion of Phase I [361].

As a large-scale neutrino experiment with the next generation of advanced detection technology, DUNE has apparent

<sup>20</sup>TPC stands for Time-Projection Chamber, while LAr TPC was first proposed by C. Rubbia [357] and realized in the ICARUS experiment [358, 359]. Due to its tracking ability and high target material density, LAr TPC was first proposed for  ${}^8\text{B}$  solar neutrino detection in the 1980s [360].

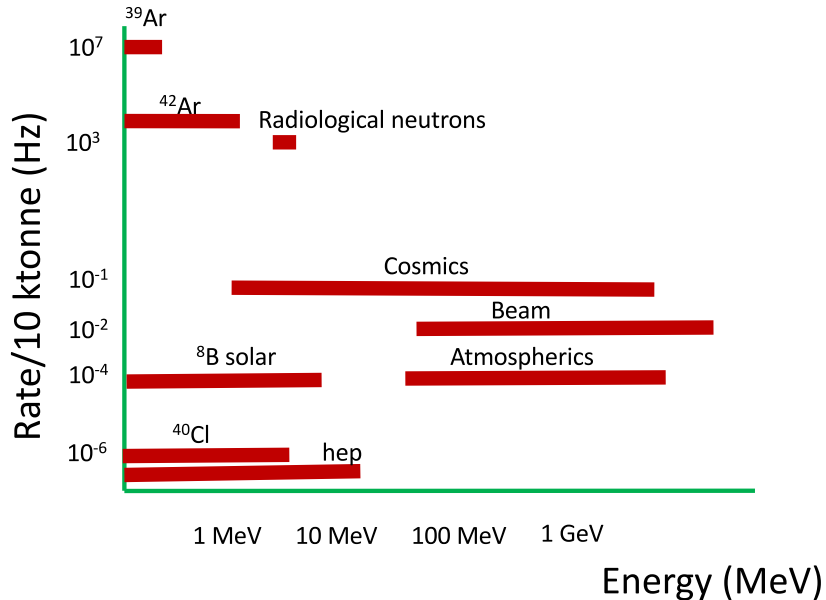


Figure 4.6: Expected solar neutrino event rates ( $^8\text{B}$  solar and hep) in DUNE far detectors and compared to other neutrinos, cosmic-ray and radioactive background sources. Figure taken from Ref. [364].

advantages for solar neutrinos above several MeV. In liquid argon, solar neutrinos can be detected either via the elastic  $\nu + e^-$  scattering or the CC process  $\nu_e + ^{40}\text{Ar} \rightarrow e^- + ^{40}\text{K}^*$ , which has a threshold of around  $4 \sim 5$  MeV [40] (see also Tab. 3.1) The large fiducial mass gives DUNE an opportunity for future solar neutrino physics study, in particular, for the measurements of  $^8\text{B}$  and hep solar neutrino fluxes [362]. Figure 4.6 shows the estimated event rates in one module adopting the single-phase far detector, indicating that DUNE would be able to detect  $^8\text{B}$  neutrinos at an event rate of about several counts/day/kT. If DUNE can well reconstruct the MeV-scale electron track, the measurement of  $^8\text{B}$  and hep fluxes can reach 2.5% and 11%, according to the study in Ref. [362]. Using the solar neutrino data, the neutrino mixing parameters  $\sin^2 \theta_{12}$  and  $\Delta m_{21}^2$  can be measured to 3% and 6%, respectively, better than the combination of all solar experiments to date.

Since the CC process of  $^{40}\text{Ar}$  has a larger cross section than  $\nu + e^-$  scattering and can directly relate the electron energy to the neutrino energy, DUNE will have the best chance to improve  $^8\text{B}$  flux precision and discover hep neutrinos — the last undiscovered solar neutrino component in the pp chain. However, these prospects rely on the performance of LAr TPC working in a large target volume and MeV energy scale. The challenging issues include the suppression of the radioactive background and the improvement of calibration at low energies [363].

## 4.5. Other experimental approaches

Despite many efforts to build large solar neutrino experiments, there are other experimental approaches to solar neutrino observations using small detectors. The smallness is a consequence of either large neutrino cross sections (in dark matter detectors) or higher neutrino fluxes (in space-based detectors).

### 4.5.1. Dark matter detectors

Dark matter (DM) detectors have the potential to measure solar neutrinos, which comprise the low-energy part of the ultimate background for DM direct detection, known as *the neutrino floor* in the literature. As the scales and detection



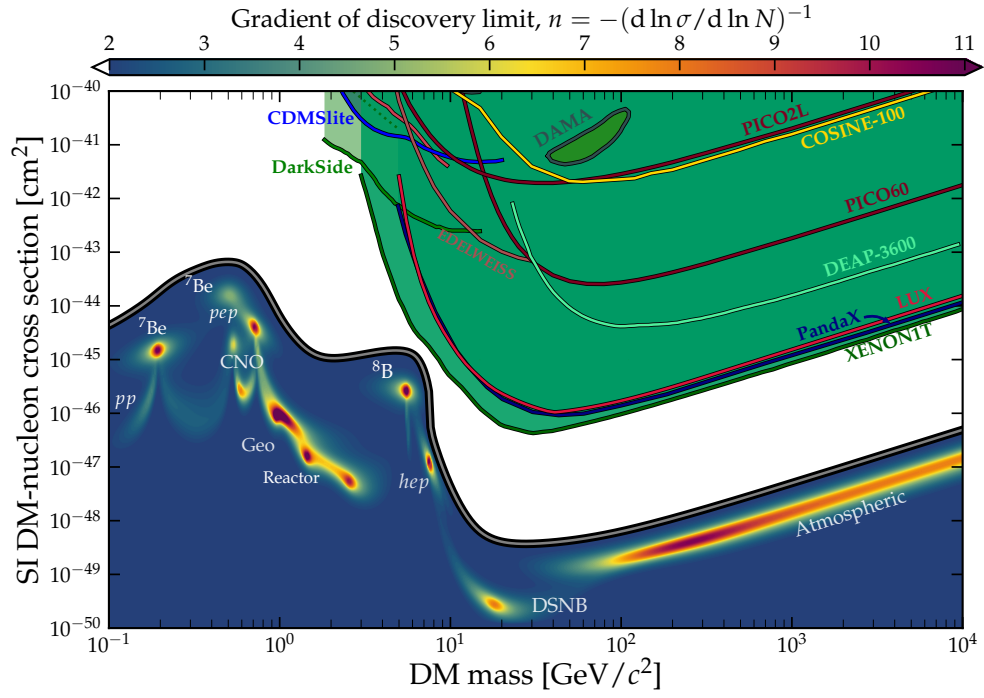


Figure 4.7: Solar neutrinos in the neutrino floor for DM direct detection. Upcoming liquid Xe experiments will soon be able to detect  $^8\text{B}$  solar neutrinos. Figure from Refs. [365, 366].

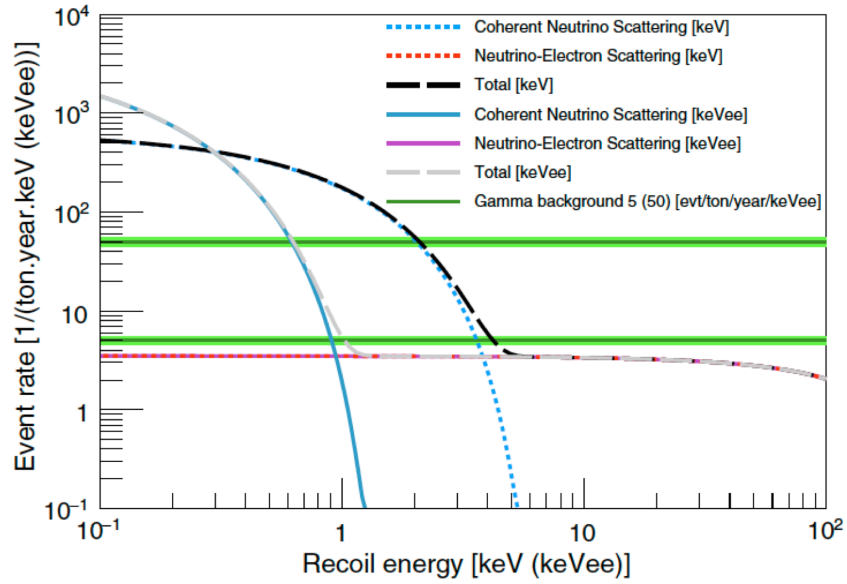


Figure 4.8: Solar neutrino event rates in a low-threshold Ge DM detector. The true recoil energy is presented in units of keV and the corresponding ionization energy, which is smaller than the true recoil energy due to quenching, is in units of keVee. Figure taken from Ref. [155].

thresholds of DM detectors have been improved drastically in recent years, they will soon be able to touch the solar neutrino floor—see Ref. [366] for a recent review. Figure 4.7 shows the status as of 2021.

It is known that the neutrino floor does not strictly stop DM detectors from detecting DM signals underneath the floor. First, the recoil spectra of DM and neutrinos do not have exactly the same shape. Second, their cross-sections with nuclei may have different dependencies on the neutron and proton composition. These differences could be used to distinguish between DM and neutrino signals if the statistics are high [367]. In addition, for the solar neutrino floor, one could employ the directionality of events to separate DM and neutrino signals [368]. Finally, annual or diurnal modulation might be present in DM signals [369, 370]. All these possibilities of searching for DM signals below the neutrino floor imply an important interplay between DM and solar neutrino detection in the future.

Detecting solar neutrinos in DM detectors relies on elastic neutrino scattering with electrons or nuclei. The latter is always coherent for solar neutrinos and the process is referred to as  $\text{CE}\nu\text{NS}$ —see discussions in Sec. 3.3. In the latest results of XENON-1T [371] and PandaX-4T [372] searching for solar neutrinos via  $\text{CE}\nu\text{NS}$ , no significant excess of events has been observed.

$\text{CE}\nu\text{NS}$  generically has a much larger cross section than elastic  $\nu + e^-$  scattering, but the recoil energy of a nucleus is much lower than that of an electron. Regarding this aspect, ultra-low threshold detectors such as those based on Germanium semiconductors might have certain advantages. In semiconductor detectors, nuclear recoils lead to ionization and generate electronic signals. The ionization (measured in units of keVee) is quantitatively related to the recoil energy (in units of keV) via quenching models, which have not been well calibrated yet in the sub-keV regime. Figure 4.8 shows the event rates of solar neutrinos expected in a Ge detector using the Lindhard ionization quenching factor model [155].

Elastic  $\nu + e^-$  scattering has a relatively small cross section. Hence detecting solar neutrinos via this process would require a large fiducial mass. Regarding this aspect, liquid Xe (e.g., LUX, PandaX, XENONnT) and Ar (DarkSide-20k [373]) detectors have a significant advantage over semiconductor detectors because the former can be easily scaled up to very large fiducial volumes (multi-ton scales or higher).

Successful detection of solar neutrinos in DM detectors is foreseeable for the upcoming multi-ton scale experiments. It will not only be crucial to the background study of DM detectors but also provides an important cross-check on conventional measurements of solar neutrino fluxes. Potential discrepancies would imply new physics such as quark NSI, neutrino magnetic moments, etc.

#### 4.5.2. Space-based detectors

The Neutrino Solar Observatory ( $\nu\text{SOL}$ ) has been proposed [374]. The idea is to send a neutrino detector with Gadolinium-Aluminum-Gallium Garnet scintillating crystal into space and operate in orbit close to the Sun. According to the inverse radius square law, the detector can detect the high-intensity solar neutrinos with a not-too-large target volume practicable for space programme. At  $r = 9R_{\odot}$ , which has been proven feasible by NASA’s Parker Solar Probe launched in 2018 [375], the solar neutrino intensity is increased by a factor of 600. Further enhancement up to  $10^4$  (corresponding to  $r = 10^{-2}\text{AU} \approx 2.2R_{\odot}$ ) might be possible [376].

Due to the enhanced flux, such a detector can be orders of magnitude smaller than those terrestrial neutrino detectors and yet reach the same high statistics. However, the background would be the severest concern since high-energy cosmic rays cannot be passively shielded in an effective way, though the iron shield can stop low-energy particles (e.g. electrons below 15 MeV). Active veto rejection techniques are required for background reduction. The technology developed in

such an experiment might also be useful for space-based DM direct detection if DM detectors are delivered to locations far away from the Sun to evade the limitation of the neutrino floor.

The physics gain of space-based solar neutrino detectors is yet to be investigated. One interesting possibility would be to probe off-axis solar neutrinos, which would allow us to verify the distribution of the neutrino production rate, as previously shown in Fig. 2.5. If neutrinos from the outer layers of the Sun (e.g.  $r > 0.3R_{\odot}$ ) are observed, it might be an important hint of DM accumulating in the Sun and annihilating to neutrinos—see discussions in Sec. 2.3.6.

## 5. Summary

*“For centuries the heavens have been a natural laboratory to test the classical laws of motion, and more recently to test Einstein’s theory of gravity. Today, astrophysics has become a vast playing ground for applications of the laws of microscopic physics, especially the properties of elementary particles and their interactions.”*<sup>21</sup> Indeed, the great achievement of solar neutrino observations, which eventually led to one of the most profound and surprising discoveries in particle physics—neutrino masses, is a perfect example.

With the upcoming next-generation neutrino detectors featuring higher statistics, lower backgrounds, and novel detection technologies, can we make another surprising discovery in future solar neutrino observations? The finding of neutrino masses implies the existence of new physics beyond the SM, which includes a variety of possibilities. Among them, some could potentially modify the standard MSW-LMA solution to the solar neutrino problem, as we have reviewed in Sec. 2. In addition, a few experimental anomalies and inconsistencies among existing measurements might be hints of the underlying new physics. Moreover, dark matter, with its abundant astrophysical and cosmological evidence of the existence and yet rather elusive particle physics nature, may have been affecting solar neutrino observations in an unnoticed way, calling for further experimental and theoretical investigations.

We can see that some predictions are still waiting for experimental confirmation, even within the most conservative framework. For example, the present experiments are still struggling to justify the day-night asymmetry and the up-turn expected from the standard neutrino oscillation theory. In addition, several components of the solar neutrino spectrum, including both old ones from the pp chain (hep,  ${}^7\text{Be}$ -II) and new ones from the CNO cycle (e.g.  ${}^{17}\text{F}$  decay,  $e$  ${}^{13}\text{N}$  electron capture, etc.), still await experimental probe. Observations of CNO neutrinos have just started, with the first success reported recently by Borexino. Future precision measurements of CNO neutrinos will help resolve the long-standing solar metallicity problem and also be of great importance to studying stellar nucleosynthesis in large-mass stars.

In summary, future solar neutrino observations will produce exciting new results and might make another surprising discovery. As history has demonstrated, studying solar neutrino physics may offer unique insight into not only our nearest star but also the most fundamental physics laws.

## Acknowledgments

We gratefully acknowledge useful discussions with Evgeny Akhmedov, John F. Beacom, Steven Biller, Alexei Yu. Smirnov, Ya-Kun Wang and Hanyu Wei. This work is funded by the National Natural Science Foundation of China, under grant No. 12127808 and No. 12141501.

---

<sup>21</sup>Quoted from Georg G. Raffelt’s book *Stars as Laboratories for Fundamental Physics* [377].

## References

- [1] J. N. Bahcall, Neutrino Astrophysics, Cambridge University Press, 1989. [doi:ISBN0-521-37975-X](#).
- [2] A. S. Eddington, The internal constitution of the stars, *The Observatory* 43 (1920) 341–358.
- [3] R. Davis, Jr., D. S. Harmer, K. C. Hoffman, Search for neutrinos from the sun, *Phys. Rev. Lett.* 20 (1968) 1205–1209. [doi:10.1103/PhysRevLett.20.1205](#).
- [4] B. Pontecorvo, Chalk River Report PD (1946) 205.
- [5] L. W. Alvarez, University of California Radiation Laboratory Report (1949) UCRL 328.
- [6] J. N. Bahcall, N. A. Bahcall, G. Shaviv, Present status of the theoretical predictions for the Cl-36 solar neutrino experiment, *Phys. Rev. Lett.* 20 (1968) 1209–1212. [doi:10.1103/PhysRevLett.20.1209](#).
- [7] B. T. Cleveland, T. Daily, R. Davis, Jr., J. R. Distel, K. Lande, C. K. Lee, P. S. Wildenhain, J. Ullman, Measurement of the solar electron neutrino flux with the Homestake chlorine detector, *Astrophys. J.* 496 (1998) 505–526. [doi:10.1086/305343](#).
- [8] J. N. Bahcall, R. K. Ulrich, Solar Models, Neutrino Experiments and Helioseismology, *Rev. Mod. Phys.* 60 (1988) 297–372. [doi:10.1103/RevModPhys.60.297](#).
- [9] P. Anselmann, et al., Solar neutrinos observed by GALLEX at Gran Sasso., *Phys. Lett. B* 285 (1992) 376–389. [doi:10.1016/0370-2693\(92\)91521-A](#).
- [10] J. N. Abdurashitov, et al., Solar neutrino flux measurements by the Soviet-American Gallium Experiment (SAGE) for half the 22 year solar cycle, *J. Exp. Theor. Phys.* 95 (2002) 181–193. [arXiv:astro-ph/0204245](#), [doi:10.1134/1.1506424](#).
- [11] K. S. Hirata, et al., Observation of B-8 Solar Neutrinos in the Kamiokande-II Detector, *Phys. Rev. Lett.* 63 (1989) 16. [doi:10.1103/PhysRevLett.63.16](#).
- [12] Y. Fukuda, et al., Measurements of the solar neutrino flux from Super-Kamiokande’s first 300 days, *Phys. Rev. Lett.* 81 (1998) 1158–1162, [Erratum: *Phys.Rev.Lett.* 81, 4279 (1998)]. [arXiv:hep-ex/9805021](#), [doi:10.1103/PhysRevLett.81.1158](#).
- [13] Q. R. Ahmad, et al., Direct evidence for neutrino flavor transformation from neutral current interactions in the Sudbury Neutrino Observatory, *Phys. Rev. Lett.* 89 (2002) 011301. [arXiv:nucl-ex/0204008](#), [doi:10.1103/PhysRevLett.89.011301](#).
- [14] A. B. McDonald, Nobel Lecture: The Sudbury Neutrino Observatory: Observation of flavor change for solar neutrinos, *Rev. Mod. Phys.* 88 (3) (2016) 030502. [doi:10.1103/RevModPhys.88.030502](#).
- [15] B. Pontecorvo, Mesonium and anti-mesonium, *Sov. Phys. JETP* 6 (1957) 429.
- [16] B. Pontecorvo, Inverse beta processes and nonconservation of lepton charge, *Zh. Eksp. Teor. Fiz.* 34 (1957) 247.
- [17] Z. Maki, M. Nakagawa, S. Sakata, Remarks on the unified model of elementary particles, *Prog. Theor. Phys.* 28 (1962) 870–880. [doi:10.1143/PTP.28.870](#).

- [18] B. Pontecorvo, Neutrino experiments and the problem of conservation of leptonic charge, *Zh. Eksp. Teor. Fiz.* 53 (1967) 1717–1725.
- [19] L. Wolfenstein, Neutrino Oscillations in Matter, *Phys.Rev. D17* (1978) 2369–2374. [doi:10.1103/PhysRevD.17.2369](https://doi.org/10.1103/PhysRevD.17.2369).
- [20] S. P. Mikheev, A. Yu. Smirnov, Resonance Amplification of Oscillations in Matter and Spectroscopy of Solar Neutrinos, *Sov. J. Nucl. Phys.* 42 (1985) 913–917, [*Yad. Fiz.*42,1441(1985)].
- [21] S. P. Mikheev, A. Yu. Smirnov, Resonant amplification of neutrino oscillations in matter and solar neutrino spectroscopy, *Nuovo Cim. C9* (1986) 17–26. [doi:10.1007/BF02508049](https://doi.org/10.1007/BF02508049).
- [22] S. L. Glashow, L. M. Krauss, 'just so' neutrino oscillations, *Phys. Lett. B* 190 (1987) 199–207. [doi:10.1016/0370-2693\(87\)90867-7](https://doi.org/10.1016/0370-2693(87)90867-7).
- [23] A. Cisneros, Effect of neutrino magnetic moment on solar neutrino observations, *Astrophys. Space Sci.* 10 (1971) 87–92. [doi:10.1007/BF00654607](https://doi.org/10.1007/BF00654607).
- [24] L. B. Okun, M. B. Voloshin, M. I. Vysotsky, Neutrino electrodynamics and possible effects for solar neutrinos, *Sov. Phys. JETP* 64 (1986) 446–452.
- [25] C.-S. Lim, W. J. Marciano, Resonant Spin - Flavor Precession of Solar and Supernova Neutrinos, *Phys. Rev. D* 37 (1988) 1368–1373. [doi:10.1103/PhysRevD.37.1368](https://doi.org/10.1103/PhysRevD.37.1368).
- [26] E. K. Akhmedov, Resonant Amplification of Neutrino Spin Rotation in Matter and the Solar Neutrino Problem, *Phys. Lett. B* 213 (1988) 64–68. [doi:10.1016/0370-2693\(88\)91048-9](https://doi.org/10.1016/0370-2693(88)91048-9).
- [27] L. Wolfenstein, Neutrino oscillations and stellar collapse, *Phys. Rev. D* 20 (1979) 2634–2635. [doi:10.1103/PhysRevD.20.2634](https://doi.org/10.1103/PhysRevD.20.2634).
- [28] E. Roulet, Msw effect with flavor changing neutrino interactions, *Phys. Rev. D* 44 (1991) R935–R938. [doi:10.1103/PhysRevD.44.R935](https://doi.org/10.1103/PhysRevD.44.R935).
- [29] M. M. Guzzo, A. Masiero, S. T. Petcov, On the msw effect with massless neutrinos and no mixing in the vacuum, *Phys. Lett. B* 260 (1991) 154–160. [doi:10.1016/0370-2693\(91\)90984-X](https://doi.org/10.1016/0370-2693(91)90984-X).
- [30] J. N. Bahcall, N. Cabibbo, A. Yahil, Are neutrinos stable particles?, *Phys. Rev. Lett.* 28 (1972) 316–318. [doi:10.1103/PhysRevLett.28.316](https://doi.org/10.1103/PhysRevLett.28.316).
- [31] Z. G. Berezhiani, M. I. Vysotsky, Neutrino decay in matter, *Phys. Lett. B* 199 (1987) 281. [doi:10.1016/0370-2693\(87\)91375-X](https://doi.org/10.1016/0370-2693(87)91375-X).
- [32] S. Fukuda, et al., Solar B-8 and hep neutrino measurements from 1258 days of Super-Kamiokande data, *Phys. Rev. Lett.* 86 (2001) 5651–5655. [arXiv:hep-ex/0103032](https://arxiv.org/abs/hep-ex/0103032), [doi:10.1103/PhysRevLett.86.5651](https://doi.org/10.1103/PhysRevLett.86.5651).
- [33] C. Arpesella, et al., First real time detection of Be-7 solar neutrinos by Borexino, *Phys. Lett. B* 658 (2008) 101–108. [arXiv:0708.2251](https://arxiv.org/abs/0708.2251), [doi:10.1016/j.physletb.2007.09.054](https://doi.org/10.1016/j.physletb.2007.09.054).

- [34] G. Bellini, et al., Neutrinos from the primary proton–proton fusion process in the Sun, *Nature* 512 (7515) (2014) 383–386. [doi:10.1038/nature13702](https://doi.org/10.1038/nature13702).
- [35] M. Agostini, et al., First Simultaneous Precision Spectroscopy of  $pp$ ,  ${}^7\text{Be}$ , and  $pep$  Solar Neutrinos with Borexino Phase-II, *Phys. Rev. D* 100 (8) (2019) 082004. [arXiv:1707.09279](https://arxiv.org/abs/1707.09279), [doi:10.1103/PhysRevD.100.082004](https://doi.org/10.1103/PhysRevD.100.082004).
- [36] M. Agostini, et al., Comprehensive measurement of  $pp$ -chain solar neutrinos, *Nature* 562 (7728) (2018) 505–510. [doi:10.1038/s41586-018-0624-y](https://doi.org/10.1038/s41586-018-0624-y).
- [37] M. Agostini, et al., Experimental evidence of neutrinos produced in the cno fusion cycle in the sun, *Nature* 587 (2020) 577–582. [arXiv:2006.15115](https://arxiv.org/abs/2006.15115), [doi:10.1038/s41586-020-2934-0](https://doi.org/10.1038/s41586-020-2934-0).
- [38] K. Abe, et al., Hyper-Kamiokande Design Report (5 2018). [arXiv:1805.04163](https://arxiv.org/abs/1805.04163).
- [39] F. An, et al., Neutrino Physics with JUNO, *J. Phys. G* 43 (3) (2016) 030401. [arXiv:1507.05613](https://arxiv.org/abs/1507.05613), [doi:10.1088/0954-3899/43/3/030401](https://doi.org/10.1088/0954-3899/43/3/030401).
- [40] R. Acciarri, et al., Long-Baseline Neutrino Facility (LBNF) and Deep Underground Neutrino Experiment (DUNE): Conceptual Design Report, Volume 2: The Physics Program for DUNE at LBNF (12 2015). [arXiv:1512.06148](https://arxiv.org/abs/1512.06148).
- [41] J. F. Beacom, et al., Physics prospects of the Jinping neutrino experiment, *Chin. Phys. C* 41 (2) (2017) 023002. [arXiv:1602.01733](https://arxiv.org/abs/1602.01733), [doi:10.1088/1674-1137/41/2/023002](https://doi.org/10.1088/1674-1137/41/2/023002).
- [42] M. Askins, et al., THEIA: an advanced optical neutrino detector, *Eur. Phys. J. C* 80 (5) (2020) 416. [arXiv:1911.03501](https://arxiv.org/abs/1911.03501), [doi:10.1140/epjc/s10052-020-7977-8](https://doi.org/10.1140/epjc/s10052-020-7977-8).
- [43] D. Z. Freedman, Coherent Neutrino Nucleus Scattering as a Probe of the Weak Neutral Current, *Phys. Rev. D* 9 (1974) 1389–1392. [doi:10.1103/PhysRevD.9.1389](https://doi.org/10.1103/PhysRevD.9.1389).
- [44] S. Appel, et al., Improved measurement of solar neutrinos from the Carbon-Nitrogen-Oxygen cycle by Borexino and its implications for the Standard Solar Model (5 2022). [arXiv:2205.15975](https://arxiv.org/abs/2205.15975).
- [45] G. Bellini, et al., First evidence of pep solar neutrinos by direct detection in borexino, *Phys. Rev. Lett.* 108 (2012) 051302. [arXiv:1110.3230](https://arxiv.org/abs/1110.3230), [doi:10.1103/PhysRevLett.108.051302](https://doi.org/10.1103/PhysRevLett.108.051302).
- [46] J. P. Cravens, et al., Solar neutrino measurements in Super-Kamiokande-II, *Phys. Rev. D* 78 (2008) 032002. [arXiv:0803.4312](https://arxiv.org/abs/0803.4312), [doi:10.1103/PhysRevD.78.032002](https://doi.org/10.1103/PhysRevD.78.032002).
- [47] B. Aharmim, et al., Combined analysis of all three phases of solar neutrino data from the sudbury neutrino observatory, *Phys. Rev. C* 88 (2013) 025501. [arXiv:1109.0763](https://arxiv.org/abs/1109.0763), [doi:10.1103/PhysRevC.88.025501](https://doi.org/10.1103/PhysRevC.88.025501).
- [48] G. D. O. Gann, K. Zuber, D. Bemmerer, A. Serenelli, The Future of Solar Neutrinos, *Ann. Rev. Nucl. Part. Sci.* 71 (2021) 491–528. [arXiv:2107.08613](https://arxiv.org/abs/2107.08613), [doi:10.1146/annurev-nucl-011921-061243](https://doi.org/10.1146/annurev-nucl-011921-061243).
- [49] V. Antonelli, L. Miramonti, C. Pena Garay, A. Serenelli, Solar neutrinos, *Adv. High Energy Phys.* 2013 (2013) 351926. [arXiv:1208.1356](https://arxiv.org/abs/1208.1356), [doi:10.1155/2013/351926](https://doi.org/10.1155/2013/351926).
- [50] M. Wurm, Solar neutrino spectroscopy, *Phys. Rept.* 685 (2017) 1–52. [arXiv:1704.06331](https://arxiv.org/abs/1704.06331), [doi:10.1016/j.physrep.2017.04.002](https://doi.org/10.1016/j.physrep.2017.04.002).

- [51] A. Ianni, Solar neutrinos, *Prog. Part. Nucl. Phys.* 94 (2017) 257–281. [doi:10.1016/j.pnpnp.2017.01.001](https://doi.org/10.1016/j.pnpnp.2017.01.001).
- [52] M. Maltoni, A. Y. Smirnov, Solar neutrinos and neutrino physics, *Eur. Phys. J. A* 52 (4) (2016) 87. [arXiv:1507.05287](https://arxiv.org/abs/1507.05287), [doi:10.1140/epja/i2016-16087-0](https://doi.org/10.1140/epja/i2016-16087-0).
- [53] J. Christensen-Dalsgaard, Solar structure and evolution (7 2020). [arXiv:2007.06488](https://arxiv.org/abs/2007.06488), [doi:10.1007/s41116-020-00028-3](https://doi.org/10.1007/s41116-020-00028-3).
- [54] N. Vinyoles, A. M. Serenelli, F. L. Villante, S. Basu, J. Bergström, M. C. Gonzalez-Garcia, M. Maltoni, C. Peña Garay, N. Song, A new Generation of Standard Solar Models, *Astrophys. J.* 835 (2) (2017) 202. [arXiv:1611.09867](https://arxiv.org/abs/1611.09867), [doi:10.3847/1538-4357/835/2/202](https://doi.org/10.3847/1538-4357/835/2/202).
- [55] W. C. Haxton, R. G. Hamish Robertson, A. M. Serenelli, Solar Neutrinos: Status and Prospects, *Ann. Rev. Astron. Astrophys.* 51 (2013) 21–61. [arXiv:1208.5723](https://arxiv.org/abs/1208.5723), [doi:10.1146/annurev-astro-081811-125539](https://doi.org/10.1146/annurev-astro-081811-125539).
- [56] W. C. Haxton, P. D. Parker, C. E. Rolfs, Solar hydrogen burning and neutrinos, *Nucl. Phys. A* 777 (2006) 226–253. [arXiv:nuc1-th/0501020](https://arxiv.org/abs/nuc1-th/0501020), [doi:10.1016/j.nuclphysa.2005.02.088](https://doi.org/10.1016/j.nuclphysa.2005.02.088).
- [57] M. Salaris, S. Cassisi, *Evolution of Stars and Stellar Populations*, John Wiley & Sons Ltd., 2005.
- [58] E. G. Adelberger, et al., Solar fusion cross sections II: the pp chain and CNO cycles, *Rev. Mod. Phys.* 83 (2011) 195. [arXiv:1004.2318](https://arxiv.org/abs/1004.2318), [doi:10.1103/RevModPhys.83.195](https://doi.org/10.1103/RevModPhys.83.195).
- [59] H. A. Bethe, Energy production in stars, *Phys. Rev.* 55 (1939) 434–456. [doi:10.1103/PhysRev.55.434](https://doi.org/10.1103/PhysRev.55.434).
- [60] J. N. Bahcall, LINE VERSUS CONTINUUM SOLAR NEUTRINOS, *Phys. Rev. D* 41 (1990) 2964. [doi:10.1103/PhysRevD.41.2964](https://doi.org/10.1103/PhysRevD.41.2964).
- [61] L. C. Stonehill, J. A. Formaggio, R. G. H. Robertson, Solar neutrinos from CNO electron capture, *Phys. Rev. C* 69 (2004) 015801. [arXiv:hep-ph/0309266](https://arxiv.org/abs/hep-ph/0309266), [doi:10.1103/PhysRevC.69.015801](https://doi.org/10.1103/PhysRevC.69.015801).
- [62] F. L. Villante, ecCNO Solar Neutrinos: A Challenge for Gigantic Ultra-Pure Liquid Scintillator Detectors, *Phys. Lett. B* 742 (2015) 279–284. [arXiv:1410.2796](https://arxiv.org/abs/1410.2796), [doi:10.1016/j.physletb.2015.01.043](https://doi.org/10.1016/j.physletb.2015.01.043).
- [63] J. N. Bahcall, A. M. Serenelli, S. Basu, 10,000 standard solar models: a Monte Carlo simulation, *Astrophys. J. Suppl.* 165 (2006) 400–431. [arXiv:astro-ph/0511337](https://arxiv.org/abs/astro-ph/0511337), [doi:10.1086/504043](https://doi.org/10.1086/504043).
- [64] N. Grevesse, A. J. Sauval, Standard Solar Composition, *Space Sci. Rev.* 85 (1998) 161–174. [doi:10.1023/A:1005161325181](https://doi.org/10.1023/A:1005161325181).
- [65] M. Asplund, N. Grevesse, J. Sauval, The Solar chemical composition, *ASP Conf. Ser.* 336 (2005) 25. [arXiv:astro-ph/0410214](https://arxiv.org/abs/astro-ph/0410214), [doi:10.1016/j.nuclphysa.2005.06.010](https://doi.org/10.1016/j.nuclphysa.2005.06.010).
- [66] M. Asplund, N. Grevesse, A. J. Sauval, P. Scott, The chemical composition of the Sun, *Ann. Rev. Astron. Astrophys.* 47 (2009) 481–522. [arXiv:0909.0948](https://arxiv.org/abs/0909.0948), [doi:10.1146/annurev.astro.46.060407.145222](https://doi.org/10.1146/annurev.astro.46.060407.145222).
- [67] J. N. Bahcall, B. R. Holstein, Solar Neutrinos From the Decay of  $^8\text{B}$ , *Phys. Rev. C* 33 (1986) 2121–2127. [doi:10.1103/PhysRevC.33.2121](https://doi.org/10.1103/PhysRevC.33.2121).



- [68] W. T. Winter, S. J. Freedman, K. E. Rehm, J. P. Schiffer, The B-8 neutrino spectrum, *Phys. Rev. C* 73 (2006) 025503. [arXiv:nucl-ex/0406019](https://arxiv.org/abs/nucl-ex/0406019), [doi:10.1103/PhysRevC.73.025503](https://doi.org/10.1103/PhysRevC.73.025503).
- [69] M. Bhattacharya, E. G. Adelberger, H. E. Swanson, Precise study of the final-state continua in Li8 and B8 decays, *Phys. Rev. C* 73 (2006) 055802. [doi:10.1103/PhysRevC.73.055802](https://doi.org/10.1103/PhysRevC.73.055802).
- [70] M. K. Bacrania, N. M. Boyd, R. G. H. Robertson, D. W. Storm, Search for the second forbidden beta decay of B-8 to the ground state of Be-8, *Phys. Rev. C* 76 (2007) 055806. [arXiv:0710.5197](https://arxiv.org/abs/0710.5197), [doi:10.1103/PhysRevC.76.055806](https://doi.org/10.1103/PhysRevC.76.055806).
- [71] I. V. Moskalenko, S. Karakula, W. Tkaczyk, The Sun as the source of VHE neutrinos, *Astron. Astrophys.* 248 (1991) L5–L6.
- [72] D. Seckel, T. Stanev, T. K. Gaisser, Signatures of cosmic-ray interactions on the solar surface, *Astrophys. J.* 382 (1991) 652–666. [doi:10.1086/170753](https://doi.org/10.1086/170753).
- [73] I. V. Moskalenko, S. Karakula, Very high-energy neutrinos from the sun, *J. Phys. G* 19 (1993) 1399–1406. [doi:10.1088/0954-3899/19/9/019](https://doi.org/10.1088/0954-3899/19/9/019).
- [74] G. Ingelman, M. Thunman, High-energy neutrino production by cosmic ray interactions in the sun, *Phys. Rev. D* 54 (1996) 4385–4392. [arXiv:hep-ph/9604288](https://arxiv.org/abs/hep-ph/9604288), [doi:10.1103/PhysRevD.54.4385](https://doi.org/10.1103/PhysRevD.54.4385).
- [75] C. A. Argüelles, G. de Wasseige, A. Fedynitch, B. J. P. Jones, Solar Atmospheric Neutrinos and the Sensitivity Floor for Solar Dark Matter Annihilation Searches, *JCAP* 07 (2017) 024. [arXiv:1703.07798](https://arxiv.org/abs/1703.07798), [doi:10.1088/1475-7516/2017/07/024](https://doi.org/10.1088/1475-7516/2017/07/024).
- [76] K. C. Y. Ng, J. F. Beacom, A. H. G. Peter, C. Rott, Solar Atmospheric Neutrinos: A New Neutrino Floor for Dark Matter Searches, *Phys. Rev. D* 96 (10) (2017) 103006. [arXiv:1703.10280](https://arxiv.org/abs/1703.10280), [doi:10.1103/PhysRevD.96.103006](https://doi.org/10.1103/PhysRevD.96.103006).
- [77] J. Edsjo, J. Elevant, R. Enberg, C. Niblaeus, Neutrinos from cosmic ray interactions in the Sun, *JCAP* 06 (2017) 033. [arXiv:1704.02892](https://arxiv.org/abs/1704.02892), [doi:10.1088/1475-7516/2017/06/033](https://doi.org/10.1088/1475-7516/2017/06/033).
- [78] F. L. Villante, A. Serenelli, The relevance of nuclear reactions for Standard Solar Models construction, *Front. Astron. Space Sci.* 7 (2021) 112. [arXiv:2101.03077](https://arxiv.org/abs/2101.03077), [doi:10.3389/fspas.2020.618356](https://doi.org/10.3389/fspas.2020.618356).
- [79] E. Magg, et al., Observational constraints on the origin of the elements - IV. Standard composition of the Sun, *Astron. Astrophys.* 661 (2022) A140. [arXiv:2203.02255](https://arxiv.org/abs/2203.02255), [doi:10.1051/0004-6361/202142971](https://doi.org/10.1051/0004-6361/202142971).
- [80] G. Buldgen, P. Eggenberger, A. Noels, R. Scuflaire, A. M. Amarsi, N. Grevesse, S. Salmon, Higher metal abundances do not solve the solar problem, *Astron. Astrophys.* 669 (2023) L9. [arXiv:2212.06473](https://arxiv.org/abs/2212.06473), [doi:10.1051/0004-6361/202245448](https://doi.org/10.1051/0004-6361/202245448).
- [81] R. L. Workman, et al., Review of Particle Physics, *PTEP* 2022 (2022) 083C01. [doi:10.1093/ptep/ptac097](https://doi.org/10.1093/ptep/ptac097).
- [82] <http://www.nu-fit.org>.
- [83] M. C. Gonzalez-Garcia, M. Maltoni, T. Schwetz, Updated fit to three neutrino mixing: status of leptonic CP violation, *JHEP* 11 (2014) 052. [arXiv:1409.5439](https://arxiv.org/abs/1409.5439), [doi:10.1007/JHEP11\(2014\)052](https://doi.org/10.1007/JHEP11(2014)052).



- [84] I. Esteban, M. C. Gonzalez-Garcia, M. Maltoni, T. Schwetz, A. Zhou, The fate of hints: updated global analysis of three-flavor neutrino oscillations, *JHEP* 09 (2020) 178. [arXiv:2007.14792](#), [doi:10.1007/JHEP09\(2020\)178](#).
- [85] A. Gando, et al., Reactor On-Off Antineutrino Measurement with KamLAND, *Phys. Rev. D* 88 (3) (2013) 033001. [arXiv:1303.4667](#), [doi:10.1103/PhysRevD.88.033001](#).
- [86] K. Abe, et al., Solar Neutrino Measurements in Super-Kamiokande-IV, *Phys. Rev. D* 94 (5) (2016) 052010. [arXiv:1606.07538](#), [doi:10.1103/PhysRevD.94.052010](#).
- [87] Y. Koshio, Overview of the solar neutrino observation, Talk given at the XXX International Conference on Neutrino Physics and Astrophysics, Seoul, Korea, May 30-June 4, 2022. <https://indico.kps.or.kr/event/30/contributions/893>.
- [88] W. C. Haxton, Adiabatic Conversion of Solar Neutrinos, *Phys. Rev. Lett.* 57 (1986) 1271–1274. [doi:10.1103/PhysRevLett.57.1271](#).
- [89] S. J. Parke, Nonadiabatic Level Crossing in Resonant Neutrino Oscillations, *Phys. Rev. Lett.* 57 (1986) 1275–1278. [arXiv:2212.06978](#), [doi:10.1103/PhysRevLett.57.1275](#).
- [90] S. T. Petcov, Exact analytic description of two neutrino oscillations in matter with exponentially varying density, *Phys. Lett. B* 200 (1988) 373–379. [doi:10.1016/0370-2693\(88\)90791-5](#).
- [91] P. C. de Holanda, W. Liao, A. Y. Smirnov, Toward precision measurements in solar neutrinos, *Nucl. Phys. B* 702 (2004) 307–332. [arXiv:hep-ph/0404042](#), [doi:10.1016/j.nuclphysb.2004.09.027](#).
- [92] M. Blennow, T. Ohlsson, H. Snellman, Day-night effect in solar neutrino oscillations with three flavors, *Phys. Rev. D* 69 (2004) 073006. [arXiv:hep-ph/0311098](#), [doi:10.1103/PhysRevD.69.073006](#).
- [93] A. N. Ioannian, A. Y. Smirnov, Neutrino oscillations in low density medium, *Phys. Rev. Lett.* 93 (2004) 241801. [arXiv:hep-ph/0404060](#), [doi:10.1103/PhysRevLett.93.241801](#).
- [94] A. Renshaw, et al., First Indication of Terrestrial Matter Effects on Solar Neutrino Oscillation, *Phys. Rev. Lett.* 112 (9) (2014) 091805. [arXiv:1312.5176](#), [doi:10.1103/PhysRevLett.112.091805](#).
- [95] E. K. Akhmedov, M. A. Tortola, J. W. F. Valle, Geotomography with solar and supernova neutrinos, *JHEP* 06 (2005) 053. [arXiv:hep-ph/0502154](#), [doi:10.1088/1126-6708/2005/06/053](#).
- [96] A. Ioannian, A. Smirnov, D. Wyler, Scanning the Earth with solar neutrinos and DUNE, *Phys. Rev. D* 96 (3) (2017) 036005. [arXiv:1702.06097](#), [doi:10.1103/PhysRevD.96.036005](#).
- [97] P. Bakhti, A. Y. Smirnov, Oscillation tomography of the Earth with solar neutrinos and future experiments, *Phys. Rev. D* 101 (12) (2020) 123031. [arXiv:2001.08030](#), [doi:10.1103/PhysRevD.101.123031](#).
- [98] P. S. Bhupal Dev, et al., Neutrino Non-Standard Interactions: A Status Report, *SciPost Phys. Proc.* 2 (2019) 001. [arXiv:1907.00991](#), [doi:10.21468/SciPostPhysProc.2.001](#).
- [99] S. Davidson, C. Pena-Garay, N. Rius, A. Santamaria, Present and future bounds on nonstandard neutrino interactions, *JHEP* 03 (2003) 011. [arXiv:hep-ph/0302093](#), [doi:10.1088/1126-6708/2003/03/011](#).

- [100] T. Ohlsson, Status of non-standard neutrino interactions, Rept. Prog. Phys. 76 (2013) 044201. [arXiv:1209.2710](#), [doi:10.1088/0034-4885/76/4/044201](#).
- [101] Y. Farzan, M. Tortola, Neutrino oscillations and Non-Standard Interactions, Front. in Phys. 6 (2018) 10. [arXiv:1710.09360](#), [doi:10.3389/fphy.2018.00010](#).
- [102] I. Esteban, M. C. Gonzalez-Garcia, M. Maltoni, I. Martinez-Soler, J. Salvado, Updated constraints on non-standard interactions from global analysis of oscillation data, JHEP 08 (2018) 180, [Addendum: JHEP 12, 152 (2020)]. [arXiv:1805.04530](#), [doi:10.1007/JHEP08\(2018\)180](#).
- [103] W. Konetschny, W. Kummer, Nonconservation of Total Lepton Number with Scalar Bosons, Phys. Lett. B 70 (1977) 433–435. [doi:10.1016/0370-2693\(77\)90407-5](#).
- [104] T. P. Cheng, L.-F. Li, Neutrino Masses, Mixings and Oscillations in SU(2) x U(1) Models of Electroweak Interactions, Phys. Rev. D 22 (1980) 2860. [doi:10.1103/PhysRevD.22.2860](#).
- [105] J. Schechter, J. W. F. Valle, Neutrino Masses in SU(2) x U(1) Theories, Phys. Rev. D 22 (1980) 2227. [doi:10.1103/PhysRevD.22.2227](#).
- [106] R. N. Mohapatra, G. Senjanovic, Neutrino Masses and Mixings in Gauge Models with Spontaneous Parity Violation, Phys. Rev. D 23 (1981) 165. [doi:10.1103/PhysRevD.23.165](#).
- [107] M. Malinsky, T. Ohlsson, H. Zhang, Non-Standard Neutrino Interactions from a Triplet Seesaw Model, Phys. Rev. D 79 (2009) 011301. [arXiv:0811.3346](#), [doi:10.1103/PhysRevD.79.011301](#).
- [108] S. Mandal, O. G. Miranda, G. Sanchez Garcia, J. W. F. Valle, X.-J. Xu, Toward deconstructing the simplest seesaw mechanism, Phys. Rev. D 105 (9) (2022) 095020. [arXiv:2203.06362](#), [doi:10.1103/PhysRevD.105.095020](#).
- [109] J. Heeck, M. Lindner, W. Rodejohann, S. Vogl, Non-Standard Neutrino Interactions and Neutral Gauge Bosons, SciPost Phys. 6 (3) (2019) 038. [arXiv:1812.04067](#), [doi:10.21468/SciPostPhys.6.3.038](#).
- [110] K. S. Babu, P. S. B. Dev, S. Jana, A. Thapa, Non-Standard Interactions in Radiative Neutrino Mass Models, JHEP 03 (2020) 006. [arXiv:1907.09498](#), [doi:10.1007/JHEP03\(2020\)006](#).
- [111] I. Bischer, W. Rodejohann, X.-J. Xu, Loop-induced Neutrino Non-Standard Interactions, JHEP 10 (2018) 096. [arXiv:1807.08102](#), [doi:10.1007/JHEP10\(2018\)096](#).
- [112] G. Chauhan, X.-J. Xu, How dark is the  $\nu_R$ -philic dark photon?, JHEP 04 (2021) 003. [arXiv:2012.09980](#), [doi:10.1007/JHEP04\(2021\)003](#).
- [113] A. Friedland, C. Lunardini, C. Pena-Garay, Solar neutrinos as probes of neutrino matter interactions, Phys. Lett. B 594 (2004) 347. [arXiv:hep-ph/0402266](#), [doi:10.1016/j.physletb.2004.05.047](#).
- [114] O. G. Miranda, M. A. Tortola, J. W. F. Valle, Are solar neutrino oscillations robust?, JHEP 10 (2006) 008. [arXiv:hep-ph/0406280](#), [doi:10.1088/1126-6708/2006/10/008](#).
- [115] A. Bolanos, O. G. Miranda, A. Palazzo, M. A. Tortola, J. W. F. Valle, Probing non-standard neutrino-electron interactions with solar and reactor neutrinos, Phys. Rev. D 79 (2009) 113012. [arXiv:0812.4417](#), [doi:10.1103/PhysRevD.79.113012](#).

- [116] F. J. Escrivuela, O. G. Miranda, M. A. Tortola, J. W. F. Valle, Constraining nonstandard neutrino-quark interactions with solar, reactor and accelerator data, *Phys. Rev. D* 80 (2009) 105009, [Erratum: *Phys.Rev.D* 80, 129908 (2009)]. [arXiv:0907.2630](https://arxiv.org/abs/0907.2630), [doi:10.1103/PhysRevD.80.129908](https://doi.org/10.1103/PhysRevD.80.129908).
- [117] A. Palazzo, J. W. F. Valle, Confusing non-zero  $\theta_{13}$  with non-standard interactions in the solar neutrino sector, *Phys. Rev. D* 80 (2009) 091301. [arXiv:0909.1535](https://arxiv.org/abs/0909.1535), [doi:10.1103/PhysRevD.80.091301](https://doi.org/10.1103/PhysRevD.80.091301).
- [118] A. Palazzo, Hint of non-standard dynamics in solar neutrino conversion, *Phys. Rev. D* 83 (2011) 101701. [arXiv:1101.3875](https://arxiv.org/abs/1101.3875), [doi:10.1103/PhysRevD.83.101701](https://doi.org/10.1103/PhysRevD.83.101701).
- [119] M. C. Gonzalez-Garcia, M. Maltoni, Determination of matter potential from global analysis of neutrino oscillation data, *JHEP* 09 (2013) 152. [arXiv:1307.3092](https://arxiv.org/abs/1307.3092), [doi:10.1007/JHEP09\(2013\)152](https://doi.org/10.1007/JHEP09(2013)152).
- [120] S. Fukasawa, O. Yasuda, The possibility to observe the non-standard interaction by the Hyperkamiokande atmospheric neutrino experiment, *Nucl. Phys. B* 914 (2017) 99–116. [arXiv:1608.05897](https://arxiv.org/abs/1608.05897), [doi:10.1016/j.nuclphysb.2016.11.004](https://doi.org/10.1016/j.nuclphysb.2016.11.004).
- [121] J. Liao, D. Marfatia, K. Whisnant, Nonstandard interactions in solar neutrino oscillations with Hyper-Kamiokande and JUNO, *Phys. Lett. B* 771 (2017) 247–253. [arXiv:1704.04711](https://arxiv.org/abs/1704.04711), [doi:10.1016/j.physletb.2017.05.054](https://doi.org/10.1016/j.physletb.2017.05.054).
- [122] A. N. Khan, D. W. McKay,  $\sin^2 \theta_W$  estimate and bounds on nonstandard interactions at source and detector in the solar neutrino low-energy regime, *JHEP* 07 (2017) 143. [arXiv:1704.06222](https://arxiv.org/abs/1704.06222), [doi:10.1007/JHEP07\(2017\)143](https://doi.org/10.1007/JHEP07(2017)143).
- [123] P. Weatherly, et al., Testing Non-Standard Interactions Between Solar Neutrinos and Quarks with Super-Kamiokande (3 2022). [arXiv:2203.11772](https://arxiv.org/abs/2203.11772).
- [124] B. Dutta, S. Liao, L. E. Strigari, J. W. Walker, Non-standard interactions of solar neutrinos in dark matter experiments, *Phys. Lett. B* 773 (2017) 242–246. [arXiv:1705.00661](https://arxiv.org/abs/1705.00661), [doi:10.1016/j.physletb.2017.08.031](https://doi.org/10.1016/j.physletb.2017.08.031).
- [125] A. N. Khan, W. Rodejohann, X.-J. Xu, Borexino and general neutrino interactions, *Phys. Rev. D* 101 (5) (2020) 055047. [arXiv:1906.12102](https://arxiv.org/abs/1906.12102), [doi:10.1103/PhysRevD.101.055047](https://doi.org/10.1103/PhysRevD.101.055047).
- [126] P. Bakhti, M. Rajaei, Sensitivities of future solar neutrino observatories to nonstandard neutrino interactions, *Phys. Rev. D* 102 (3) (2020) 035024. [arXiv:2003.12984](https://arxiv.org/abs/2003.12984), [doi:10.1103/PhysRevD.102.035024](https://doi.org/10.1103/PhysRevD.102.035024).
- [127] P. Martínez-Miravé, S. M. Sedgwick, M. Tórtola, Nonstandard interactions from the future neutrino solar sector, *Phys. Rev. D* 105 (3) (2022) 035004. [arXiv:2111.03031](https://arxiv.org/abs/2111.03031), [doi:10.1103/PhysRevD.105.035004](https://doi.org/10.1103/PhysRevD.105.035004).
- [128] P. Coloma, M. C. Gonzalez-Garcia, M. Maltoni, J. a. P. Pinheiro, S. Urrea, Constraining New Physics with Borexino Phase-II spectral data (4 2022). [arXiv:2204.03011](https://arxiv.org/abs/2204.03011).
- [129] T. Schwemberger, T.-T. Yu, Detecting Beyond the Standard Model Interactions of Solar Neutrinos in Low-Threshold Dark Matter Detectors (2 2022). [arXiv:2202.01254](https://arxiv.org/abs/2202.01254).
- [130] P. Bakhti, Y. Farzan, Shedding light on LMA-Dark solar neutrino solution by medium baseline reactor experiments: JUNO and RENO-50, *JHEP* 07 (2014) 064. [arXiv:1403.0744](https://arxiv.org/abs/1403.0744), [doi:10.1007/JHEP07\(2014\)064](https://doi.org/10.1007/JHEP07(2014)064).
- [131] Y. Farzan, A model for large non-standard interactions of neutrinos leading to the LMA-Dark solution, *Phys. Lett. B* 748 (2015) 311–315. [arXiv:1505.06906](https://arxiv.org/abs/1505.06906), [doi:10.1016/j.physletb.2015.07.015](https://doi.org/10.1016/j.physletb.2015.07.015).

- [132] M. Chaves, T. Schwetz, Resolving the LMA-dark NSI degeneracy with coherent neutrino-nucleus scattering, *JHEP* 05 (2021) 042. [arXiv:2102.11981](#), [doi:10.1007/JHEP05\(2021\)042](#).
- [133] J. M. Link, X.-J. Xu, Searching for BSM neutrino interactions in dark matter detectors, *JHEP* 08 (2019) 004. [arXiv:1903.09891](#), [doi:10.1007/JHEP08\(2019\)004](#).
- [134] A. Bolanos, O. G. Miranda, A. Palazzo, M. A. Tortola, J. W. F. Valle, Probing non-standard neutrino-electron interactions with solar and reactor neutrinos, *Phys. Rev. D* 79 (2009) 113012. [arXiv:0812.4417](#), [doi:10.1103/PhysRevD.79.113012](#).
- [135] L. E. Strigari, Neutrino Coherent Scattering Rates at Direct Dark Matter Detectors, *New J. Phys.* 11 (2009) 105011. [arXiv:0903.3630](#), [doi:10.1088/1367-2630/11/10/105011](#).
- [136] A. J. Anderson, J. M. Conrad, E. Figueroa-Feliciano, K. Scholberg, J. Spitz, Coherent Neutrino Scattering in Dark Matter Detectors, *Phys. Rev. D* 84 (2011) 013008. [arXiv:1103.4894](#), [doi:10.1103/PhysRevD.84.013008](#).
- [137] D. Aristizabal Sierra, B. Dutta, S. Liao, L. E. Strigari, Coherent elastic neutrino-nucleus scattering in multi-ton scale dark matter experiments: Classification of vector and scalar interactions new physics signals, *JHEP* 12 (2019) 124. [arXiv:1910.12437](#), [doi:10.1007/JHEP12\(2019\)124](#).
- [138] A. de Gouvea, W.-C. Huang, J. Jenkins, Pseudo-Dirac Neutrinos in the New Standard Model, *Phys. Rev. D* 80 (2009) 073007. [arXiv:0906.1611](#), [doi:10.1103/PhysRevD.80.073007](#).
- [139] K. N. Abazajian, et al., Light Sterile Neutrinos: A White Paper (4 2012). [arXiv:1204.5379](#).
- [140] J. Kopp, P. A. N. Machado, M. Maltoni, T. Schwetz, Sterile Neutrino Oscillations: The Global Picture, *JHEP* 05 (2013) 050. [arXiv:1303.3011](#), [doi:10.1007/JHEP05\(2013\)050](#).
- [141] S. Gariazzo, C. Giunti, M. Laveder, Y. F. Li, E. M. Zanvanin, Light sterile neutrinos, *J. Phys. G* 43 (2016) 033001. [arXiv:1507.08204](#), [doi:10.1088/0954-3899/43/3/033001](#).
- [142] M. Lindner, W. Rodejohann, X.-J. Xu, Sterile neutrinos in the light of IceCube, *JHEP* 01 (2016) 124. [arXiv:1510.00666](#), [doi:10.1007/JHEP01\(2016\)124](#).
- [143] J. Hamann, S. Hannestad, G. G. Raffelt, Y. Y. Y. Wong, Sterile neutrinos with eV masses in cosmology: How disfavoured exactly?, *JCAP* 09 (2011) 034. [arXiv:1108.4136](#), [doi:10.1088/1475-7516/2011/09/034](#).
- [144] N. Aghanim, et al., Planck 2018 results. VI. Cosmological parameters, *Astron. Astrophys.* 641 (2020) A6, [Erratum: *Astron. Astrophys.* 652, C4 (2021)]. [arXiv:1807.06209](#), [doi:10.1051/0004-6361/201833910](#).
- [145] C. Giunti, M. C. Gonzalez-Garcia, C. Pena-Garay, Four-neutrino oscillation solutions of the solar neutrino problem, *Phys. Rev. D* 62 (2000) 013005. [arXiv:hep-ph/0001101](#), [doi:10.1103/PhysRevD.62.013005](#).
- [146] M. C. Gonzalez-Garcia, M. Maltoni, C. Pena-Garay, Solar and atmospheric four neutrino oscillations, *Phys. Rev. D* 64 (2001) 093001. [arXiv:hep-ph/0105269](#), [doi:10.1103/PhysRevD.64.093001](#).
- [147] J. N. Bahcall, M. C. Gonzalez-Garcia, C. Pena-Garay, If sterile neutrinos exist, how can one determine the total neutrino fluxes?, *Phys. Rev. C* 66 (2002) 035802. [arXiv:hep-ph/0204194](#), [doi:10.1103/PhysRevC.66.035802](#).

- [148] P. C. de Holanda, A. Y. Smirnov, Homestake result, sterile neutrinos and low-energy solar neutrino experiments, Phys. Rev. D 69 (2004) 113002. [arXiv:hep-ph/0307266](#), [doi:10.1103/PhysRevD.69.113002](#).
- [149] C. R. Das, J. Pulido, M. Picariello, Light sterile neutrinos, spin flavour precession and the solar neutrino experiments, Phys. Rev. D 79 (2009) 073010. [arXiv:0902.1310](#), [doi:10.1103/PhysRevD.79.073010](#).
- [150] C. Giunti, Y. F. Li, Matter Effects in Active-Sterile Solar Neutrino Oscillations, Phys. Rev. D 80 (2009) 113007. [arXiv:0910.5856](#), [doi:10.1103/PhysRevD.80.113007](#).
- [151] P. C. de Holanda, A. Y. Smirnov, Solar neutrino spectrum, sterile neutrinos and additional radiation in the Universe, Phys. Rev. D 83 (2011) 113011. [arXiv:1012.5627](#), [doi:10.1103/PhysRevD.83.113011](#).
- [152] A. Palazzo, Testing the very-short-baseline neutrino anomalies at the solar sector, Phys. Rev. D 83 (2011) 113013. [arXiv:1105.1705](#), [doi:10.1103/PhysRevD.83.113013](#).
- [153] H. W. Long, Y. F. Li, C. Giunti, Day-Night Asymmetries in Active-Sterile Solar Neutrino Oscillations, JHEP 08 (2013) 056. [arXiv:1306.4051](#), [doi:10.1007/JHEP08\(2013\)056](#).
- [154] H. W. Long, Y. F. Li, C. Giunti, CP-violating Phases in Active-Sterile Solar Neutrino Oscillations, Phys. Rev. D 87 (11) (2013) 113004. [arXiv:1304.2207](#), [doi:10.1103/PhysRevD.87.113004](#).
- [155] J. Billard, L. E. Strigari, E. Figueroa-Feliciano, Solar neutrino physics with low-threshold dark matter detectors, Phys. Rev. D 91 (9) (2015) 095023. [arXiv:1409.0050](#), [doi:10.1103/PhysRevD.91.095023](#).
- [156] Ankush, R. Verma, G. Sharma, B. C. Chauhan, Investigating Sterile Neutrino Flux in the Solar Neutrino Data, Adv. High Energy Phys. 2019 (2019) 2598953. [arXiv:1812.03634](#), [doi:10.1155/2019/2598953](#).
- [157] M. Hostert, M. Pospelov, Constraints on decaying sterile neutrinos from solar antineutrinos, Phys. Rev. D 104 (5) (2021) 055031. [arXiv:2008.11851](#), [doi:10.1103/PhysRevD.104.055031](#).
- [158] K. Goldhagen, M. Maltoni, S. E. Reichard, T. Schwetz, Testing sterile neutrino mixing with present and future solar neutrino data, Eur. Phys. J. C 82 (2) (2022) 116. [arXiv:2109.14898](#), [doi:10.1140/epjc/s10052-022-10052-2](#).
- [159] S. T. Petcov, The Processes  $\mu \rightarrow e \gamma$ ,  $\mu \rightarrow e e \text{ anti-}e$ , Neutrino'  $\rightarrow$  Neutrino gamma in the Weinberg-Salam Model with Neutrino Mixing, Sov. J. Nucl. Phys. 25 (1977) 340, [Erratum: Yad. Fiz.25,1336(1977)].
- [160] W. J. Marciano, A. I. Sanda, Exotic Decays of the Muon and Heavy Leptons in Gauge Theories, Phys. Lett. 67B (1977) 303–305. [doi:10.1016/0370-2693\(77\)90377-X](#).
- [161] B. W. Lee, R. E. Shrock, Natural Suppression of Symmetry Violation in Gauge Theories: Muon - Lepton and Electron Lepton Number Nonconservation, Phys. Rev. D16 (1977) 1444. [doi:10.1103/PhysRevD.16.1444](#).
- [162] K. Fujikawa, R. Shrock, The Magnetic Moment of a Massive Neutrino and Neutrino Spin Rotation, Phys. Rev. Lett. 45 (1980) 963. [doi:10.1103/PhysRevLett.45.963](#).
- [163] P. B. Pal, L. Wolfenstein, Radiative Decays of Massive Neutrinos, Phys. Rev. D25 (1982) 766. [doi:10.1103/PhysRevD.25.766](#).

- [164] R. E. Shrock, Electromagnetic Properties and Decays of Dirac and Majorana Neutrinos in a General Class of Gauge Theories, Nucl. Phys. B206 (1982) 359–379. [doi:10.1016/0550-3213\(82\)90273-5](https://doi.org/10.1016/0550-3213(82)90273-5).
- [165] M. B. Voloshin, On Compatibility of Small Mass with Large Magnetic Moment of Neutrino, Sov. J. Nucl. Phys. 48 (1988) 512, [Yad. Fiz.48,804(1988)].
- [166] S. M. Barr, E. M. Freire, A. Zee, A Mechanism for large neutrino magnetic moments, Phys. Rev. Lett. 65 (1990) 2626–2629. [doi:10.1103/PhysRevLett.65.2626](https://doi.org/10.1103/PhysRevLett.65.2626).
- [167] S. M. Barr, E. M. Freire, Large neutrino magnetic moments and the existence of singly charged scalar fields, Phys. Rev. D43 (1991) 2989–2998. [doi:10.1103/PhysRevD.43.2989](https://doi.org/10.1103/PhysRevD.43.2989).
- [168] K. S. Babu, R. N. Mohapatra, Radiative fermion masses and large neutrino magnetic moment: A Unified picture, Phys. Rev. D43 (1991) 2278–2282. [doi:10.1103/PhysRevD.43.2278](https://doi.org/10.1103/PhysRevD.43.2278).
- [169] K. S. Babu, D. Chang, W.-Y. Keung, I. Phillips, Simple mechanism for large neutrino magnetic moments, Phys. Rev. D46 (1992) 2268–2269. [doi:10.1103/PhysRevD.46.2268](https://doi.org/10.1103/PhysRevD.46.2268).
- [170] M. Lindner, B. Radovic, J. Welter, Revisiting Large Neutrino Magnetic Moments, JHEP 07 (2017) 139. [arXiv:1706.02555](https://arxiv.org/abs/1706.02555), [doi:10.1007/JHEP07\(2017\)139](https://doi.org/10.1007/JHEP07(2017)139).
- [171] X.-J. Xu, Tensor and scalar interactions of neutrinos may lead to observable neutrino magnetic moments, Phys. Rev. D99 (7) (2019) 075003. [arXiv:1901.00482](https://arxiv.org/abs/1901.00482), [doi:10.1103/PhysRevD.99.075003](https://doi.org/10.1103/PhysRevD.99.075003).
- [172] C. Giunti, A. Studenikin, Neutrino electromagnetic interactions: a window to new physics, Rev. Mod. Phys. 87 (2015) 531. [arXiv:1403.6344](https://arxiv.org/abs/1403.6344), [doi:10.1103/RevModPhys.87.531](https://doi.org/10.1103/RevModPhys.87.531).
- [173] P. Vogel, J. Engel, Neutrino Electromagnetic Form-Factors, Phys. Rev. D 39 (1989) 3378. [doi:10.1103/PhysRevD.39.3378](https://doi.org/10.1103/PhysRevD.39.3378).
- [174] W. Grimus, M. Maltoni, T. Schwetz, M. A. Tortola, J. W. F. Valle, Constraining Majorana neutrino electromagnetic properties from the LMA-MSW solution of the solar neutrino problem, Nucl. Phys. B 648 (2003) 376–396. [arXiv:hep-ph/0208132](https://arxiv.org/abs/hep-ph/0208132), [doi:10.1016/S0550-3213\(02\)00973-2](https://doi.org/10.1016/S0550-3213(02)00973-2).
- [175] B. C. Canas, O. G. Miranda, A. Parada, M. Tortola, J. W. F. Valle, Updating neutrino magnetic moment constraints, Phys. Lett. B 753 (2016) 191–198, [Addendum: Phys.Lett.B 757, 568–568 (2016)]. [arXiv:1510.01684](https://arxiv.org/abs/1510.01684), [doi:10.1016/j.physletb.2015.12.011](https://doi.org/10.1016/j.physletb.2015.12.011).
- [176] M. Agostini, et al., Limiting neutrino magnetic moments with Borexino Phase-II solar neutrino data, Phys. Rev. D 96 (9) (2017) 091103. [arXiv:1707.09355](https://arxiv.org/abs/1707.09355), [doi:10.1103/PhysRevD.96.091103](https://doi.org/10.1103/PhysRevD.96.091103).
- [177] G.-Y. Huang, S. Zhou, Constraining Neutrino Lifetimes and Magnetic Moments via Solar Neutrinos in the Large Xenon Detectors, JCAP 02 (2019) 024. [arXiv:1810.03877](https://arxiv.org/abs/1810.03877), [doi:10.1088/1475-7516/2019/02/024](https://doi.org/10.1088/1475-7516/2019/02/024).
- [178] X. Zhou, et al., A Search for Solar Axions and Anomalous Neutrino Magnetic Moment with the Complete PandaX-II Data, Chin. Phys. Lett. 38 (1) (2021) 011301, [Erratum: Chin.Phys.Lett. 38, 109902 (2021)]. [arXiv:2008.06485](https://arxiv.org/abs/2008.06485), [doi:10.1088/0256-307X/38/10/109902](https://doi.org/10.1088/0256-307X/38/10/109902).

- [179] Z. Ye, F. Zhang, D. Xu, J. Liu, Unambiguously Resolving the Potential Neutrino Magnetic Moment Signal at Large Liquid Scintillator Detectors, *Chin. Phys. Lett.* 38 (11) (2021) 111401. [arXiv:2103.11771](#), [doi:10.1088/0256-307X/38/11/111401](#).
- [180] B. Yue, J. Liao, J. Ling, Probing neutrino magnetic moment at the Jinping neutrino experiment, *JHEP* 08 (068) (2021) 068. [arXiv:2102.12259](#), [doi:10.1007/JHEP08\(2021\)068](#).
- [181] O. G. Miranda, D. K. Papoulias, O. Sanders, M. Tórtola, J. W. F. Valle, Low-energy probes of sterile neutrino transition magnetic moments, *JHEP* 12 (2021) 191. [arXiv:2109.09545](#), [doi:10.1007/JHEP12\(2021\)191](#).
- [182] E. Akhmedov, P. Martínez-Miravé, Solar  $\bar{\nu}_e$  flux: revisiting bounds on neutrino magnetic moments and solar magnetic field, *JHEP* 10 (2022) 144. [arXiv:2207.04516](#), [doi:10.1007/JHEP10\(2022\)144](#).
- [183] E. Aprile, et al., Excess electronic recoil events in XENON1T, *Phys. Rev. D* 102 (7) (2020) 072004. [arXiv:2006.09721](#), [doi:10.1103/PhysRevD.102.072004](#).
- [184] J. Aalbers, et al., First Dark Matter Search Results from the LUX-ZEPLIN (LZ) Experiment (7 2022). [arXiv:2207.03764](#).
- [185] M. Atzori Corona, W. M. Bonivento, M. Cadeddu, N. Cargioli, F. Dordei, New constraint on neutrino magnetic moment from LZ dark matter search results (7 2022). [arXiv:2207.05036](#).
- [186] E. Aprile, et al., Search for New Physics in Electronic Recoil Data from XENONnT (7 2022). [arXiv:2207.11330](#).
- [187] R. Harnik, J. Kopp, P. A. N. Machado, Exploring  $\nu$  Signals in Dark Matter Detectors, *JCAP* 07 (2012) 026. [arXiv:1202.6073](#), [doi:10.1088/1475-7516/2012/07/026](#).
- [188] D. K. Papoulias, R. Sahu, T. S. Kosmas, V. K. B. Kota, B. Nayak, Novel neutrino-floor and dark matter searches with deformed shell model calculations, *Adv. High Energy Phys.* 2018 (2018) 6031362. [arXiv:1804.11319](#), [doi:10.1155/2018/6031362](#).
- [189] Y.-F. Li, S.-y. Xia, Probing neutrino magnetic moments and the Xenon1T excess with coherent elastic solar neutrino scattering, *Phys. Rev. D* 106 (9) (2022) 095022. [arXiv:2203.16525](#), [doi:10.1103/PhysRevD.106.095022](#).
- [190] M. Bauer, P. Foldenauer, J. Jaeckel, Hunting All the Hidden Photons, *JHEP* 07 (2018) 094. [arXiv:1803.05466](#), [doi:10.1007/JHEP07\(2018\)094](#).
- [191] M. Abdullah, J. B. Dent, B. Dutta, G. L. Kane, S. Liao, L. E. Strigari, Coherent elastic neutrino nucleus scattering as a probe of a  $Z'$  through kinetic and mass mixing effects, *Phys. Rev. D* 98 (1) (2018) 015005. [arXiv:1803.01224](#), [doi:10.1103/PhysRevD.98.015005](#).
- [192] D. W. P. d. Amaral, D. G. Cerdeno, P. Foldenauer, E. Reid, Solar neutrino probes of the muon anomalous magnetic moment in the gauged  $U(1)_{L_\mu-L_\tau}$ , *JHEP* 12 (2020) 155. [arXiv:2006.11225](#), [doi:10.1007/JHEP12\(2020\)155](#).
- [193] S. Gninenko, D. Gorbunov, Refining constraints from Borexino measurements on a light  $Z'$ -boson coupled to  $L_\mu-L_\tau$  current, *Phys. Lett. B* 823 (2021) 136739. [arXiv:2007.16098](#), [doi:10.1016/j.physletb.2021.136739](#).
- [194] Y.-F. Li, S.-y. Xia, Constraining light mediators via detection of coherent elastic solar neutrino nucleus scattering, *Nucl. Phys. B* 977 (2022) 115737. [arXiv:2201.05015](#), [doi:10.1016/j.nuclphysb.2022.115737](#).



- [195] G. Chauhan, P. S. B. Dev, X.-J. Xu, Probing the  $\nu_R$ -philic  $Z'$  at DUNE near detectors (2022). [arXiv:2204.11876](#).
- [196] R. Coy, X.-J. Xu, Probing the muon  $g - 2$  with future beam dump experiments, JHEP 10 (2021) 189. [arXiv:2108.05147](#), [doi:10.1007/JHEP10\(2021\)189](#).
- [197] E. K. Akhmedov, J. Pulido, Solar neutrino oscillations and bounds on neutrino magnetic moment and solar magnetic field, Phys. Lett. B 553 (2003) 7–17. [arXiv:hep-ph/0209192](#), [doi:10.1016/S0370-2693\(02\)03182-9](#).
- [198] S. M. Usman, G. R. Jocher, S. T. Dye, W. F. McDonough, J. G. Learned, AGM2015: Antineutrino Global Map 2015, Sci. Rep. 5 (2015) 13945.
- [199] L. Wan, G. Hussain, Z. Wang, S. Chen, Geoneutrinos at Jinping: Flux prediction and oscillation analysis, Phys. Rev. D 95 (5) (2017) 053001.
- [200] A. Gando, et. al., KamLAND collaboration, A study of extraterrestrial antineutrino sources with the KamLAND detector, Astrophys. J. 745 (2012) 193.
- [201] M. Agostini, et. al., Borexino collaboration, Search for low-energy neutrinos from astrophysical sources with Borexino, Astropart. Phys. 125 (2021) 102509.
- [202] B. Aharmim, et. al., SNO collaboration, Electron antineutrino search at the Sudbury Neutrino Observatory, Phys. Rev. D 70 (2004) 093014.
- [203] K. Abe, et. al., Super-Kamiokande collaboration, Search for solar electron anti-neutrinos due to spin-flavor precession in the Sun with Super-Kamiokande-IV, Astropart. Phys. 139 (2022) 102702.
- [204] D. N. Spergel, W. H. Press, Effect of hypothetical, weakly interacting, massive particles on energy transport in the solar interior, Astrophys. J. 294 (1985) 663–673. [doi:10.1086/163336](#).
- [205] A. Gould, WIMP Distribution in and Evaporation From the Sun, Astrophys. J. 321 (1987) 560. [doi:10.1086/165652](#).
- [206] A. Gould, Resonant Enhancements in WIMP Capture by the Earth, Astrophys. J. 321 (1987) 571. [doi:10.1086/165653](#).
- [207] M. Blennow, J. Edsjo, T. Ohlsson, Neutrinos from WIMP annihilations using a full three-flavor Monte Carlo, JCAP 01 (2008) 021. [arXiv:0709.3898](#), [doi:10.1088/1475-7516/2008/01/021](#).
- [208] A. R. Zentner, High-Energy Neutrinos From Dark Matter Particle Self-Capture Within the Sun, Phys. Rev. D 80 (2009) 063501. [arXiv:0907.3448](#), [doi:10.1103/PhysRevD.80.063501](#).
- [209] N. F. Bell, K. Petraki, Enhanced neutrino signals from dark matter annihilation in the Sun via metastable mediators, JCAP 04 (2011) 003. [arXiv:1102.2958](#), [doi:10.1088/1475-7516/2011/04/003](#).
- [210] C. Rott, J. Siegal-Gaskins, J. F. Beacom, New Sensitivity to Solar WIMP Annihilation using Low-Energy Neutrinos, Phys. Rev. D 88 (2013) 055005. [arXiv:1208.0827](#), [doi:10.1103/PhysRevD.88.055005](#).
- [211] N. Bernal, J. Martín-Albo, S. Palomares-Ruiz, A novel way of constraining WIMPs annihilations in the Sun: MeV neutrinos, JCAP 08 (2013) 011. [arXiv:1208.0834](#), [doi:10.1088/1475-7516/2013/08/011](#).



- [212] G. Busoni, A. De Simone, W.-C. Huang, On the Minimum Dark Matter Mass Testable by Neutrinos from the Sun, JCAP 07 (2013) 010. [arXiv:1305.1817](#), [doi:10.1088/1475-7516/2013/07/010](#).
- [213] C.-S. Chen, F.-F. Lee, G.-L. Lin, Y.-H. Lin, Probing Dark Matter Self-Interaction in the Sun with IceCube-PINGU, JCAP 10 (2014) 049. [arXiv:1408.5471](#), [doi:10.1088/1475-7516/2014/10/049](#).
- [214] W.-L. Guo, Detecting electron neutrinos from solar dark matter annihilation by JUNO, JCAP 01 (2016) 039. [arXiv:1511.04888](#), [doi:10.1088/1475-7516/2016/01/039](#).
- [215] P. W. Gorham, B. J. Rotter, Stringent neutrino flux constraints on antiquark nugget dark matter, Phys. Rev. D 95 (10) (2017) 103002. [arXiv:1507.03545](#), [doi:10.1103/PhysRevD.95.103002](#).
- [216] K. Lawson, A. R. Zhitnitsky, Solar neutrino spectrum of quark nugget dark matter, Phys. Rev. D 95 (6) (2017) 063521. [arXiv:1510.07646](#), [doi:10.1103/PhysRevD.95.063521](#).
- [217] C. Gaidau, J. Shelton, A Solar System Test of Self-Interacting Dark Matter, JCAP 06 (2019) 022. [arXiv:1811.00557](#), [doi:10.1088/1475-7516/2019/06/022](#).
- [218] A. Gupta, D. Majumdar, A. Halder, KM3NeT upper bounds of detection rates of solar neutrinos from annihilations of dark matter at the solar core (3 2022). [arXiv:2203.13697](#).
- [219] K. Choi, et al., Search for neutrinos from annihilation of captured low-mass dark matter particles in the Sun by Super-Kamiokande, Phys. Rev. Lett. 114 (14) (2015) 141301. [arXiv:1503.04858](#), [doi:10.1103/PhysRevLett.114.141301](#).
- [220] M. G. Aartsen, et al., Improved limits on dark matter annihilation in the Sun with the 79-string IceCube detector and implications for supersymmetry, JCAP 04 (2016) 022. [arXiv:1601.00653](#), [doi:10.1088/1475-7516/2016/04/022](#).
- [221] M. G. Aartsen, et al., Search for annihilating dark matter in the Sun with 3 years of IceCube data, Eur. Phys. J. C 77 (3) (2017) 146, [Erratum: Eur.Phys.J.C 79, 214 (2019)]. [arXiv:1612.05949](#), [doi:10.1140/epjc/s10052-017-4689-9](#).
- [222] S. Adrian-Martinez, et al., Limits on Dark Matter Annihilation in the Sun using the ANTARES Neutrino Telescope, Phys. Lett. B 759 (2016) 69–74. [arXiv:1603.02228](#), [doi:10.1016/j.physletb.2016.05.019](#).
- [223] G. T. Zatsepin, A. Y. Smirnov, Neutrino Decay in Gauge Theories, Yad. Fiz. 28 (1978) 1569–1579.
- [224] A. Y. Smirnov, How Heavy Are Neutrinos? (In Russian), Yad. Fiz. 34 (1981) 1547–1553.
- [225] A. S. Joshipura, E. Masso, S. Mohanty, Constraints on decay plus oscillation solutions of the solar neutrino problem, Phys. Rev. D 66 (2002) 113008. [arXiv:hep-ph/0203181](#), [doi:10.1103/PhysRevD.66.113008](#).
- [226] J. F. Beacom, N. F. Bell, Do Solar Neutrinos Decay?, Phys. Rev. D 65 (2002) 113009. [arXiv:hep-ph/0204111](#), [doi:10.1103/PhysRevD.65.113009](#).
- [227] A. Bandyopadhyay, S. Choubey, S. Goswami, Neutrino decay confronts the SNO data, Phys. Lett. B 555 (2003) 33–42. [arXiv:hep-ph/0204173](#), [doi:10.1016/S0370-2693\(03\)00044-3](#).

- [228] S. Cecchini, D. Centomo, G. Giacomelli, R. Giacomelli, V. Popa, C. G. Serbanut, R. Serra, Search for possible neutrino radiative decays during the 2001 total solar eclipse, *Astropart. Phys.* 21 (2004) 183–194. [arXiv:hep-ex/0402008](#), [doi:10.1016/j.astropartphys.2003.12.011](#).
- [229] J. M. Berryman, A. de Gouvea, D. Hernandez, Solar Neutrinos and the Decaying Neutrino Hypothesis, *Phys. Rev. D* 92 (7) (2015) 073003. [arXiv:1411.0308](#), [doi:10.1103/PhysRevD.92.073003](#).
- [230] R. Picoreti, M. M. Guzzo, P. C. de Holanda, O. L. G. Peres, Neutrino Decay and Solar Neutrino Seasonal Effect, *Phys. Lett. B* 761 (2016) 70–73. [arXiv:1506.08158](#), [doi:10.1016/j.physletb.2016.08.007](#).
- [231] A. de Gouvêa, M. Sen, J. Weill, Visible Neutrino Decays and the Impact of the Daughter-Neutrino Mass (3 2022). [arXiv:2203.14976](#).
- [232] A. S. Joshipura, S. Mohanty, Constraints on flavor dependent long range forces from atmospheric neutrino observations at super-Kamiokande, *Phys. Lett. B* 584 (2004) 103–108. [arXiv:hep-ph/0310210](#), [doi:10.1016/j.physletb.2004.01.057](#).
- [233] J. A. Grifols, E. Masso, Neutrino oscillations in the sun probe long range leptonic forces, *Phys. Lett. B* 579 (2004) 123–126. [arXiv:hep-ph/0311141](#), [doi:10.1016/j.physletb.2003.10.078](#).
- [234] A. Bandyopadhyay, A. Dighe, A. S. Joshipura, Constraints on flavor-dependent long range forces from solar neutrinos and KamLAND, *Phys. Rev. D* 75 (2007) 093005. [arXiv:hep-ph/0610263](#), [doi:10.1103/PhysRevD.75.093005](#).
- [235] M. C. Gonzalez-Garcia, P. C. de Holanda, E. Masso, R. Zukanovich Funchal, Probing long-range leptonic forces with solar and reactor neutrinos, *JCAP* 0701 (2007) 005. [arXiv:hep-ph/0609094](#), [doi:10.1088/1475-7516/2007/01/005](#).
- [236] A. E. Nelson, J. Walsh, Short Baseline Neutrino Oscillations and a New Light Gauge Boson, *Phys. Rev. D* 77 (2008) 033001. [arXiv:0711.1363](#), [doi:10.1103/PhysRevD.77.033001](#).
- [237] M. C. Gonzalez-Garcia, P. C. de Holanda, R. Zukanovich Funchal, Constraints from Solar and Reactor Neutrinos on Unparticle Long-Range Forces, *JCAP* 0806 (2008) 019. [arXiv:0803.1180](#), [doi:10.1088/1475-7516/2008/06/019](#).
- [238] A. Samanta, Long-range Forces : Atmospheric Neutrino Oscillation at a magnetized Detector, *JCAP* 1109 (2011) 010. [arXiv:1001.5344](#), [doi:10.1088/1475-7516/2011/09/010](#).
- [239] J. Heeck, W. Rodejohann, Gauged  $L_\mu - L_\tau$  and different Muon Neutrino and Anti-Neutrino Oscillations: MINOS and beyond, *J. Phys. G* 38 (2011) 085005. [arXiv:1007.2655](#), [doi:10.1088/0954-3899/38/8/085005](#).
- [240] H. Davoudiasl, H.-S. Lee, W. J. Marciano, Long-Range Lepton Flavor Interactions and Neutrino Oscillations, *Phys. Rev. D* 84 (2011) 013009. [arXiv:1102.5352](#), [doi:10.1103/PhysRevD.84.013009](#).
- [241] S. S. Chatterjee, A. Dasgupta, S. K. Agarwalla, Exploring Flavor-Dependent Long-Range Forces in Long-Baseline Neutrino Oscillation Experiments, *JHEP* 12 (2015) 167. [arXiv:1509.03517](#), [doi:10.1007/JHEP12\(2015\)167](#).
- [242] M. Bustamante, S. K. Agarwalla, Universe’s Worth of Electrons to Probe Long-Range Interactions of High-Energy Astrophysical Neutrinos, *Phys. Rev. Lett.* 122 (6) (2019) 061103. [arXiv:1808.02042](#), [doi:10.1103/PhysRevLett.122.061103](#).

- [243] A. Khatun, T. Thakore, S. Kumar Agarwalla, Can INO be Sensitive to Flavor-Dependent Long-Range Forces?, JHEP 04 (2018) 023. [arXiv:1801.00949](#), [doi:10.1007/JHEP04\(2018\)023](#).
- [244] M. B. Wise, Y. Zhang, Lepton Flavorful Fifth Force and Depth-dependent Neutrino Matter Interactions, JHEP 06 (2018) 053. [arXiv:1803.00591](#), [doi:10.1007/JHEP06\(2018\)053](#).
- [245] A. Y. Smirnov, X.-J. Xu, Wolfenstein potentials for neutrinos induced by ultra-light mediators, JHEP 12 (2019) 046. [arXiv:1909.07505](#), [doi:10.1007/JHEP12\(2019\)046](#).
- [246] K. S. Babu, G. Chauhan, P. S. Bhupal Dev, Neutrino nonstandard interactions via light scalars in the Earth, Sun, supernovae, and the early Universe, Phys. Rev. D 101 (9) (2020) 095029. [arXiv:1912.13488](#), [doi:10.1103/PhysRevD.101.095029](#).
- [247] A. Berlin, Neutrino Oscillations as a Probe of Light Scalar Dark Matter, Phys. Rev. Lett. 117 (23) (2016) 231801. [arXiv:1608.01307](#), [doi:10.1103/PhysRevLett.117.231801](#).
- [248] G. Krnjaic, P. A. N. Machado, L. Necib, Distorted neutrino oscillations from time varying cosmic fields, Phys. Rev. D 97 (7) (2018) 075017. [arXiv:1705.06740](#), [doi:10.1103/PhysRevD.97.075017](#).
- [249] F. Capozzi, I. M. Shoemaker, L. Vecchi, Solar Neutrinos as a Probe of Dark Matter-Neutrino Interactions, JCAP 07 (2017) 021. [arXiv:1702.08464](#), [doi:10.1088/1475-7516/2017/07/021](#).
- [250] V. Brdar, J. Kopp, J. Liu, P. Prass, X.-P. Wang, Fuzzy dark matter and nonstandard neutrino interactions, Phys. Rev. D 97 (4) (2018) 043001. [arXiv:1705.09455](#), [doi:10.1103/PhysRevD.97.043001](#).
- [251] J. Liao, D. Marfatia, K. Whisnant, Light scalar dark matter at neutrino oscillation experiments, JHEP 04 (2018) 136. [arXiv:1803.01773](#), [doi:10.1007/JHEP04\(2018\)136](#).
- [252] G.-Y. Huang, N. Nath, Neutrinophilic axion-like dark matter, Eur. Phys. J. C 78 (11) (2018) 922. [arXiv:1809.01111](#), [doi:10.1140/epjc/s10052-018-6391-y](#).
- [253] I. Lopes, The Sun: Light Dark Matter and Sterile Neutrinos, Astrophys. J. 905 (1) (2020) 22. [arXiv:2101.00210](#), [doi:10.3847/1538-4357/abfb6](#).
- [254] R. Fardon, A. E. Nelson, N. Weiner, Dark energy from mass varying neutrinos, JCAP 10 (2004) 005. [arXiv:astro-ph/0309800](#), [doi:10.1088/1475-7516/2004/10/005](#).
- [255] D. B. Kaplan, A. E. Nelson, N. Weiner, Neutrino oscillations as a probe of dark energy, Phys. Rev. Lett. 93 (2004) 091801. [arXiv:hep-ph/0401099](#), [doi:10.1103/PhysRevLett.93.091801](#).
- [256] V. Barger, P. Huber, D. Marfatia, Solar mass-varying neutrino oscillations, Phys. Rev. Lett. 95 (2005) 211802. [arXiv:hep-ph/0502196](#), [doi:10.1103/PhysRevLett.95.211802](#).
- [257] M. Cirelli, M. C. Gonzalez-Garcia, C. Pena-Garay, Mass varying neutrinos in the sun, Nucl. Phys. B 719 (2005) 219–233. [arXiv:hep-ph/0503028](#), [doi:10.1016/j.nuclphysb.2005.04.034](#).
- [258] I. Lopes, J. Silk, Solar neutrinos: Probing the quasiisothermal solar core produced by SUSY dark matter particles, Phys. Rev. Lett. 88 (2002) 151303. [arXiv:astro-ph/0112390](#), [doi:10.1103/PhysRevLett.88.151303](#).

- [259] A. Bottino, G. Fiorentini, N. Fornengo, B. Ricci, S. Scopel, F. L. Villante, Does solar physics provide constraints to weakly interacting massive particles?, *Phys. Rev. D* 66 (2002) 053005. [arXiv:hep-ph/0206211](#), [doi:10.1103/PhysRevD.66.053005](#).
- [260] M. Taoso, F. Iocco, G. Meynet, G. Bertone, P. Eggenberger, Effect of low mass dark matter particles on the Sun, *Phys. Rev. D* 82 (2010) 083509. [arXiv:1005.5711](#), [doi:10.1103/PhysRevD.82.083509](#).
- [261] D. T. Cumberbatch, J. A. Guzik, J. Silk, L. S. Watson, S. M. West, Light WIMPs in the Sun: Constraints from Helioseismology, *Phys. Rev. D* 82 (2010) 103503. [arXiv:1005.5102](#), [doi:10.1103/PhysRevD.82.103503](#).
- [262] I. Lopes, J. Silk, Solar constraints on asymmetric dark matter, *Astrophys. J.* 757 (2012) 130. [arXiv:1209.3631](#), [doi:10.1088/0004-637X/757/2/130](#).
- [263] I. Lopes, J. Silk, Solar neutrino physics: Sensitivity to light dark matter particles, *Astrophys. J. Lett.* 752 (2012) L129. [arXiv:1309.7573](#), [doi:10.1088/0004-637X/752/2/129](#).
- [264] I. Lopes, P. Panci, J. Silk, Helioseismology with long range dark matter-baryon interactions, *Astrophys. J.* 795 (2014) 162. [arXiv:1402.0682](#), [doi:10.1088/0004-637X/795/2/162](#).
- [265] J. Casanellas, I. M. Brandão, Y. Lebreton, Stellar convective cores as dark matter probes, *Phys. Rev. D* 91 (10) (2015) 103535. [arXiv:1505.01362](#), [doi:10.1103/PhysRevD.91.103535](#).
- [266] I. Lopes, J. Silk, Dark matter imprint on  $^8\text{B}$  neutrino spectrum, *Phys. Rev. D* 99 (2) (2019) 023008. [arXiv:1812.07426](#), [doi:10.1103/PhysRevD.99.023008](#).
- [267] J. N. Bahcall, Neutrino - Electron Scattering and Solar Neutrino Experiments, *Rev. Mod. Phys.* 59 (1987) 505. [doi:10.1103/RevModPhys.59.505](#).
- [268] C. Giunti, C. W. Kim, *Fundamentals of Neutrino Physics and Astrophysics*, Oxford University Press, 2007.
- [269] IAEA Nuclear Data Section, <https://www-nds.iaea.org/relnsd/NdsEnsd/QueryForm.html>, <https://www-nds.iaea.org/relnsd/vcharthtml/VChartHTML.html>.
- [270] M. K. Pavićević, G. Amthauer, V. Cvetković, B. Boev, V. Pejović, W. F. Henning, F. Bosch, Y. A. Litvinov, R. Wagner, Lorandite from Allchar as geochemical detector for pp-solar neutrinos, *Nucl. Instrum. Meth. A* 895 (2018) 62–73. [doi:10.1016/j.nima.2018.03.039](#).
- [271] J. Kostensalo, J. Suhonen, K. Zuber, Calculated solar-neutrino capture rate for a radiochemical  $^{205}\text{Tl}$ -based solar-neutrino detector, *Phys. Rev. C* 101 (3) (2020) 031302. [arXiv:1912.05334](#), [doi:10.1103/PhysRevC.101.031302](#).
- [272] A. Kopylov, V. Petukhov, Perspectives to Study a Solar CNO Cycle by Means of a Lithium Detector of Neutrinos, *JCAP* 10 (2008) 007. [arXiv:0806.0460](#), [doi:10.1088/1475-7516/2008/10/007](#).
- [273] A. V. Kopylov, I. V. Orekhov, V. V. Petukhov, A. E. Solomatin, A Lithium-Beryllium Method for the Detection of Solar Neutrinos (10 2009). [arXiv:0910.3889](#).
- [274] Y. Fujita, K. Zuber, H. Fujita, Constraining the solar neutrino survival probability curve by using  $\text{Li6}$ ,  $\text{Li7}$ ,  $\text{C12}$ ,  $\text{O18}$ ,  $\text{F19}$ , and  $\text{Ca42}$  nuclear targets, *Phys. Rev. D* 104 (1) (2021) 013004. [doi:10.1103/PhysRevD.104.013004](#).

- [275] W. Shao, W. Xu, Y. Liang, W. Luo, T. Xu, M. Qi, J. Zhang, B. Xu, Z. Wang, S. Chen, The Potential to Probe Solar Neutrino Physics with LiCl Water Solution (3 2022). [arXiv:2203.01860](#).
- [276] H.R.Crane, J. Halpern, New Experimental Evidence for the Existence of a Neutrino, *Phys.Rev.* 53 (1938) 789.
- [277] H.R.Crane, An attempt to observe the absorption of neutrinos, *Phys. Rev.* 55 (1939) 501.
- [278] H.R.Crane, J. Halpern, Further Experiments on the Recoil of the Nucleus in Beta-Decay, *Phys.Rev.* 56 (1939) 232.
- [279] K.C.Wang, A Suggestion on the Detection of the Neutrino, *Phys.Rev.* 61 (1942) 97.
- [280] J. N. Bahcall, Solar neutrino experiments, *Rev. Mod. Phys.* 50 (1978) 881. [doi:10.1103/RevModPhys.50.881](#).
- [281] J. N. Bahcall, Phase-space integrals for beta decay and nuclear matrix elements, *Nuclear Physics* 75 (1966) 10.
- [282] V. Barinov, B. Cleveland, V. Gavrin, D. Gorbunov, T. Ibragimova, Revised neutrino-gallium cross section and prospects of BEST in resolving the Gallium anomaly, *Phys. Rev. D* 97 (7) (2018) 073001. [doi:10.1103/PhysRevD.97.073001](#).
- [283] Y. Fujita, Nuclei as neutrino detectors, Proceedings, 5th International Solar Neutrino Conference, Dresden, Germany, 2019. [doi:10.1142/9789811204296\\_0009](#).
- [284] Y. Fujita, K. Zuber, H. Fujita, Constraining the solar neutrino survival probability curve by using Li6, Li7, C12, O18, F19, and Ca42 nuclear targets, *Phys. Rev. D* 104 (1) (2021) 013004. [doi:10.1103/PhysRevD.104.013004](#).
- [285] W. E. Ormand, P. M. Pizzochero, P. F. Bortignon, R. A. Broglia, Neutrino capture cross-sections for Ar-40 and Beta decay of Ti-40, *Phys. Lett. B* 345 (1995) 343–350. [arXiv:nucl-th/9405007](#), [doi:10.1016/0370-2693\(94\)01605-C](#).
- [286] W. Trinder, et al., Ti-40 beta decay and the neutrino capture cross-section of Ar-40, *Phys. Lett. B* 415 (1997) 211–216. [doi:10.1016/S0370-2693\(97\)01243-4](#).
- [287] J.N.Bahcall, Neutrino-spectroscopy of the solar interior, *Phys. Lett. B* 13 (1964) 332–333.
- [288] T. Kovacs, et al., Borex: Solar neutrino experiment via weak neutral and charged currents in boron-11, *Solar Phys.* 128 (1) (1990) 61. [doi:10.1007/BF00154147](#).
- [289] L. Pfeiffer, A. P. Mills, R. S. Raghavan, E. A. Chandross, Indium-Loaded Liquid Scintillator for Low-Energy Solar-Neutrino Spectroscopy, *Phys. Rev. Lett.* 41 (1978) 63. [doi:10.1103/PhysRevLett.41.63](#).
- [290] S. Haselschwardt, B. Lenardo, P. Pirinen, J. Suhonen, Solar neutrino detection in liquid xenon detectors via charged-current scattering to excited states, *Phys. Rev. D* 102 (7) (2020) 072009. [doi:10.1103/PhysRevD.102.072009](#).
- [291] R. S. Raghavan, Inverse beta decay of 115-In to 115-Sn\*: a new possibility for detecting solar neutrinos from the proton-proton reaction, *Phys. Rev. Lett.* 37 (1976) 259–262. [doi:10.1103/PhysRevLett.37.259](#).
- [292] H. Ejiri, J. Engel, R. Hazama, P. Krastev, N. Kudomi, R. G. H. Robertson, Spectroscopy of double beta and inverse beta decays from Mo-100 for neutrinos, *Phys. Rev. Lett.* 85 (2000) 2917–2920. [arXiv:nucl-ex/9911008](#), [doi:10.1103/PhysRevLett.85.2917](#).

- [293] R. S. Raghavan, New prospects for real time spectroscopy of low-energy electron neutrinos from the sun, *Phys. Rev. Lett.* 78 (1997) 3618–3621. doi:[10.1103/PhysRevLett.78.3618](https://doi.org/10.1103/PhysRevLett.78.3618).
- [294] K. Zuber, Spectroscopy of low energy solar neutrinos using CdTe detectors, *Phys. Lett. B* 571 (2003) 148. doi:[10.1016/j.physletb.2003.07.070](https://doi.org/10.1016/j.physletb.2003.07.070).
- [295] Z. Wang, B. Xu, S. Chen, Delayed coincidence in electron-neutrino capture on gallium for neutrino spectroscopy, *Astropart. Phys.* 126 (2021) 102519. doi:[10.1016/j.astropartphys.2020.102519](https://doi.org/10.1016/j.astropartphys.2020.102519).
- [296] M. Lindner, W. Rodejohann, X.-J. Xu, Coherent Neutrino-Nucleus Scattering and new Neutrino Interactions, *JHEP* 03 (2017) 097. arXiv:[1612.04150](https://arxiv.org/abs/1612.04150), doi:[10.1007/JHEP03\(2017\)097](https://doi.org/10.1007/JHEP03(2017)097).
- [297] R. H. Helm, Inelastic and Elastic Scattering of 187-Mev Electrons from Selected Even-Even Nuclei, *Phys. Rev.* 104 (1956) 1466–1475. doi:[10.1103/PhysRev.104.1466](https://doi.org/10.1103/PhysRev.104.1466).
- [298] D. Akimov, et al., Observation of Coherent Elastic Neutrino-Nucleus Scattering, *Science* 357 (6356) (2017) 1123–1126. arXiv:[1708.01294](https://arxiv.org/abs/1708.01294), doi:[10.1126/science.aao0990](https://doi.org/10.1126/science.aao0990).
- [299] M. F. L’Annunziata, *2 - beta radiation*, in: M. F. L’Annunziata (Ed.), *Radioactivity*, Elsevier Science B.V., Amsterdam, 2007, pp. 119–140. doi:<https://doi.org/10.1016/B978-044452715-8.50005-0>. URL <https://www.sciencedirect.com/science/article/pii/B9780444527158500050>
- [300] K. Abe, et al., Solar neutrino results in Super-Kamiokande-III, *Phys. Rev. D* 83 (2011) 052010. arXiv:[1010.0118](https://arxiv.org/abs/1010.0118), doi:[10.1103/PhysRevD.83.052010](https://doi.org/10.1103/PhysRevD.83.052010).
- [301] G. Bellini, et al., Final results of Borexino Phase-I on low energy solar neutrino spectroscopy, *Phys. Rev. D* 89 (11) (2014) 112007. arXiv:[1308.0443](https://arxiv.org/abs/1308.0443), doi:[10.1103/PhysRevD.89.112007](https://doi.org/10.1103/PhysRevD.89.112007).
- [302] M. Agostini, et al., Search for low-energy neutrinos from astrophysical sources with Borexino, *Astropart. Phys.* 125 (2021) 102509. arXiv:[1909.02422](https://arxiv.org/abs/1909.02422), doi:[10.1016/j.astropartphys.2020.102509](https://doi.org/10.1016/j.astropartphys.2020.102509).
- [303] M. Agostini, et al., First Directional Measurement of Sub-MeV Solar Neutrinos with Borexino, *Phys. Rev. Lett.* 128 (9) (2022) 091803. arXiv:[2112.11816](https://arxiv.org/abs/2112.11816), doi:[10.1103/PhysRevLett.128.091803](https://doi.org/10.1103/PhysRevLett.128.091803).
- [304] T. K. Gaisser, *Cosmic Rays and Particle Physics*, Cambridge University Press, 1990, Page69.
- [305] M. Guan, M.-C. Chu, J. Cao, K.-B. Luk, C. Yang, A parametrization of the cosmic-ray muon flux at sea-level (9 2015). arXiv:[1509.06176](https://arxiv.org/abs/1509.06176).
- [306] Z. Guo, et al., Muon flux measurement at China Jinping Underground Laboratory, *Chin. Phys. C* 45 (2) (2021) 025001. arXiv:[2007.15925](https://arxiv.org/abs/2007.15925), doi:[10.1088/1674-1137/abccae](https://doi.org/10.1088/1674-1137/abccae).
- [307] J. Hosaka, et al., Solar neutrino measurements in Super-Kamiokande-I, *Phys. Rev. D* 73 (2006) 112001. arXiv:[hep-ex/0508053](https://arxiv.org/abs/hep-ex/0508053), doi:[10.1103/PhysRevD.73.112001](https://doi.org/10.1103/PhysRevD.73.112001).
- [308] M. Anderson, et al., Measurement of the  $^8\text{B}$  solar neutrino flux in SNO+ with very low backgrounds, *Phys. Rev. D* 99 (1) (2019) 012012. arXiv:[1812.03355](https://arxiv.org/abs/1812.03355), doi:[10.1103/PhysRevD.99.012012](https://doi.org/10.1103/PhysRevD.99.012012).

- [309] H. Back, et. al., Borexino collaboration, CNO and pep neutrino spectroscopy in Borexino: Measurement of the deep underground production of cosmogenic  $^{11}\text{C}$  in organic liquid scintillator, Phys. Rev. C 74 (2006) 045805.
- [310] S. Abe, et. al., KamLAND collaboration, Production of Radioactive Isotopes through Cosmic Muon Spallation in KamLAND, Phys. Rev. C 81 (2010) 025807.
- [311] Y. Zhang, et. al., Super-Kamiokande collaboration, First measurement of radioactive isotope production through cosmic-ray muon spallation in Super-Kamiokande IV, Phys. Rev. D 93 (2016) 012004.
- [312] H. M. O’Keefe, Low Energy Background in the NCD Phase of the Sudbury Neutrino Observatory, PhD thesis, Lincoln College, Oxford (2008).
- [313] F. Gatti, et. al., Liquid scintillators for large mass and low background detectors, Nucl.Instrum.Meth.A 370 (1996) 609–620.
- [314] C. Arpesella, et. al., Borexino collaboration, First real time detection of Be-7 solar neutrinos by Borexino, Phys. Lett. B 658 (2008) 58.
- [315] M. Balata, et. al., The water purification system for the low background counting test facility of the Borexino experiment at Gran Sasso, Nucl.Instrum.Meth.A 370 (1996) 605–608.
- [316] G. Alimonti, et. al., Borexino collaboration, The liquid handling systems for the Borexino solar neutrino detector, Nucl.Instrum.Meth.A 609 (2009) 58–78.
- [317] M. Altmann, et al., Complete results for five years of GNO solar neutrino observations, Phys. Lett. B 616 (2005) 174–190. [arXiv:hep-ex/0504037](https://arxiv.org/abs/hep-ex/0504037), [doi:10.1016/j.physletb.2005.04.068](https://doi.org/10.1016/j.physletb.2005.04.068).
- [318] J. N. Abdurashitov, et al., Measurement of the solar neutrino capture rate with gallium metal. III: Results for the 2002–2007 data-taking period, Phys. Rev. C 80 (2009) 015807. [arXiv:0901.2200](https://arxiv.org/abs/0901.2200), [doi:10.1103/PhysRevC.80.015807](https://doi.org/10.1103/PhysRevC.80.015807).
- [319] B. Aharmim, et al., Search for *hep* solar neutrinos and the diffuse supernova neutrino background using all three phases of the Sudbury Neutrino Observatory, Phys. Rev. D 102 (6) (2020) 062006. [arXiv:2007.08018](https://arxiv.org/abs/2007.08018), [doi:10.1103/PhysRevD.102.062006](https://doi.org/10.1103/PhysRevD.102.062006).
- [320] B. Aharmim, et al., Measurement of the Cosmic Ray and Neutrino-Induced Muon Flux at the Sudbury Neutrino Observatory, Phys. Rev. D 80 (2009) 012001. [arXiv:0902.2776](https://arxiv.org/abs/0902.2776), [doi:10.1103/PhysRevD.80.012001](https://doi.org/10.1103/PhysRevD.80.012001).
- [321] K. Abe, et al., Letter of Intent: The Hyper-Kamiokande Experiment — Detector Design and Physics Potential — (9 2011). [arXiv:1109.3262](https://arxiv.org/abs/1109.3262).
- [322] S. Abe, et al., Measurement of the 8B Solar Neutrino Flux with the KamLAND Liquid Scintillator Detector, Phys. Rev. C 84 (2011) 035804. [arXiv:1106.0861](https://arxiv.org/abs/1106.0861), [doi:10.1103/PhysRevC.84.035804](https://doi.org/10.1103/PhysRevC.84.035804).
- [323] A. Gando, et al.,  $^7\text{Be}$  Solar Neutrino Measurement with KamLAND, Phys. Rev. C 92 (5) (2015) 055808. [arXiv:1405.6190](https://arxiv.org/abs/1405.6190), [doi:10.1103/PhysRevC.92.055808](https://doi.org/10.1103/PhysRevC.92.055808).
- [324] V. Albanese, et al., The SNO+ experiment, JINST 16 (08) (2021) P08059. [arXiv:2104.11687](https://arxiv.org/abs/2104.11687), [doi:10.1088/1748-0221/16/08/P08059](https://doi.org/10.1088/1748-0221/16/08/P08059).



- [325] L. Marti Magro, SK-Gd looks forward, PoS ICRC2021 (2021) 1088. [doi:10.22323/1.395.1088](https://doi.org/10.22323/1.395.1088).
- [326] A. Goldsack, The New Phase of Super-Kamiokande: SK-Gd, PoS NuFact2021 (2022) 170. [doi:10.22323/1.402.0170](https://doi.org/10.22323/1.402.0170).
- [327] A. Abusleme, et al., JUNO Physics and Detector (4 2021). [arXiv:2104.02565](https://arxiv.org/abs/2104.02565).
- [328] B. Abi, et al., Deep Underground Neutrino Experiment (DUNE), Far Detector Technical Design Report, Volume II: DUNE Physics (2 2020). [arXiv:2002.03005](https://arxiv.org/abs/2002.03005).
- [329] G. Bellini, et al., Precision measurement of the  ${}^7\text{Be}$  solar neutrino interaction rate in Borexino, Phys. Rev. Lett. 107 (2011) 141302. [arXiv:1104.1816](https://arxiv.org/abs/1104.1816), [doi:10.1103/PhysRevLett.107.141302](https://doi.org/10.1103/PhysRevLett.107.141302).
- [330] K. S. Hirata, et al., Observation of B-8 Solar Neutrinos in the Kamiokande-II Detector, Phys. Rev. Lett. 63 (1989) 16. [doi:10.1103/PhysRevLett.63.16](https://doi.org/10.1103/PhysRevLett.63.16).
- [331] K. S. Hirata, et al., Observation of a small atmospheric muon-neutrino / electron-neutrino ratio in Kamiokande, Phys. Lett. B 280 (1992) 146–152. [doi:10.1016/0370-2693\(92\)90788-6](https://doi.org/10.1016/0370-2693(92)90788-6).
- [332] K. Hirata, et al., Observation of a Neutrino Burst from the Supernova SN 1987a, Phys. Rev. Lett. 58 (1987) 1490–1493. [doi:10.1103/PhysRevLett.58.1490](https://doi.org/10.1103/PhysRevLett.58.1490).
- [333] Y. Fukuda, et al., Solar neutrino data covering solar cycle 22, Phys. Rev. Lett. 77 (1996) 1683–1686. [doi:10.1103/PhysRevLett.77.1683](https://doi.org/10.1103/PhysRevLett.77.1683).
- [334] D. Casper, et al., Measurement of atmospheric neutrino composition with IMB-3, Phys. Rev. Lett. 66 (1991) 2561–2564. [doi:10.1103/PhysRevLett.66.2561](https://doi.org/10.1103/PhysRevLett.66.2561).
- [335] C. B. Bratton, et al., Angular Distribution of Events From Sn1987a, Phys. Rev. D 37 (1988) 3361. [doi:10.1103/PhysRevD.37.3361](https://doi.org/10.1103/PhysRevD.37.3361).
- [336] J. F. Beacom, M. R. Vagins, GADZOOKS! Anti-neutrino spectroscopy with large water Cherenkov detectors, Phys. Rev. Lett. 93 (2004) 171101. [arXiv:hep-ph/0309300](https://arxiv.org/abs/hep-ph/0309300), [doi:10.1103/PhysRevLett.93.171101](https://doi.org/10.1103/PhysRevLett.93.171101).
- [337] C. Simpson, et al., Sensitivity of Super-Kamiokande with Gadolinium to Low Energy Anti-neutrinos from Pre-supernova Emission, Astrophys. J. 885 (2019) 133. [arXiv:1908.07551](https://arxiv.org/abs/1908.07551), [doi:10.3847/1538-4357/ab4883](https://doi.org/10.3847/1538-4357/ab4883).
- [338] M. Malek, et al., Search for supernova relic neutrinos at SUPER-KAMIOKANDE, Phys. Rev. Lett. 90 (2003) 061101. [arXiv:hep-ex/0209028](https://arxiv.org/abs/hep-ex/0209028), [doi:10.1103/PhysRevLett.90.061101](https://doi.org/10.1103/PhysRevLett.90.061101).
- [339] K. Bays, et al., Supernova Relic Neutrino Search at Super-Kamiokande, Phys. Rev. D 85 (2012) 052007. [arXiv:1111.5031](https://arxiv.org/abs/1111.5031), [doi:10.1103/PhysRevD.85.052007](https://doi.org/10.1103/PhysRevD.85.052007).
- [340] M. Fukugita, M. Kawasaki, Constraints on the star formation rate from supernova relic neutrino observations, Mon. Not. Roy. Astron. Soc. 340 (2003) L7. [arXiv:astro-ph/0204376](https://arxiv.org/abs/astro-ph/0204376), [doi:10.1046/j.1365-8711.2003.06507.x](https://doi.org/10.1046/j.1365-8711.2003.06507.x).
- [341] S. Ando, K. Sato, Supernova relic neutrinos and observational implications for neutrino oscillation, Phys. Lett. B 559 (2003) 113. [arXiv:astro-ph/0210502](https://arxiv.org/abs/astro-ph/0210502), [doi:10.1016/S0370-2693\(03\)00374-5](https://doi.org/10.1016/S0370-2693(03)00374-5).



- [342] L. E. Strigari, M. Kaplinghat, G. Steigman, T. P. Walker, The Supernova relic neutrino backgrounds at KamLAND and Super-Kamiokande, JCAP 03 (2004) 007. [arXiv:astro-ph/0312346](#), [doi:10.1088/1475-7516/2004/03/007](#).
- [343] J. F. Beacom, L. E. Strigari, New test of supernova electron neutrino emission using Sudbury neutrino observatory sensitivity to the diffuse supernova neutrino background, Phys. Rev. C 73 (2006) 035807. [arXiv:hep-ph/0508202](#), [doi:10.1103/PhysRevC.73.035807](#).
- [344] L. E. Strigari, J. F. Beacom, T. P. Walker, P. Zhang, The Concordance Cosmic Star Formation Rate: Implications from and for the supernova neutrino and gamma ray backgrounds, JCAP 04 (2005) 017. [arXiv:astro-ph/0502150](#), [doi:10.1088/1475-7516/2005/04/017](#).
- [345] J. F. Beacom, The Diffuse Supernova Neutrino Background, Ann. Rev. Nucl. Part. Sci. 60 (2010) 439–462. [arXiv:1004.3311](#), [doi:10.1146/annurev.nucl.010909.083331](#).
- [346] T. Tashiro, Hyper-Kamiokande experiment, PoS EPS-HEP2021 (2022) 234. [doi:10.22323/1.398.0234](#).
- [347] A. Abusleme, et al., Feasibility and physics potential of detecting  $^8\text{B}$  solar neutrinos at JUNO, Chin. Phys. C 45 (2) (2021) 023004. [arXiv:2006.11760](#), [doi:10.1088/1674-1137/abd92a](#).
- [348] T. Suzuki, A. B. Balantekin, T. Kajino, Neutrino Capture on  $^{13}\text{C}$ , Phys. Rev. C 86 (2012) 015502. [arXiv:1204.4231](#), [doi:10.1103/PhysRevC.86.015502](#).
- [349] T. Suzuki, A. B. Balantekin, T. Kajino, S. Chiba, Neutrino- $^{13}\text{C}$  Cross Sections at Supernova Neutrino Energies, J. Phys. G 46 (7) (2019) 075103. [arXiv:1904.11291](#), [doi:10.1088/1361-6471/ab1c11](#).
- [350] S. Andringa, et al., Current Status and Future Prospects of the SNO+ Experiment, Adv. High Energy Phys. 2016 (2016) 6194250. [arXiv:1508.05759](#), [doi:10.1155/2016/6194250](#).
- [351] M. Yeh, S. Hans, W. Beriguete, R. Rosero, L. Hu, R. L. Hahn, M. V. Diwan, D. E. Jaffe, S. H. Kettell, L. Littenberg, A new water-based liquid scintillator and potential applications, Nucl. Instrum. Meth. A 660 (2011) 51–56. [doi:10.1016/j.nima.2011.08.040](#).
- [352] L. Zhao, et al., Measurement of muon-induced neutron yield at the China Jinping Underground Laboratory \*, Chin. Phys. C 46 (8) (2022) 085001. [arXiv:2108.04010](#), [doi:10.1088/1674-1137/ac66cc](#).
- [353] J.-P. Cheng, et al., The China Jinping Underground Laboratory and its Early Science, Ann. Rev. Nucl. Part. Sci. 67 (2017) 231–251. [arXiv:1801.00587](#), [doi:10.1146/annurev-nucl-102115-044842](#).
- [354] The Power Reactor Information System (PRIS), International Atomic Energy Agency, <https://pris.iaea.org/pris/> (2021).
- [355] Z. Guo, M. Yeh, R. Zhang, D.-W. Cao, M. Qi, Z. Wang, S. Chen, Slow Liquid Scintillator Candidates for MeV-scale Neutrino Experiments, Astropart. Phys. 109 (2019) 33–40. [arXiv:1708.07781](#), [doi:10.1016/j.astropartphys.2019.02.001](#).
- [356] S. D. Biller, E. J. Leming, J. L. Paton, Slow fluors for effective separation of Cherenkov light in liquid scintillators, Nucl. Instrum. Meth. A 972 (2020) 164106. [arXiv:2001.10825](#), [doi:10.1016/j.nima.2020.164106](#).

- [357] C. Rubbia, The liquid Argon Time Projection Chamber: a new concept for neutrino detector, CERN EP/77-8, 1977.
- [358] P. Cennini, et. al., Performance of a three-ton liquid argon time projection chamber, Nucl. Instrum. Methods Phys. Res. A 345 (1994) 230–243.
- [359] F. Arneodo, et. al., Performance of the 10 m<sup>3</sup> ICARUS liquid argon prototype, Nucl. Instrum. Methods Phys. Res. A 498 (2003) 292–311.
- [360] H. H. Chen, P. J. Doe, H. J. Mahler, A Proton Decay and Solar Neutrino Experiment with a Liquid Argon Time Projection Chamber, AIP Conf. Proc. 96 (1983) 182–185. [doi:10.1063/1.33934](https://doi.org/10.1063/1.33934).
- [361] A. Abed Abud, et al., Snowmass Neutrino Frontier: DUNE Physics Summary (3 2022). [arXiv:2203.06100](https://arxiv.org/abs/2203.06100).
- [362] F. Capozzi, S. W. Li, G. Zhu, J. F. Beacom, DUNE as the Next-Generation Solar Neutrino Experiment, Phys. Rev. Lett. 123 (13) (2019) 131803. [arXiv:1808.08232](https://arxiv.org/abs/1808.08232), [doi:10.1103/PhysRevLett.123.131803](https://doi.org/10.1103/PhysRevLett.123.131803).
- [363] S. Parsa, et al., SoLAR: Solar Neutrinos in Liquid Argon, in: 2022 Snowmass Summer Study, 2022. [arXiv:2203.07501](https://arxiv.org/abs/2203.07501).
- [364] B. Abi, et al., Deep Underground Neutrino Experiment (DUNE), Far Detector Technical Design Report, Volume IV: Far Detector Single-phase Technology, JINST 15 (08) (2020) T08010. [arXiv:2002.03010](https://arxiv.org/abs/2002.03010), [doi:10.1088/1748-0221/15/08/T08010](https://doi.org/10.1088/1748-0221/15/08/T08010).
- [365] C. A. J. O’Hare, New definition of the neutrino floor for direct dark matter searches, Phys. Rev. Lett. 127 (25) (2021) 251802. [arXiv:2109.03116](https://arxiv.org/abs/2109.03116), [doi:10.1103/PhysRevLett.127.251802](https://doi.org/10.1103/PhysRevLett.127.251802).
- [366] C. A. J. O’Hare, et al., Recoil imaging for dark matter, neutrinos, and physics beyond the Standard Model, in: 2022 Snowmass Summer Study, 2022. [arXiv:2203.05914](https://arxiv.org/abs/2203.05914).
- [367] F. Ruppin, J. Billard, E. Figueroa-Feliciano, L. Strigari, Complementarity of dark matter detectors in light of the neutrino background, Phys. Rev. D 90 (8) (2014) 083510. [arXiv:1408.3581](https://arxiv.org/abs/1408.3581), [doi:10.1103/PhysRevD.90.083510](https://doi.org/10.1103/PhysRevD.90.083510).
- [368] F. Mayet, et al., A review of the discovery reach of directional Dark Matter detection, Phys. Rept. 627 (2016) 1–49. [arXiv:1602.03781](https://arxiv.org/abs/1602.03781), [doi:10.1016/j.physrep.2016.02.007](https://doi.org/10.1016/j.physrep.2016.02.007).
- [369] J. H. Davis, Dark Matter vs. Neutrinos: The effect of astrophysical uncertainties and timing information on the neutrino floor, JCAP 03 (2015) 012. [arXiv:1412.1475](https://arxiv.org/abs/1412.1475), [doi:10.1088/1475-7516/2015/03/012](https://doi.org/10.1088/1475-7516/2015/03/012).
- [370] S. Sassi, A. Dinmohammadi, M. Heikinheimo, N. Mirabolfathi, K. Nordlund, H. Safari, K. Tuominen, Solar neutrinos and dark matter detection with diurnal modulation, Phys. Rev. D 104 (6) (2021) 063037. [arXiv:2103.08511](https://arxiv.org/abs/2103.08511), [doi:10.1103/PhysRevD.104.063037](https://doi.org/10.1103/PhysRevD.104.063037).
- [371] E. Aprile, et al., Search for Coherent Elastic Scattering of Solar <sup>8</sup>B Neutrinos in the XENON1T Dark Matter Experiment, Phys. Rev. Lett. 126 (2021) 091301. [arXiv:2012.02846](https://arxiv.org/abs/2012.02846), [doi:10.1103/PhysRevLett.126.091301](https://doi.org/10.1103/PhysRevLett.126.091301).
- [372] W. Ma, et al., Search for Solar B8 Neutrinos in the PandaX-4T Experiment Using Neutrino-Nucleus Coherent Scattering, Phys. Rev. Lett. 130 (2) (2023) 021802. [arXiv:2207.04883](https://arxiv.org/abs/2207.04883), [doi:10.1103/PhysRevLett.130.021802](https://doi.org/10.1103/PhysRevLett.130.021802).

- [373] C. E. Aalseth, et al., DarkSide-20k: A 20 tonne two-phase LAr TPC for direct dark matter detection at LNGS, Eur. Phys. J. Plus 133 (2018) 131. [arXiv:1707.08145](https://arxiv.org/abs/1707.08145), [doi:10.1140/epjp/i2018-11973-4](https://doi.org/10.1140/epjp/i2018-11973-4).
- [374] N. Solomey, et al., Design of a Space-based Near-Solar Neutrino Detector for the  $\nu$ SOL Experiment (6 2022). [arXiv:2206.00703](https://arxiv.org/abs/2206.00703).
- [375] <http://parkersolarprobe.jhuapl.edu/The-Mission/index.php>.
- [376] N. Solomey, Studying the Sun's Nuclear Furnace with a Neutrino Detector Spacecraft in Close Solar Orbit, in: AAS/Solar Physics Division Abstracts #47, Vol. 47 of AAS/Solar Physics Division Meeting, 2016, p. 209.03.
- [377] G. G. Raffelt, Stars as laboratories for fundamental physics: The astrophysics of neutrinos, axions, and other weakly interacting particles, University of Chicago Press, 1996.